UNIVERSITY OF CAPE TOWN

DEPARTMENT OF CIVIL ENGINEERING

CONCRETE MATERIALS AND STRUCTURAL INTEGRITY RESEARCH UNIT (CoMSIRU)

ASSESSING THE INFLUENCE OF CRACK WIDTH ON THE DURABILITY POTENTIAL OF CRACKED CONCRETE USING THE DURABILITY INDEX APPROACH

AUTHOR

Janina P. Kanjee

Supervisor: Assoc. Prof Hans-Dieter Beushausen

Co-Supervisors: Prof Mark Gavin Alexander, Dr Mike Benjamin Otieno

A Dissertation submitted to the Faculty of Engineering and The Built Environment, University of Cape Town, in partial fulfilment of the requirements for the degree of Master of Science in Engineering

South Africa, 2015

DECLARATION

I, Janina Kanjee, hereby declare that this Dissertation is my own, unaided work. I know the meaning of plagiarism and declare that all the work in this document, save for that which is properly acknowledged, is my own. It is being submitted for the degree of Master of Science in Engineering in the University of Cape Town. It has not been submitted before for any degree or examination in any other University.

SIGNED:

_____

JANINA P. KANJEE

2015

DEDICATION

This dissertation is dedicated with all my love to my Mother,

~ Harsila Kanjee ~

for always being the driving force in my life.

ABSTRACT

Durability is a major concern for reinforced concrete (RC) structures. RC structures both in service and new, are subject to cracking. Irrespective of the cause of the cracking, cracks can increase the rate of penetration of aggressive species into concrete and modify the transport properties. Consequently, the service life of corrosion-affected RC structures may be drastically reduced in the presence of cracks. However, no modifications are made for the influence of cracking on the penetration of aggressive species into concrete when analysing durability test results or making service life predictions, even through concrete is very often in a cracked state.

This study focused on the influence of cracks on the ingress of aggressive species (carbon dioxide and chlorides) into cracked concrete in comparison to uncracked concrete. The aim was to establish any correlations between the transport properties in uncracked and cracked concrete. Furthermore, in a broader context, the aim was to assess to what extent the modified cracked concrete parameters used in service life predictions affect the service life outputs, when compared with service life outputs obtained using the uncracked concrete parameters. Six concretes mixes were investigated comprising two water/binder (w/b) ratios (0.40 and 0.55) and three binder types (100% CEM I 52.5N (PC), 70/30 PC/FA and 50/50 PC/GGBS). 100 x 100 x 500 mm beams were cast and cracks were induced after seven days in the mid-span of each beam using three-point loading. Two crack width ranges were investigated; 0.1-0.4 mm (w_{cr1}) and 0.5-0.8 mm (w_{cr2}). The central section of the beam that contained the crack was sawn from the rest of the beam and used for either accelerated carbonation or bulk chloride diffusion testing. Cores were drilled from the outer sections of the beam and used as specimens for the Durability Index tests. The cracked specimens were monitored for carbonation (accelerated carbonation) and chloride ingress (bulk diffusion), while the uncracked ones were monitored for durability parameters (OPI, WSI & CCI) after 8 and 16 weeks of exposure.

Firstly, it can be concluded that the presence of cracks modifies the transport properties of concrete by promoting rapid increase of ingress of aggressive species (CO_2 & Cl^-) into the concrete matrix. It was found that the degree to which the transport properties were modified increased as the crack width increased. This was primarily attributed to the increase in surface area created by the crack, which allowed increased amounts of species (CO_2 & Cl^-) to penetrate into the concrete matrix.

In the case of carbon dioxide ingress, the presence of cracks significantly increased the rate of carbonation (up to 50 %) in the concrete specimens that contained blended cements PC/FA and PC/GGBS when compared to the PC concrete specimens. However, in the case of chloride ingress the effects of cracks in the PC mix resulted in the highest presence of chlorides (up to 78 %) in the concrete specimens in comparison to the chlorides present in the PC/FA and PC/GGBS concrete specimens.

Secondly, when the sound (DI) and cracked durability parameters (carbonation and diffusion coefficient) where used in carbonation and chloride ingress service predictions, it was found that the DI service life prediction outputs were more conservative in relation to service life outputs from the durability parameters obtained from cracked concrete specimens. These results highlighted the degree of influence which the presence of cracks had on modifying transport properties in concrete. Furthermore, it also highlights the impact of the presence of cracks on the service life of RC structures and the prediction of long-term carbonation- and chloride- induced corrosion.

Due to the significant influence that cracks have on modifying the transport properties of concrete, the results show that some reduction factors need to be applied to the results from the DI approach to reflect a more realistic durability potential of the concrete. Further research into understanding how other crack parameters (crack depth, frequency etc.) modify transport properties in concrete will lead to a more accurate insight into dealing with and accounting for the presence of cracks in RC structures.

ACKNOWLEDGEMENTS

I would like to acknowledge, with much gratitude, the assistance of the following people for their assistance during this study:

My supervisors, Assoc. Prof. Hans Beushausen and Prof. Mark Alexander, who gave me the opportunity to take on this project and provided guidance and enthusiasm;

Dr Mike Otieno, who co-supervised this project and provided continual guidance, critical evaluation, encouragement and who served as a constant source of inspiration;

The laboratory staff within the department of civil engineering for their continued assistance during the laboratory-related phases of the dissertation, in particular, Mr C. May, Mr E. Witbooi, Mr H. Mafungwa, Mr D. Ferus and Mr L. Adams. I would like to specially acknowledge Mr. N. Hassen, for ensuring that my experimental work ran smoothly and being a pillar of support in my life, which I could always rely on for my well-being.

Ms. Elly Yelverton for her assistance with regards to any CoMSIRU-related matters and in obtaining relevant literature material.

I would like to thank the staff at the erstwhile South African Cement and Concrete Institute, especially Susan Battison for her help in sourcing much needed literature.

Special thanks to my fellow postgraduate colleagues in the Concrete Materials and Structural Integrity Research Group (CoMSIRU), Philemon Arito, Simon Starck, Matteo Angellucci, Benjamin Walker, Micheal Loseby and all others who provided support in one way or another. Your effort is greatly appreciated.

The Concrete Materials and Structural Integrity Research Unit (CoMSIRU), the National Research Fund (NRF), the erstwhile Cement and Concrete Institute (cnci) and lastly Aurecon for their financial support towards my study.

I would like to also thank my close friends Beejal Govan, Azni November, Keegan de Waal and Travys Munthree for their love, support and always being there for me.

Lastly, I would also like to thank my loving parents and sister for their support, motivation and encouragement through my thesis.

"I would maintain that thanks are the highest form of thought, and that gratitude is happiness doubled by wonder."- Gilbert Chesterton

TABLE OF CONTENTS

TABLE OF FIGURES

LIST OF TABLES

1 INTRODUCTION

1.1 Background

The concrete construction industry is currently refocusing its attention towards monitoring, rehabilitating and retrofitting ageing infrastructure. This change has been as a result of a number of factors. Firstly, resources are spent on repairing, strengthening and maintaining existing civil infrastructure to ensure their serviceability and to extend their service life (Maage *et al.,* 1996; Nedhi *et al.*, 2010). It is much more economical to extend the service life of existing structures with little repair and/or maintenance than to construct new ones (Richardson, 2002). This is true for the increasing amount of ageing infrastructure. Secondly, several cases of new structures exhibiting premature deterioration have been reported (Metha & Burrows, 2001) and require financial resources for inspection, maintenance and repair. Lastly, ensuring the preservation of historic buildings for future generations due to their architectural style or their affiliation with historic people or events (Miller, 2006) is important. In view of all these issues, it has become essential for structural engineers to aim at ensuring the durability of structures during their life.

Reinforced concrete (RC) is a composite constructed material, that is usually strong and durable, performing well during its service life. However in spite of the perceived durability of these structures, many have continued to deteriorate. Corrosion of steel reinforcement is reported (Broomfield, 2007; El-Reedy, 2008) to be the greatest cause of durability failure of RC structures in most parts of the world today. The two main causes of reinforcement corrosion are carbonation and chloride ingress (Broomfield, 2007). Other forms of deterioration include sulphate attack (for example, due to ingress of sulphate ions from groundwater) and freeze/thaw (due to the flow of water and its distribution within the pore structure). The damage and related cost of repair as a result of reinforcing steel corrosion has led to one of the largest infrastructural problems facing both developing and developed countries.

Folic (2009) noted that RC structures often experience premature deterioration because not enough attention is given to durability design for service life during the design stage, furthermore most standards for structural design do not cover durability design explicitly. Corrosion of steel in RC structures not only has severe economic implications with regards to repair, but also has an environmental burden associated with it (Koch *et al.,* 1999). Some structures can be replaced, however others (for example, public utilities, bridges and chemical plants) would cause great inconvenience if they were taken out of commission as they serve a critical purpose with respect to the economic, political and social functioning of a society (ASM International, 2000). Hence it is crucial that existing infrastructure achieve their design life and is maintained effectively.

1.2 Motivation and Research significance

In order to ensure that structures maintain adequate durability during their service life, engineers need to thoroughly understand the different parameters governing the deterioration of RC structures such as the aggressiveness of the environment, quality of the concrete and resistance of the structure to carry load. Durability- related deterioration processes are usually initiated due to the ingress of aggressive species (via various transport mechanisms) from the exterior environment into concrete. Failure to understand what drives deterioration processes can eventually lead to loss of durability and ultimately structural failure in the long-term (EN1992, 2004).

There are a several transport mechanisms that facilitate the ingress of harmful species into concrete (Richardson, 2002) including gaseous diffusion (oxygen, carbon dioxide), vapour diffusion (moisture movements), ionic diffusion (chlorides, sulphates), absorption and capillary rise (chlorides dissolved in water) and pressure-induced flow (aggressive groundwater, freeze/thaw). The ease with which these aggressive species can ingress concrete is termed 'penetrability'. The degree of penetrability of aggressive species into the concrete matrix is dependent on a number of factors such as permeability, pore size distribution, connectivity between pores and tortuosity. These properties are inherently determined by the volume fraction of the materials used in the mix design, the casting of concrete and the degree of hydration (Ballim *et al.,* 2009). Penetrability is considered a significant characteristic governing concrete durability, as it controls the ability to impede the ingress of deleterious substances into the concrete pore structure. It is well established in literature that the quality and thickness of the cover concrete greatly governs the durability of RC structures (Basheer *et al.*, 2001). In addition, its condition, for example whether cracked or uncracked, is also important.

The interaction between the environment and the structure determines the long-term durability performance and service life of the structure, in which the rate of penetration of aggressive species is highly significant. Tuutti (1982) defined service life as *the period when the maximum level of tolerable damage is reached for a given structure.* In the Eurocode (EN1990, 2002) it is defined as *the period of time after construction during which all properties exceed the minimum acceptable values when routinely maintained.*

The deterioration of RC structures with respect to corrosion was initially described in terms of an initiation and propagation period. It was then later modified by Heckrood (2002) to include three periods (initiation, propagation and acceleration) as shown in Figure 1.1

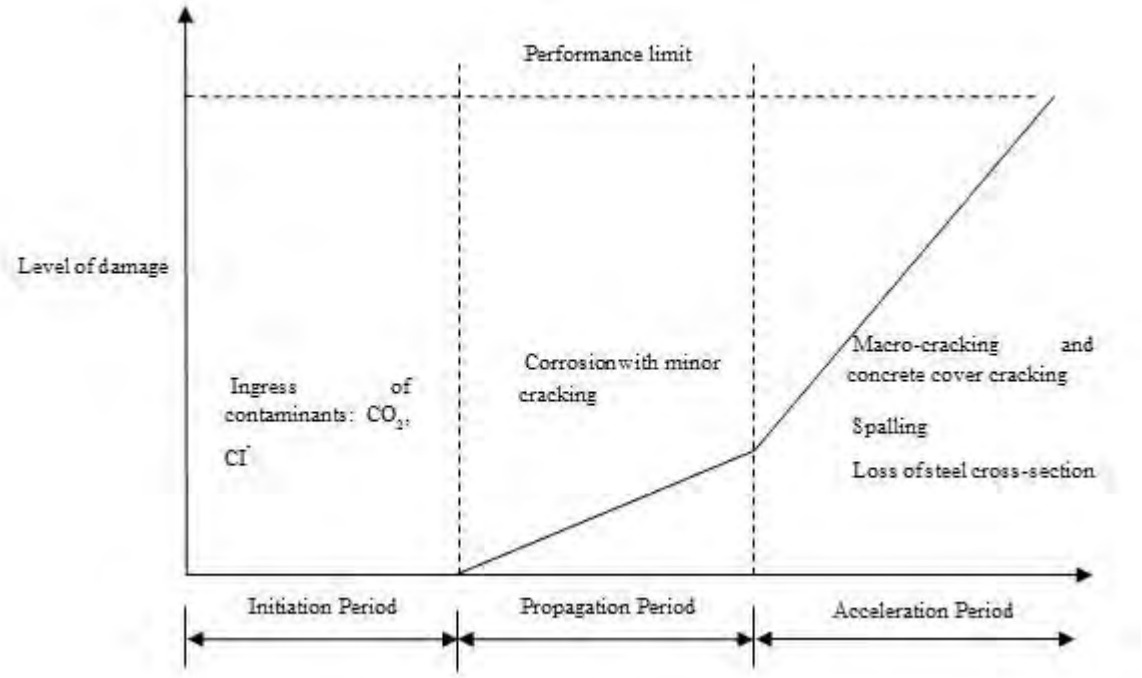

Figure 1.1 Three stage deterioration model (Heckroodt, 2002)

The first period (initiation) describes the phase when there are no visible signs of corrosion on the RC structure. During this period aggressive species from the exterior environment penetrate the bulk concrete material and accumulate at the level of the steel in sufficient concentration to break down the passive protective layer on the steel surface. The end of this period is marked by the initiation of active corrosion.

The propagation period describes the phase when corrosion–induced deterioration occurs with time. This phase presents minor damage such as cover cracking on the RC structure.

The acceleration period is marked by widespread cracking and spalling of the cover concrete. The length of this period directly depends on the rate of the corrosion. The corrosion rate in this phase is governed by the access of aggressive species through the cracks and areas were concrete has spalled.

Although concrete deterioration due to the ingress of aggressive species is usually a medium to long-term process, the onset of deterioration and its rate may relate to the damage that originates at the time of construction such as defects or during the initial stages such as plastic and drying shrinkage cracking. Premature damage to the concrete cover in the form of cracks can aid the movement of gases, ions and liquids into concrete. Subsequently, this leads to modification of the transport properties of the concrete. Depending on the nature and the driving force of aggressive species, there is a distinction between the different transport processes which are diffusion, absorption and permeation. This is of interest because the interaction of these species with the constituents of the pore water can alter the properties of the concrete and indirectly lead to the deterioration of the structure (Basheer *et al.,* 2001).

To fully understand the cause and extent of deterioration of a given structure, a thorough evaluation of the structure's construction material needs to be undertaken. Firstly, this involves characterizing the nature of the problem by carrying out a visual survey of the structure. Particular attention should be given to the serviceability and structural integrity of the structure (i.e. cracking or concrete spalling or steel cross-section loss). The next stage involves confirming the cause of deterioration and quantifying the extent of the problem by conducting tests on the concrete and measuring the severity of deterioration. Many techniques and test methods have been developed and can be used to carry out a service life assessment of an existing structure or an evaluation of the expected corrosion resistance of RC structures.

Most of these test methods are based on the rate of penetration of aggressive species into concrete and relate transport mechanisms to various deterioration processes (Basheer *et al.,* 2001). Results from these tests give an indication of the concrete's resistance to the ingress of aggressive species and are used as input parameters in service life prediction models. Lastly, based on the service life model outputs, an appropriate repair and rehabilitation system can be chosen for the structure depending on its type, condition and expected future use.

1.2.1 The influence of cracks on transport properties and the effect on concrete durability

The key to attaining concrete durability is to ensure a highly impermeable pore structure of the concrete matrix. Shah and Slate (1965) found that microcracks at the interface between coarse aggregate and the mortar exist in concrete even before it is subjected to external load, even in concrete kept continuously wet from the time it is cast. Although microcracks may not affect the structural intergrity of a RC strcucture immediately, they can affect its long-term durability performance and hence strcuctural intergrity. Interestingly, the majority of research that has been conducted on the penetration of deteriorious species into concrete has been performed primarly on uncracked concrete. This can be attributed to the difficulty of creating desired crack patterns in concrete and the lack of availability of appropriate testing apparatus. It is only recently that attention has shifted towards accounting for the presence of cracks and their influence on the penetration of species into the concrete, and consequently on deterioration processes.

Knowledge of the transport properties of cracked concrete is essential for predicting its durability since the deterioration mechanisms depend on the movement of aggressive agents within the cracked concrete. The presence of cracks at an early age facilitates the ingress of moisture and other aggressive ions making concrete susceptible to deterioration. Transport in a cracked concrete is therefore viewed as a coupled phenomenon between the matrix and the crack (Mohammed *et al*., 2003).

Studies have clearly indicated that the presence of cracks can contribute to increased permeation (or absorption) coefficient of the material by several orders of magnitude (Wang et al., 1997). Parameters such as the crack network and the width of cracks, have a marked influence on the material permeability (Gerard *et al.,* 1999).

Unlike load-induced micro-cracks, which have localized effects on transport properties of concrete, shrinkage-induced micro-cracks are in most cases widely distributed and therefore have a more generalized effect on the transport properties of concrete. According to Hearn, (1991) shrinkage cracks tend to have better connectivity, thus significantly contributing to increased permeability. The focus of this study is on the impact of macrocracks, particularly flexural cracks, on transport properties in concrete, and not microcracks.

In the broader context of RC deterioration, one possible consequence of modified transport properties due to the presence of cracks can be the decreased time to the initiation of reinforcement corrosion. The limited research that has been conducted thus far on this issue has been, to some extent, conflicting. There are two opinions that exist that focus on the ingress of agressive species through cracks which result in reinforcement corrosion initiation. The first opinion is that cracks can accelerate the corrosion of reinforcing bars (Okada & Miyagawa, 1980; Shalon & Raphael, 1964) whereas research conducted by Temper (1947), Houston & Ferguson (1972) and Mohammed *et al.*,(2001) has shown that cracks have no influence on corrosion. Recent work done by Otieno *et al.*, 2009 has shown that cracks accelerate chloride-corrosion, however further work is needed to collaborate this opinion and provide a more definitive view regarding the influence of cracks on reinforcement corrosion.

1.3 Problem Statement

Both in-service and newly built RC structures are subject to cracking. Nevertheless, the fact that most of RC structures have cracks is often either ignored or not explicitly accounted for when trying to assess and predict the service life of the structures. The three statements listed below, provide the reader with a context for what needs to be addressed in order to resolve and better understanding the role of cracking on transport mechanisms in concrete and the durability of RC structures.

1) The models used to describe the fundamental transport properties with respect to the movement of species from the exterior environment into concrete bulk material have been modelled on the premise of uncracked concrete. Despite the presence of cracks in RC structures, few attempts have been made to incorporate the influence of cracking on the penetrating of aggressive species into concrete. Although there is general opinion that cracks modify transport properties in concrete, there is no accurate quantification to describe these effects.

2) The Durability Index tests (oxygen permeability, water sorptivity and chloride conductivity) that are used in South Africa to characterise the quality of the concrete cover were developed using concrete in an uncracked state. Hence the durability parameter that is obtained after testing is not a realistic representation of the in-situ concrete structure.

3) It is increasingly common to utilize numerical simulation models to predict the long-term performance of concrete structures. Service life models that have been developed are based on various deterioration mechanisms and use the durability index parameters as input parameters to predict the deterioration of the structure. These

models correlate well with laboratory investigations, however they usually fail to accurately predict the service life of real cracked RC structures. These models use well-cured undamaged specimens as a baseline and predict an overly optimistic service life performance that is not representative of the behaviour of the concrete.

An improved understanding of the influence of cracking on the transport properties of concrete will help to improve on the accuracy of predicting the durability performance and serviceability of concrete structures.

1.4 Aims

The main aim of this study is to investigate the influence of cover cracking on the ingress of chlorides and carbon dioxide in concrete.

Secondary aims of this study include:

1. Investigate the influence of water/binder (w/b) ratio on transport properties in cracked and uncracked concrete.

2. Compare the transport properties of chlorides and carbon dioxide (for a given crack width range) in concrete made using:
    - Portland Cement (PC) (CEM I 52.5 N)
    - 70/30 PC/Fly ash (PC/FA) blend
    - 50/50 PC/ Ground Granulated Blastfurnace slag (PC/GGBS) blend
3. Synthesise information so as to improve the understanding of transport properties of chlorides and carbon dioxide in cracked concrete.

4. Compare and assess the impact of service life predictions of cracked RC using cracked transport properties in relation to (ideal) uncracked transport properties.

1.5 Scope and limitations

The scope of this study is limited to the following aspects:

1. The transport properties were limited only to that of chlorides and carbon dioxide in cracked and uncracked concrete.

2. The penetration profile of chlorides and carbon dioxide into concretes of two crack width ranges:
    - 0.1-0.4 mm denoted as w_{cr1}
    - 0.5-0.8 mm denoted as w_{cr2}
3. Two water/binder ratios: 0.40 and 0.55

4. Sample testing was conducted at two ages: 8 and 16 weeks after exposure to chlorides and carbon dioxide.

1.6 Plan of development

This thesis is divided into five chapters as follows:

Chapter 2 – The first section of this chapter presents a review of literature with respect to the presence of cracks in concrete, and the transport mechanisms in both uncracked and cracked concrete. The second section deals with the influence of cracks on durability testing. The aspects that govern the durability of concrete and different test methods that are used to assess the durability are examined. The literature review will establish the need to account for the presence of cracks when conducting durability tests and making service life predictions.

Chapter 3 - This chapter discusses the laboratory testing procedures, detailing the scope of testing, the experimental variables and mix design considerations.

Chapter 4 - This chapter presents the results that were obtained from the experimental work in Chapter 3. This is accompanied by the analyses and discussion of the results.

Chapter 5 - This chapter presents the conclusions based on the findings of this study, and recommendations for future study.

2 LITERATURE REVIEW

2.1 Introduction

2.1.1 Overview

This chapter has been divided into two sections A and B as follows:

Section A: Durability of RC concrete ;
Section B: Influence of cracks on transport properties in concrete

The first section begins with providing background to the reader on the durability of RC structures. Factors that influence durability, as well as the importance of ensuring the durability of RC structures are covered. Specifically, the role of carbonation and chloride-induced corrosion is discussed and its effects in reducing the service life of RC structures. The concrete properties and environmental aspects that drive carbonation and chloride induced corrosion are touched on. International and local (South African) test methods that are used to quantify the ingress of chlorides and carbon dioxide are discussed. Lastly the South African Durability Index testing approach is examined. The limitations of using the DI approach to characterize cracked concrete are highlighted; the impacts on service life predictions are also illustrated.

The second section begins with an overview of the presence of cracks in concrete at a microscopic level. This is followed by a brief discussion of the various types of cracks that develop on reinforced concrete (RC) structures at a macroscopic level. Distinct crack features that are used to characterize cracks on RC structures are then examined. This is followed by various techniques that have been developed and used to characterize cracks in concrete. Transport mechanisms that are used to describe the movement of ions, gases and liquid in sound (uncracked) concrete are then discussed in detail. This leads to the discussion of transport mechanisms in cracked concrete. Techniques that are employed to generate artificial cracks in concrete are briefly mentioned. The section concludes by highlighting examples of the research studies that have been conducted or are currently on-going on the influence of cracks on modifying transport properties of concrete.

The chapter concludes by emphasizing the need to understand the presence of cracks in modifying the transport properties of concrete. This is important as most RC structures are subjected to cracking and this can have a significant impact on the ingress of aggressive species into the bulk concrete material. Modified transport mechanisms in cracked concrete can as a result alter the chemical and physical composition of the concrete and may ultimately lead to the onset of reinforcing steel corrosion. Based on the critical review of literature, it will be clear why the basis for the incorporation of crack parameters (such as crack widths and depth) in service life prediction models should be explored. This would ultimately provide a more accurate method of assessing and predicting the durability and inherent service life of RC structures.

2.1.2 Objectives of this chapter

The objective of this chapter is to review:

- The durability of RC structures and factors that govern the durability of such structures
- The fundamental principles of corrosion with regards to steel in concrete and the implications of corrosion on the durability and the inherent service life of RC structures.
- Provide a brief overview of carbonation- and chloride-induced corrosion. Discuss various factors that govern both types of corrosion mechanisms and models that have been developed to predict their behaviour.
- International methods that have been developed and are used for testing, measuring and monitoring the ingress of chlorides and carbon dioxide into concrete.
- The South African Durability Index (DI) testing approach. To provide an overview of the testing methodology by mentioning the relevant tests that are conducted and their relation to the service life prediction of RC structures. Highlight the short-fall of this testing approach; with regards to cracked concrete. This gap in knowledge motivates the need to understand the influence of cracks on transport properties of cracked concrete, which can be used to provide more accurate service life predictions using the Durability Index (DI) testing approach.
- The development and presence of cracks in concrete at both a micro- and macroscopic scale.
- The various methods of characterising and analysing cracks on RC structures.
- The transport mechanisms that are used to describe the movement of ions, gases and liquids from an exterior environment into (uncracked) bulk concrete material.
- The different approaches used to generate cracks in concrete specimens in the laboratory, to better understand the role of cracks on the transport mechanisms in cracked concrete and their influence on the durability of RC structures.
- Previous research that has been carried out on cracked concrete, particularly with regards to the diffusion of chlorides and gases in cracked concrete. This motivates the need to account for the presence of cracks when describing the transport mechanisms of cracked concrete.

Section A: Durability of RC structures

2.2 Durability of RC structures

Durability as defined by Ballim *et al.,* (2004) *is the ability of a material or structure to withstand the service conditions for which it is designed over a prolonged period without significant deterioration*. It is associated with the deterioration of a material over the intended service life of the structure in a given environment (Ballim *et al.,* 2009).

The key to attaining durable concrete is to achieve a dense and highly impermeable pore structure. The durability of concrete structures is greatly governed by the quality of the cover concrete (Basheer *et al.,* 2001). The long-term durability of RC is mainly controlled by its ability to impede the ingress of deleterious substances into the concrete pore structure. The interaction between the various materials and environment elements that influence the durability of RC structures can be observed in Figure 2.1

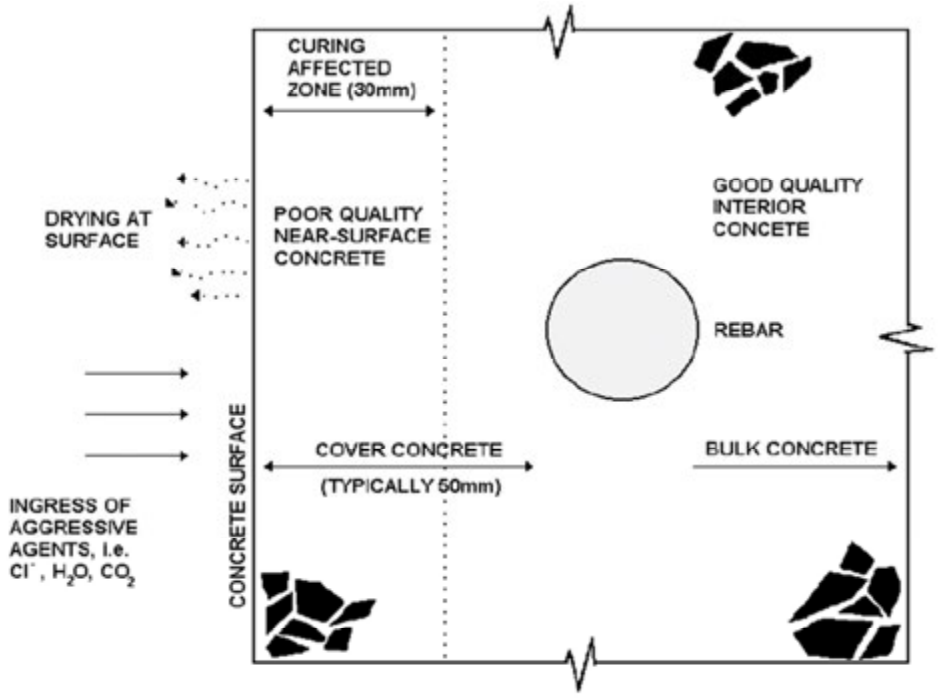

Figure 2.1 Interaction between concrete and environmental elements (Alexander *et al.,* 1999)

The porous nature of concrete permits the ingress of CO_2, Cl^-, O_2 and moisture into concrete leading to the corrosion of reinforcing bars. The penetrability of concrete, which is mainly dependant on penetrability characteristics of hardened cement paste, can be a major factor affecting durability of concrete (Song & Kwon, 2007). The important rate-controlling factors of concrete deterioration are the quality of the concrete governed by the constituent materials and their mix proportions, method of manufacturing and the subsequent surface finish of the concrete, the exposure environment and the loading history (Metha , 2006).

Corrosion is considered one of the main cause of the limited durability of steel-RC. The basic problem associated with the deterioration of RC is the corrosion product, rust, which resides at the interface between reinforcement and concrete, degrading the bond between rebar and

concrete. Damage resulting from corrosion of steel includes delamination, the reduction of steel areas, cracking, debonding between rebar and concrete, and spalling and thus reducing the service life of the structure (Huang & Yang, 1997).

A brief overview of corrosion of steel in concrete is presented in the following sections to provide basic insight of what this process entails and how it results in the deterioration of RC structures.

2.3 Transport mechanisms in uncracked concrete

The penetration of aggressive species (CO_2, Cl^-, O_2) through the concrete cover can lead to the deterioration of RC structures. In order to understand the various deterioration mechanisms, a fundamental understanding of the transport processes and properties that govern the rate of ingress of these species and their movement through concrete is necessary (Shutter & Audenaert, 2007). The kinetics of the transport mechanisms depend of the properties of the concrete (e.g. its porosity and the presence of cracks), on the binding capacity of the binder, as well as the environmental conditions existing at the surface of the concrete and their variations in time (Bertolini ***et al.,*** 2004).

The presence of moisture is an important factor controlling the various chemical deterioration processes. Moisture is continuously transported within the concrete body in the form of liquid and vapour from either the surrounding environment or the internal body of the concrete. The rate and ingress of moisture depends on the physical structure of the HCP and aspects such as the pore size, and distribution and by the presence of cracks (micro- and macro- cracks). The effective porosity of the concrete structure which is related to the degree of continuity of the pore system, significantly affects the transport properties of concrete (Hoseini ***et al.***, 2009).

Moisture is present in the hydrated cement paste in different forms. Capillary water refers to water that is contained in the capillary pores and accounts for the greatest part of moisture in concrete. This moisture has a significant role in the corrosion of RC structures, since it governs the mobility of various ions and thus the electrical conductivity of the concrete.

However, it is difficult to characterise the microstructure of concrete. In order to model the transport mechanisms in concrete, average values of permeability, porosity, diffusivity and sorptivity have to be used (Richardson, 2002).Therefore in order to predict the durability of cementitous materials, a fundamental understanding of the transport mechanisms within the concrete microstructure needs to be covered. A brief description of the transport mechanisms that are relevant to deterioration of RC structures due to carbonation and chloride ingress are mentioned below.

2.3.1 Diffusion

Diffusion is the movement of gases, ions, and/or molecules through a porous material under a concentration gradient, from an area of a high concentration to an area of low concentration (Poulsen & Mejlbro, 2006). Diffusion is the predominant transport mechanism of chlorides in

concrete. The theory of diffusion is based primarily on the mathematical models developed by Adolph Eugen Fick (1829-1901).

Fick's First Law (Equation 2.1) is commonly used to model gaseous and ionic diffusion in concrete. This law models the rate of diffusion in a one dimensional situation, of fluid or ions into a uniformly permeable material. The law states:

$$J = -D_{eff}\frac{dC}{dx}$$ **Equation 2.1**

where: J = Mass transport rate (g/m^2s)

D_{eff} = Effective diffusion coefficient (m^2/s)

C = Concentration of fluid (g/m^3)

x = Distance (m)

The negative sign denotes that the flux occurs along a negative concentration gradient. Equation 2.1 is only applicable when steady-state conditions have been reached, i.e. there is no change in concentration with time. The diffusion coefficient is dictated by the diffusion species, on the characteristics of the concrete and on the environment.

The coefficient can change following variations in pore structure (due to hydration of cement paste), or of the external humidity (degree of saturation of the pores), or the temperature (Bertolini *et al.,* 2004). Diffusion of gases occurs much faster in open pores than in water-saturated pores. In comparison to the diffusion of chloride or sulphate ions which favour the diffusion in saturated pores as a pose to partially saturated pores. Water-filled pores that are interconnected have a compounded effect on the diffusion process.

Fick's second law is used to model the ionic diffusion in concrete for non-steady state conditions:

$$\frac{\partial C}{\partial t} = D_{eff}\frac{\partial^2 C}{\partial x^2}$$ **Equation 2.2**

where: D = Diffusion coefficient (m^2/s)

t = Time parameter (s)

C and x are the same variables as in Equation 2.1. Equation 2.2 can be solved using the following Boundary conditions:

$C_x = 0$ at $t = 0$ and $0 < x < \infty$

$C_x = Cs$ at $x = 0$ and $0 < t < \infty$

where: C_x = Chloride concentration at depth x at time t

C_s = Surface chloride concentration

Equation 2.2 is usually integrated under the assumption that the concentration of the diffusing ions, measured on the surface of the concrete is constant in time and equal to the surface concentration, C_S.

2.3.2 Migration

Migration is the movement of ions in a solution under an electrical field. The ions will move along a certain direction of the gradient, depending on the valence of the ions, at an average velocity. Only free ions can contribute to the flow of migration; positive ions move towards the negative electrode and negative ions towards the positive electrode. Migration rarely exists in isolation because the migration process is always coupled with the diffusion process as a result of a concentration gradient (Tang, 1967). The flux of ions under the action of electrical field is described by Nernst-Planck equation:

$$\boldsymbol{J = D \cdot \frac{zFE}{RT} \cdot c} \qquad \textbf{Equation 2.3}$$

where J = Mass flux (g/m^2s)

D = Diffusion coefficient of the ionic species (m^2/s)

z = Electrical charge (ionic valence) (C)

F = Faraday's constant (J/V.mol)

T = Absolute temperature (K)

R = Universal gas constant (8.314 J/molK)

C = Concentration of free ions , by volume of solution (kg/m^3)

E = Electrical potential (V)

2.3.3 Permeation

Permeability is defined as the ease at which a fluid will pass through a medium under the action of a pressure differential (Richardson, 2002). Many different permeability coefficients may be defined depending on the fluid/ gases that are passed through the medium and the assumptions of viscosity and compressibility. Hence there is a clear distinction between water permeability coefficients and gas permeability coefficients.

- *Water permeability coefficient*

Water permeability coefficient (k_w) may be evaluated according D'Arcy's Law for steady state flow:

$$\boldsymbol{k_w = \frac{dq}{dt}\frac{L}{A}\frac{1}{\Delta h}} \qquad \textbf{Equation 2.4}$$

where: dq/dt = Rate of water flow (m^3/s)

L = Thickness of specimen (m)

A = Cross-sectional area of the specimen (m^2)

Δh = Change in hydraulic head in specimen (m)

- *Gas permeability coefficient*

The gas permeability coefficient (k) for Newtonian fluids is determined by using the Hagen-Poiseuille relation as stated below (Kropp, 1995):

$$\boldsymbol{k = \mu \frac{Q}{t}\frac{L}{A}\frac{2p}{(p_1 - p_2)(p_1 + p_2)}} \qquad \textbf{Equation 2.5}$$

where: k = Coefficient of gas permeability (m^2)

Q = Volume of gas flowing (m^3)

μ = Viscosity of gas (Ns/m^2)

L = Thickness of specimen (m)

A = Cross-sectional area (m^2)

p= Pressure at which volume Q is measured (N/m^2)

p_1 = Pressure at entry (N/m^2)

p_2 = Pressure at exit of gas (N/m^2)

t = Time (s)

The factors that affect the gas permeability are similar to those that affect water permeability. The transport of fluid due to a pressure gradients is depends largely on the inherent microcracking within the concrete and the interconnected pore network within the hydrated cement paste. The material porosity is basically controlled by the water/cement ratio, the degree of hydration and compaction (Neville, 1981).

2.3.4 Absorption

When water encounters a dry surface, it will be drawn into the pore structure through capillary suction. The rate of absorption is dependent on the surface tension, viscosity, density of the liquid on the angle of contact between the liquid and the concrete and the radius of the pores. Sorptivity is rate of movement of a water front through the concrete under capillary action.

$$\boldsymbol{\frac{V}{A} = S\, t^{0.5}} \qquad \textbf{Equation 2.6}$$

where V = Volume of material absorbed in time t (mm^3)

A = Surface area of specimen in contact with water (mm^2)

S = Sorptivity ($mm/min^{0.5}$)

t = Time (min)

The water absorption is calculated as a mass increase resulting in immersion as a percentage of the mass of dry concrete. Absorption is important for concrete structures that are subjected to freeze/thaw cycles or situation where chlorides are dissolved in water that has cyclical access to the structure (Richardson, 2002).

2.3.5 Convection

Convection (or *advection*) is the process that describes the transport of a solute (e.g. chloride or sulphate ions) as a result of bulk movement of water.

$$\frac{\partial C}{\partial t} = -v\frac{\partial^2 C}{\partial x^2}$$ **Equation 2.7**

where: C = concentration of solute at depth x after time t

v = average velocity of fluid flow

2.3.6 Wick action

Wick action is the transport of water and the ions it may contain through a concrete structure from a face in contact with water/salt solution to a drying face. Relatively thin structural elements are vulnerable to the effects of wicking. Wicking action occurs when a concrete face away from the chloride source is exposed to air at a relative humidity; as a result the pore water will be drawn towards this surface and evaporated. The result is increased chloride concentration inside the concrete.

2.3.7 Combined transport mechanisms

The transport mechanisms mentioned above rarely occur in isolation, the ingress of species into concrete is more likely to be a combination of various transport mechanisms that act in conjunction or in parallel with one another (Hilsdorf, 1995). In order to understand the dynamics of multiple transport mechanisms interaction, a thorough understanding of the fundamental mechanisms is essential. Furthermore, complex testing procedures and models are still required to better understand these complicated processes.

A study conducted by Boulfiza *et al.*, (2003) investigated a model that tried to capture the effects of different transport mechanisms in concrete. The results illustrated that parameters such as crack widths and crack spacing could not be effectively modelled by utilising Fick's Second Law (Weiss *et al.,* 2007).

2.4 Corrosion of steel in concrete

Corrosion, according to Van Delinder (1984), is defined as the deterioration of a material due to its interaction with its environment. The corrosion of metals in particular, occurs as a result of the electrochemical reaction by which a metal is oxidized. The natural tendency of metals to revert to their stable state allows for corrosion to take place e.g., iron in the presence of moist air will revert back to its stable oxides or hydroxides of iron.

The high alkalinity of concrete normally protects the embedded reinforcement in concrete from corrosion. The presence of dissolved oxygen in concrete and in the alkaline pore solution leads to the formation a protective oxide film on the steel surface. The oxide has very low solubility, and thus the steel is protected against corrosion (Broomfield, 2007). The steel is said to exhibit passive behaviours due to the fact that the corrosion rate is stifled to a significantly low level, by the formation of the oxide film on the steel surface. The quality and thickness of the concrete cover protects the steel from the ingress of aggressive species. If the passive film is destroyed, corrosion can be initiated (Fidjestol *et al.,* 1995).

The corrosion of steel in concrete is an electrochemical process as seen in Figure 2.2, at the anode iron is oxidised to iron ions that pass into the concrete pore solution while at the cathode oxygen is reduced to hydroxyl ions. Anode and cathode form a short-circuited corrosion cell, with the flow of electrons in the steel and of ions in the concrete pore solution (Schiessl, 1988).

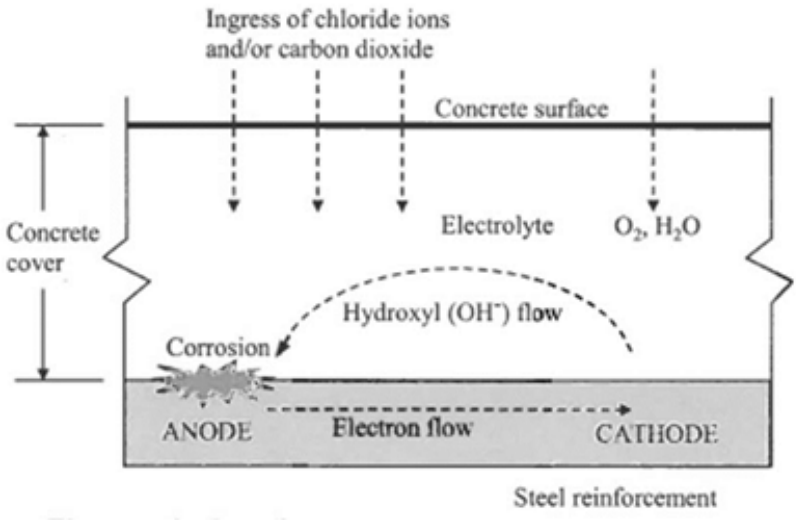

Figure 2.2 Corrosion mechanism in concrete (Broomfield, 1994)

In the case of steel in concrete, the following is a summary of the reactions that occur:

$$\textit{Anode reaction: } 2Fe \rightarrow 2Fe^{2+} + 4e^- \qquad \textbf{Equation 2.8}$$

$$\textit{Cathode reaction: } O_2 + 2H_2O + 4e^- \rightarrow 4OH^- \qquad \textbf{Equation 2.9}$$

Corrosion products have a larger volume than that of the steel that corrodes. (MacDonald *et al.,* 1991). This volume increase leads to the cracking and spalling of the concrete cover that is usually observed as a consequence of steel corrosion in RC structures.

Depending on the different spatial locations of the anode and cathode, corrosion of steel in concrete can be described as either micro-cell or macrocells corrosion.

2.4.1 Microcell corrosion

Carbonation generally causes microcell (uniform) corrosion (Jaggi *et al.,* 2007). This leads to the formation of microcells, consisting of pairs of adjacent anodes and cathodes on the steel surface. These are microscopic in size, so that externally they appear to produce uniform corrosion of the steel (Hansson *et al.,* 2006).

2.4.2 Macrocell corrosion

Macrocell corrosion is often local, with a few centimetres of corrosion (areas of rust) and then up to a metre of clean passive steel. In this case there is a clear separation of the anode and cathode, giving rise to the term 'macrocell" (Elsener *et al.,* 2003). Macrocell corrosion is prominent in chloride-induced corrosion. The presence of water and chloride ions in the concrete pores increases the electrical conductivity of the concrete. The higher conductivity allows for the separation of the anode and cathode as the ions can travel through the concrete (Hansson *et al.,* 2006).

2.4.3 Causes of steel corrosion

There are two main causes of corrosion of steel in concrete; carbonation and chloride-induced corrosion. In both cases, the aggressive species penetrate the concrete and eventually attack the steel. In practice, carbonation-induced corrosion is generally regarded as a minor problem in comparison to chloride-induced corrosion (Parrot, 1987).

Carbonation and chloride-induced corrosion are the focus of this study due to their relation to the prediction models that are utilized in the Durability Index (DI) testing approach. Factors that affect theses corrosion mechanisms, the different approaches to monitor and model their progression in concrete are discussed below in detail:

2.5 Carbonation-induced corrosion of steel in concrete

Carbonation in concrete is the consequence of the chemical reaction between the alkaline components of the cement paste (mainly $Ca(OH)_2$) and the atmospheric carbon dioxide (CO_2) to carbonates. It is essentially a neutralisation reaction which also results in the formation of carbonic acid and hence a reduction in the pH of the concrete pore solution. The calcium carbonate that is formed is deposited in the pores of the concrete (Ho & Lewis, 1987).

During carbonation the following reactions occur (Papdakis *et al.,* 1991):

1. Uptake of CO_2 in the pore water (formation of carbonic acid)

$$\boldsymbol{CO_2 + H_2O \rightarrow 2H^+ + CO_3^{2-}} \qquad \textbf{Equation 2.10}$$

2. Formation of $CaCo_3$

$$Ca(OH)_2 + H_2O + CO_2 \rightarrow CaCO_3 + 2H_2O$$ **Equation 2.11**

3. Further carbonation takes place if sufficient CO_2 and H_2O available, to soluble hydrogencarbonate

$$CaCO_3 + H_2O + CO_2 \rightarrow Ca(HCO_3)_2$$ **Equation 2.12**

The simultaneous presence of CO_3^{2-} and HCO_3^- ions buffer a further decrease of the pH as long as carbonates are still available.

Carbonation moves as a 'front' into the concrete, as seen in Figure 2.3. The front advances into the concrete (towards the steel) when all the calcium hydroxide at a given depth has been depleted. As the carbonation front moves through the matrix, it lowers the concrete pH from its high alkaline pH of 12.5 to a pH of about 9.0. Once the carbonation front reaches the steel level, the drop in pH leads to a breakdown of the passive layer on the steel surface leading to corrosion initiation if sufficient O_2 is available (Ballim *et al.,* 2009).

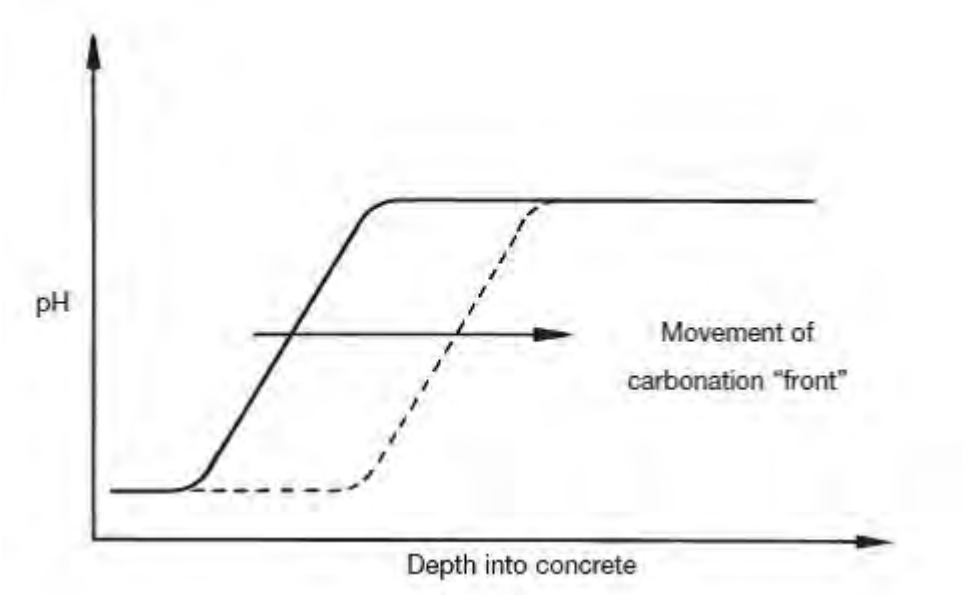

Figure 2.3 pH reduction as carbonation front moves through concrete (Ballim *et al.,* 2004)

2.5.1 Factors affecting carbonation-induced corrosion

The rate of carbonation is a function of cover thickness and quality, cover is essential to carbonation resistance. There are numerous factors that influence the rate of carbonation according to Houst & Wittmann (2002) including water-to-cement ratio, cement type, cement content, water content, alkali content, CO_2 concentration of the surrounding air, presence of damaged zones and cracks and lastly curing conditions.

These factors can be grouped into two categories that influence carbonation depth apart from time; concrete properties and environmental factors.

- *Water/cement ratio*

It is generally accepted that concrete durability is inversely proportional to permeability. Since the rate of carbonation is dependent on the permeability of the concrete, the rate of carbonation will increase with increasing water/cement ratio (St. John *et al.,* 1998). A typical relationship of water/cement ratio and carbonation depth is shown in Figure 2.4

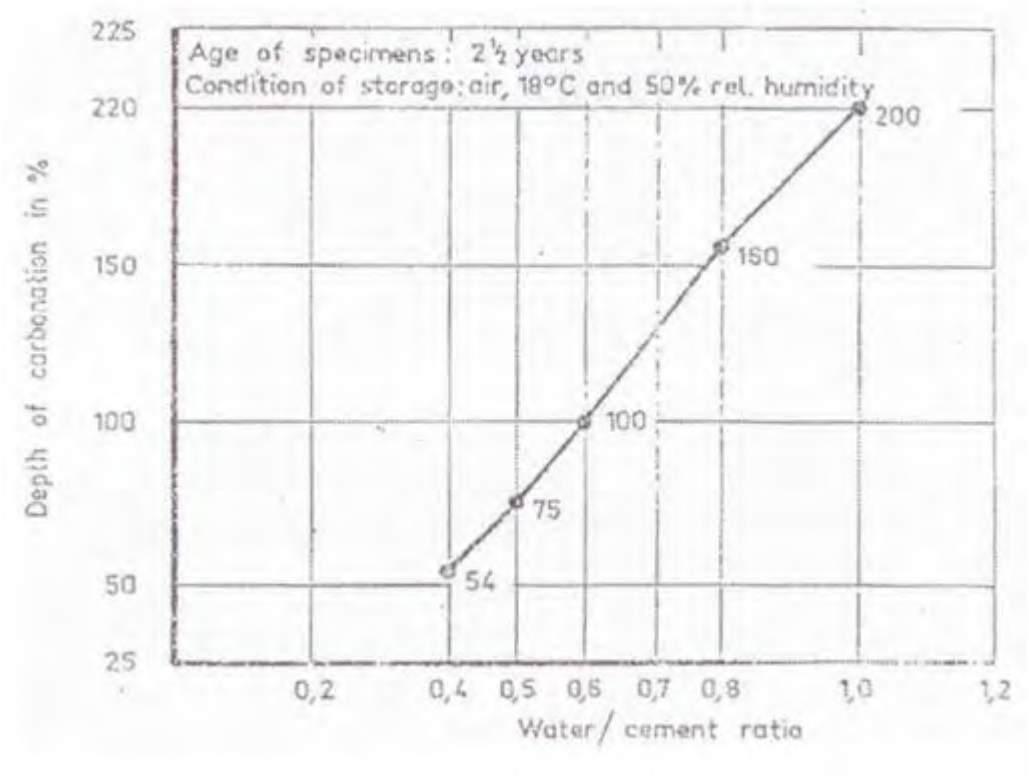

Figure 2.4 Influence of water/binder ratio on carbonation depth (Meyer, 1969)

- *Binder type (composition) and content*
  The binder composition and content influences the nature of the pore structure and the amount of $Ca(OH)_2$ available for reaction. Smaller, disconnected pores as well as increasing availability of $Ca(OH)_2$ (high cement content) will reduce the rate of carbonation.

  Work carried by Meyer (1969) showed that plain Portland cements exhibit slower rates of carbonation as compared to concrete made with from pozzolanic and blastfurnace cement in Figure 2.5 This is due to the increased percentage of $Ca(OH)_2$ that are available for carbonation in plain Portland cement. In another study conducted by Sasatani *et al.,* (1995) showed that after five years of exposure concrete made with fly ash and blast-furnace slag for cement replacement resulted in increased carbonation. Generally, it has been found that concrete made with blended cements exhibit more rapid carbonation as compared to portland cement concrete (Papadakis *et al.,* 1992; Papadakis, 2000)

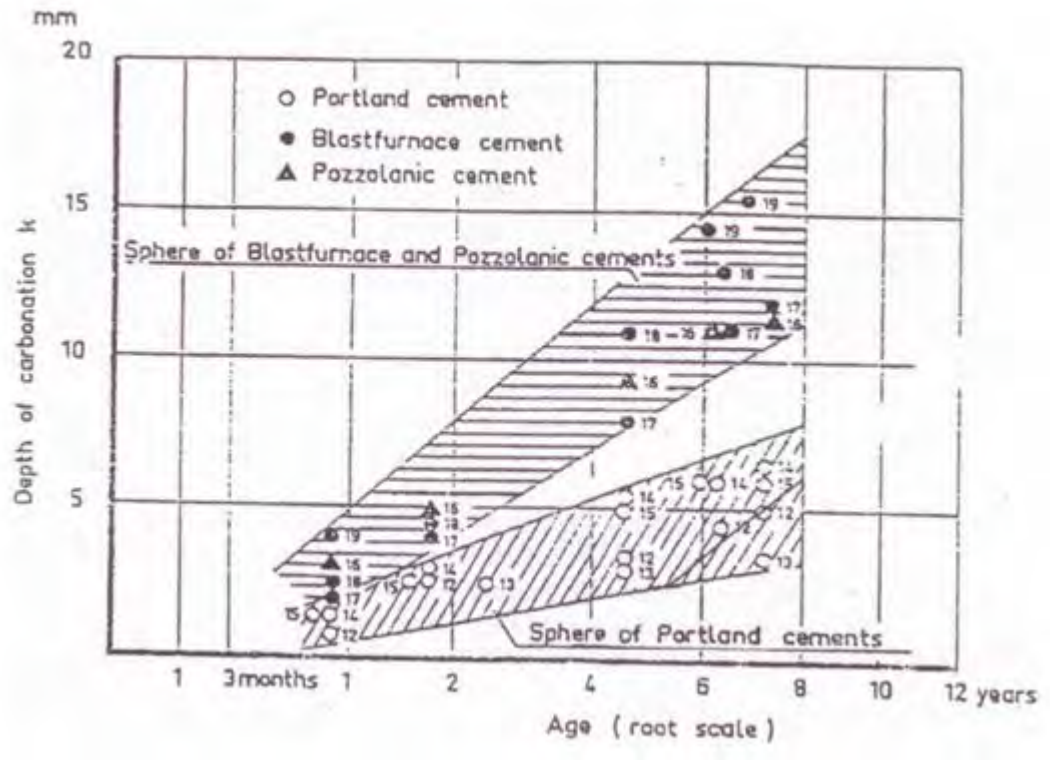

Figure 2.5 Carbonation resistance of concrete with blended cements (Meyer, 1969)

- *Degree of compaction and presence of surface cracks*

  Poor compaction of the concrete as well as surface cracking of the concrete results in an increased number and size of voids. This results in increased penetrability in the concrete which encourages the entry of CO_2 and accelerate carbonation.

- *Curing*

  Proper curing at early ages as stated by Neville, (2003) encourages hydration of cement in the cover zone and prevents the evaporation of moisture from the surface. This reduces pore sizes and the degree of inter-connection between pores, both having the effect of reducing the rate of carbonation.

2.5.1.1 Environmental factors

- *Temperature*

  Temperature has two effects on diffusivity. The CO_2 diffusion is enhanced by an increase in temperature, whereas when the moisture content is reduced, it provides more space for gas diffusion which further increases diffusivity (Houst & Wittmann, 2002).

- *Relative Humidity*

  The rate of carbonation is highly dependent upon the relativity humidity and moisture content of the concrete pore structure. Carbonation does not occur when the pores are completely dry or when fully saturated in completely dry concrete, insufficient moisture is available for the chemical reaction while in saturated concrete, water-blocked pores prevent CO_2 diffusion (Ballim *et al.*, 2009). The rate of carbonation is at a maximum when the relative humidity is between 40 and 60%.

2.5.2 Carbonation rate Prediction Models

Carbon dioxide diffuses through concrete, by utilizing Equation 2.16 Fick's first law of diffusion an approximation of the rate of carbonation front can be made. The diffusion law states that that rate of diffusion is proportional to the thickness being diffused through:

$$\frac{dx}{dt} = \frac{D_o}{x} \qquad \textbf{Equation 2.13}$$

where x = Thickness

t = Time

D_o = Diffusion coefficient

The diffusion coefficient is determined by the penetrability of the concrete. By integrating Equation 2.13, the rate of progress of carbonation is given by the Equation 2.14 (Broomfield, 2007):

$$\mathbf{d} = \boldsymbol{At^n} \qquad \textbf{Equation 2.14}$$

where d = Carbonation depth (mm)

t = Duration of carbonation (years)

n = Exponent (usually ½)

A = Carbonation coefficient for a given concrete

This formulation is based on the assumption of steady state diffusion, i.e., a constant CO_2 content at the surface, and with uniform conditions within the concrete. However, the effective diffusivity of CO_2 is not constant it may depend on time (degree of hydration), on location within the concrete (curing effect, wall effect) and on moisture content (Broomfield, 2007).

Presence of cracks in the concrete changes the composition and moisture levels in the concrete microstructure with depth, this leads to a deviation from the general diffusion equation used to model carbonation. A number of empirical models have been used to determine carbonation coefficient (A) and exponent (n) based on variables such as exposure

conditions, 28 days strength, curing, and concrete properties. A range of empirically derived equations is given in Table 2.3; they link carbonation rates to concrete quality and environment.

Table 2.1 Various carbonation depths equations (Parrot, 1987)

Equation	Parameters
$D = A \cdot B \cdot C \cdot t^{0.5}$	A = 1.0 for external exposure B = 1.7 for internal exposure $C = R(wc - 0.25)/(0.3(1.15+3wc))^{0.5}$ for water cement ratio(wc) > 0.6 C = 0.37R(4.6wc-1.7) for wc< 0.6 R = coefficient of neutralization, a function of mix design and additives (Motohashi & Masuda, 2005)
$D = A(B \cdot wc - C)t^{0.5}$	A = is a function of curing B & C are a function of the percentage of fly ash used
$D = 0.43(wc-0.4)(12(t-1))^{0.5}+0.1$	28 day cured
$D = 0.53(wc-0.3)(12t)^{0.5}+0.2$	Uncured
$D = (2.6(wc-0.3)^2+0.16)t^{0.5}$	Sheltered
$D = (wc-0.3)^2+0.007)t^{0.5}$	Unsheltered
$D = 10.3e^{-0.123f28}$	(Unsheltered at 3 years) – (fX = strength at day X)
D = 680(f28+25)-1.5-0.6at 2 years	
$D = A+B-f28^{0.5}+c/(CaO-46)^{0.5}$	CaO is alkali content expressed as CaO
$D = (0.508-f35^{0.5}-0.047)(365t)^{0.5}$	
$D= 0.846(10wc/(10f7)^{0.5}-0.193-0.076wc)(12t)^{0.5}-0.95$	
$D= A(T-ti)T^{0.75}(C1/C2)^{0.5}$	ti=initiation time T – temperature in °K $C_1 = CO_2$ concentration $C_2 = CO_2$ bound by concrete

2.6 Chloride-induced corrosion of steel in concrete

Chlorides in concrete originate from two main sources (Haque & Kayyali, 1995):

i. as contaminant of mix ingredients in the fresh concrete (water, cement, aggregate);
ii. as deicing salts or sea water from the environment in contact with the concrete while in service

In the second instance, chloride ions can penetrate the cover concrete in two different environmental conditions:

a) Chloride ions can diffuse into the pore aqueous solution in the concrete structure permanently exposed to a chloride aqueous phases, this occurs, for example, in concrete structures fully submerged in sea water.
b) Chloride ions can alternatively penetrate concrete by diffusion and/or capillary suction of salt water in the pore system of the cement matrix, this occurs, for example, in marine structures of the splash zone or in concrete slabs discontinuously exposed to de-icing salts.

Diffusion is the principal mechanism that transports chlorides into the concrete. Irrespective of the source of chlorides, chlorides may be found in different states within the concrete (Ayra *et al.,* 1990; Thangavel *et al.,* 1998):

i. Free chloride ions within the pore aqueous solution
ii. Bound chloride, chemically combined with C-A-H or adsorbed on C-S-H

When free chlorides penetrate into the concrete from the environment, some of them will be captured by the cement hydration products, this is called 'chloride binding'. Both physical and chemical processes are involved in chloride binding. The bound chlorides are generally considered not to participate in steel corrosion.

Chloride ions attack the passive layer by acting as a catalyst to corrosion. The chlorides are not consumed in the process but help to break down the passive layer of oxide on the steel and allow the corrosion process to proceed quickly as seen in Figure 2.6 below:

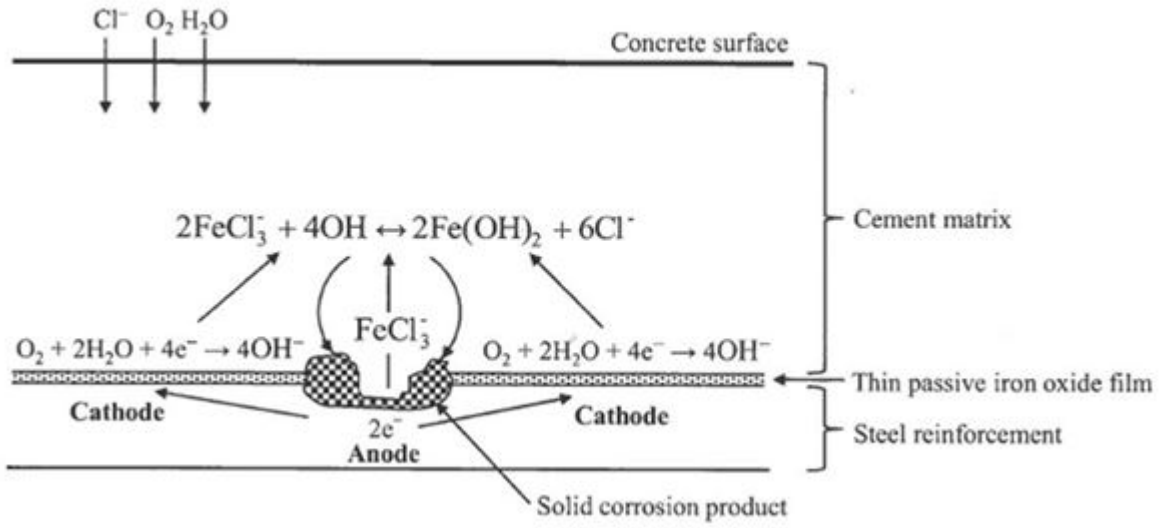

Figure 2.6 Ingress of chlorides facilitating corrosion (Broomfield, 2007)

2.6.1 Critical chloride content for corrosion initiation

The passive oxide film that forms around the reinforcement is maintained by hydroxyl ions in the concrete. However the depassivation of the steel that occurs as a result of the ingress of chlorides has led to the concept of a critical chloride threshold level or concentration. It is defined as the minimum chloride content at the depth of steel required to initiate steel corrosion. There are different ways to represent the critical chloride level. The chloride threshold is usually expressed as a ratio between the concentration of chlorides and that of hydroxyl ions ([Cl]/[OH]) or by the total amount of chlorides by weight of cement content in the material (Alonso *et al.,* 2000).

For marine application 0.4% has been commonly used (Browne) even though this is still debatable There are several parameters that have an influence on the chloride threshold according to Tuutti, (1993) and Arup & Sorensen (1995):

- Concrete quality (Water: cement ratio, cement type, supplementary cementing materials, curing and compaction, etc)
- Environmental conditions such as temperature, relative humidity, carbonation, leaching
- Surface condition of embedded steel

The diffusivity of chlorides through concrete therefore depends on the microstructure of the concrete cover. A wide range of critical chloride threshold levels that cover a number of parameters have been published to date (Angst & Vennesland, 2009).

2.6.2 Factors affecting chloride ingress in concrete

The rate of chloride ingress is dependent on both materials and environmental factor that will be discussed below:

Concrete Properties

The rate of ingress of chlorides into concrete is dependent on the pore structure of the concrete. The penetrability of concrete is related to the pore structure of the cement paste. This will be influenced by the water/cement ratio of the concrete, the inclusion of supplementary cementing materials, and the degree of hydration of the concrete.

- *Water/binder ratio*

It is well known that the concretes of low w/b ratios (0.45) have a greater resistance to chloride ingress because of their dense pore structure (Suryavanshi ***et al.,*** 1998). It is explained by the general relationship between water/binder ratio and permeability.

- *Binder type*

Concrete containing supplementary cementitious materials exhibit higher resistance to chloride ion penetration than those with plain Portland cement (Yang, 2002). Blending cement with fly ash and ground granulated blastfurnace slag (GGBS) is known to produce concrete with a dense microstructure (Kawamura & Torii, 1989) and hence an improvement in the physical protection of any embedded steel bars.

Kumar ***et al.,*** (1986) concluded that the average pore size of ordinary Portland cement concrete was 1.57–2 times larger than that of GGBS concrete because the latent hydraulicity reaction of GGBS does not only make the cement matrix more dense but also diminishes the pore size. The small pore size decreases the penetration and diffusion of chloride-ions.

Fly ash and GGBS have beneficial effect on chloride diffusivity however only at the later days of hydration (Ampadu ***et al.,*** 1999; Yeau ***et al.,*** 2005).

- *Chlorides binding capacity*

As already mentioned in previous sections, chloride binding in concrete affects both the rate of chloride penetration and the amount of chlorides available to initiate steel corrosion. The chloride binding capacity depends on varies parameters such as the local concentration of the substances, the chemical composition of the concrete and the temperature.

With regards to the chemical composition Mohammed and Hamada (2003), confirmed that the ability of concrete to bind to chloride depends on the alkalinity of the binder, its fineness, on the tricalcium (C_3A) and the tetracalcium alumina-ferrite (C_4AF) content. The alumina content of supplementary cementitious materials such as fly ash and GGBS is considerably greater than that of Portland cement. Figure 2.7 illustrates the changes in chloride concentration over a 28 day duration, particularly with mixes containing GGBS, pulverized fuel ash (PFA) and silica fume (SF). The figure highlights binding capacity of supplementary materials by showing how the chloride ion concentrations in the pore solution vary with the total chloride content.

The beneficial effect of chloride binding occurs as a result of the formation of Friedel's salt (the reaction between chlorides and C_3A), which results in a decrease in the concentration of the free chloride ions in the pore solution (Anik ***et al.,*** 1997)**.**

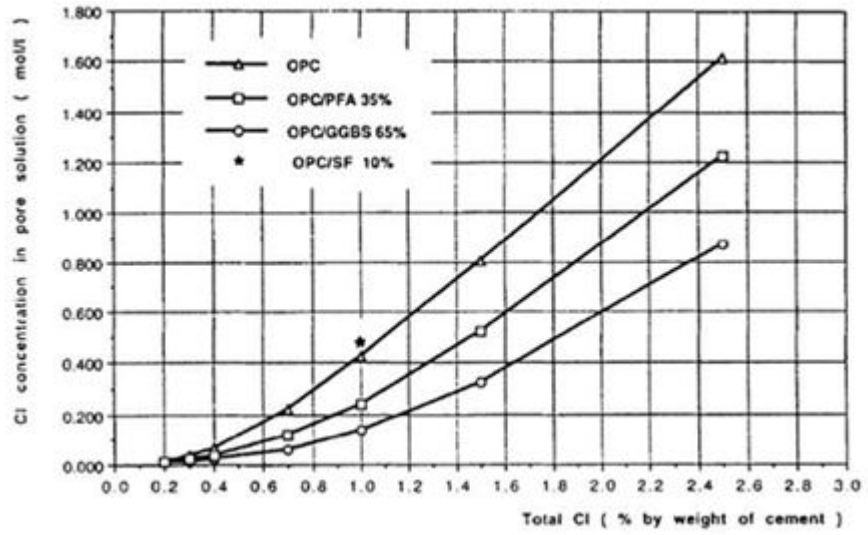

Figure 2.7 Chloride binding effect of supplementary materials (Ayra & Xu, 1995)

Once chloride binding takes place, the diffusion can no longer be effectively described using Fick's second law but requires a corrective term. Due to the difficulty of applying a corrective term, the diffusion coefficient that is derived is termed an "***apparent"*** one that is dependent on time.

Literature shows that the critical chloride concentration increases as the chloride binding capacity increases, as the hydroxyl ion concentration increases, as the degree of water saturation increases and as the water/cement ratio decreases (Hobbs, 1996).

Environmental Factors

- *Exposure to chloride source*

If the structure is constantly exposed to chloride-laden water, high amounts of chlorides will penetrate into the concrete (Lindvall, 2007). A 'constant' exposure solution may not be present all the time, occasionally being replaced by water from driving rain or undergoing

drying conditions, as in the splash zone of marine structures. An example of this are bridges that exhibit damage in areas that drain de-icing salts. The exposed area contains high concentration of salt for a short while, which dilutes and is sometimes replaced by rain water. Furthermore the concrete surface is usually exposed to drying and drying conditions.

- *Temperature*

The resistance of concrete to chloride ingress is temperature related. The diffusion coefficient is influenced by temperature and can double when average temperature increases from 10°C to 20°C (Oh & Jang, 2007). Seasonal temperatures variations may lead to bound chlorides being taken up in winter and being released as free chlorides in the summer (Richardson, 2002).

2.6.3 Chloride-diffusion Prediction Models

Models have been developed to either describe the advance of the chloride profile through the concrete, or to predict the time for the chloride front to reach a certain depth (normally the depth of reinforcement) and at a certain concentration (normally the chloride threshold value for the initiation of corrosion). The latter enables the prediction of the service life of reinforced concrete structures based on the initiation of chloride-induced corrosion.

Most of the existing models used to model the diffusion of chlorides into concrete as function of time and depth, and time to initiate corrosion are based on Fick's second law of diffusion (Hetek, 1996). The differential expression is shown below:

$$\frac{\delta C}{\delta t} = D\frac{\delta^2 C}{\delta x^2} \qquad \textbf{Equation 2.15}$$

where: C = Chloride concentration in solution

D = Apparent diffusion coefficient

Due to the fact that the model was developed over 30 years ago, it was based on a single mass transport equation limited to chloride transport. Hence it did not account for electrical coupling and chemical activity; it assumed constant temperature as well as a saturated material (Glasser *et al.*, 2008).

Many authors have come up with general solutions to Equation 2.15. One such solution is shown in Equation 2.16; it considers chloride concentration at concrete surface (Cs) and the apparent diffusion coefficient (D_a) as constant.

$$Cs\,(x,t) = C_i + (C_s - C_i)erf\left(\frac{x}{\sqrt{4(t-t_x)D_a}}\right) \qquad \textbf{Equation 2.16}$$

Where: $C_s(x,t)$ = Chloride concentration at any time t and depth x

C_i = Initial chloride concentration (constant through depth)

C_s = Chloride concentration at concrete surface (constant)

D_a = Apparent diffusion coefficient (constant)

x = Depth referred from surface

t =Time of exposure,

From this solution, considering constant diffusivity, the depth of chloride ingress and time to initiate corrosion can be evaluated or derived. Collepordi *et al.,* (1972); Browne, (1980); Tuuti, (1982);and Poulsen, (1990) are some of the authors who have proposed the use of the 'chloride diffusion coefficient' parameter in service-life prediction model of this type.

However, it is now realised that chloride transport is a complex subject, and hence the transport of chloride should not be the only variable considered. The interaction of the chlorides with other ions and the medium itself are equally important. This is partciularly the case when cements containing supplementary cementitious materials are used as binders (Luping *et al.,* 2012).

2.7 Test methods to quantify ingress of Cl^- and CO_2 in uncracked concrete

The corrosion of steel in RC structures is a serious problem which directly affects their serviceability (Bazant, 1979). Therefore earlier detection of corrosion may be an essential element in the reasonable maintenance of important civil structures.

A multitude of tests have been developed and are used to test the resistance of concrete to chloride and carbon dioxide ingress. However, to date, the complexity of these test procedures has prevented the attainment of a general consensus on a single standard test method. A brief overview of various local (South African) and international test methods that are available and used to determine Cl and CO_2 ingress is presented in the following sections.

2.7.1 International test methods for CO_2 ingress

A number of gas-permeability test procedures have been developed to date. These tests can be categorised as laboratory-based, site-based, or both. One parameter that varies between the test methods for gas-permeation is the type of gas substance that is passed through the concrete specimen. Oxygen is generally used as the preferred permeating gas as carbon dioxide results in an alteration of the concrete pore structure (Alexander *et al.*, 2008).

Several methods are available to measure the permeability of the 'covercrete' to gases, there has been a clear evolution of gas-permeability tests (Nolan *et al.,* 1995). A brief discription of the Torrent air permeability test, Hong-Parrot method, Autoclam air permeability test and accelerated carbonation tests will follow to give an idea of some of the test methods that are available.

- ***Torrent air permeability test***

The Torrent method is a non-destructive double chamber test method for measuring the air-permeability coefficient of concrete. The test method is primarily designed for on-site use, however it may also be used on laboratory specimens provided that specimens meet the size and preparation requirements (Torrent, 1992). Figure 2.8 illustrates the Torrent test set-up.

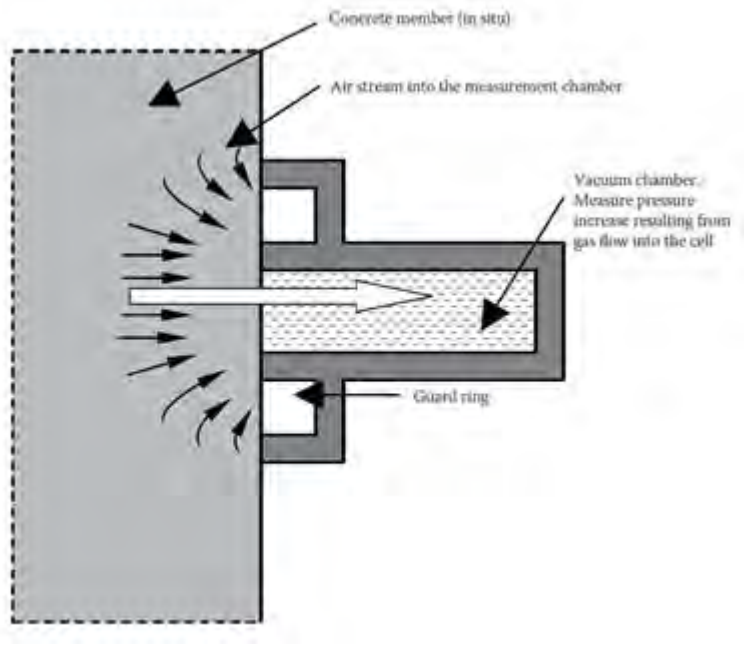

Figure 2.8 Schematic of pressure application on concrete member using the Torrent Method set-up (Beushausen & Alexander, 2008)

The apparatus is placed on to the concrete and a negative pressure is created in both cells, thus attaching the apparatus to the concrete. After applying the vacuum in both chambers, the inner chamber's valve is closed. The pressure regulator maintains an equal pressure in the inner and outer chambers, a process which forces the uni-directional air-flow into the concrete member. The pressure will start to rise in the inner chamber, and the rate of pressure increase is related to the permeability of the concrete. The instrument provides a visual display of the coefficient of air-permeability at the end of each test.

- ***Hong-Parrot method***

The Hong-parrot is an intrusive in-situ test method which requires a 35 mm deep, 20 mm diameter blind hole to be drilled into the concrete (Parrott *et al.,* 1991). A steel plug with an expanding silicone rubber is inserted into the hole and allows space for small air-filled cavity. A sealing sleeve that has a gas inlet as well as a pressure transducer is attached. The cavity is pressurized and the pressure decay through the surrounding concrete is measured by the pressure transducer (Hong *et al.,* 1989).

An initial pressure of between 1 and 3 Bars is developed inside the cavity. The time taken for the pressure to decay as well as the radius affected by the test is converted into an apparent permeability. The surrounding concrete is brushed with a soap solution to measure the influence radius of the air-flow. The radius is then detected by the presence of air bubbles on the concrete surface. It normally produces fine bubbles within the 35 mm radius around the cavity, if the concrete is cracked or poorly compacted large bubbles can be seen as the sir flows across the surrounding concrete (Torrent *et al.,* 2007). The Hong-Parrot test set-up is shown in Figure 2.9.

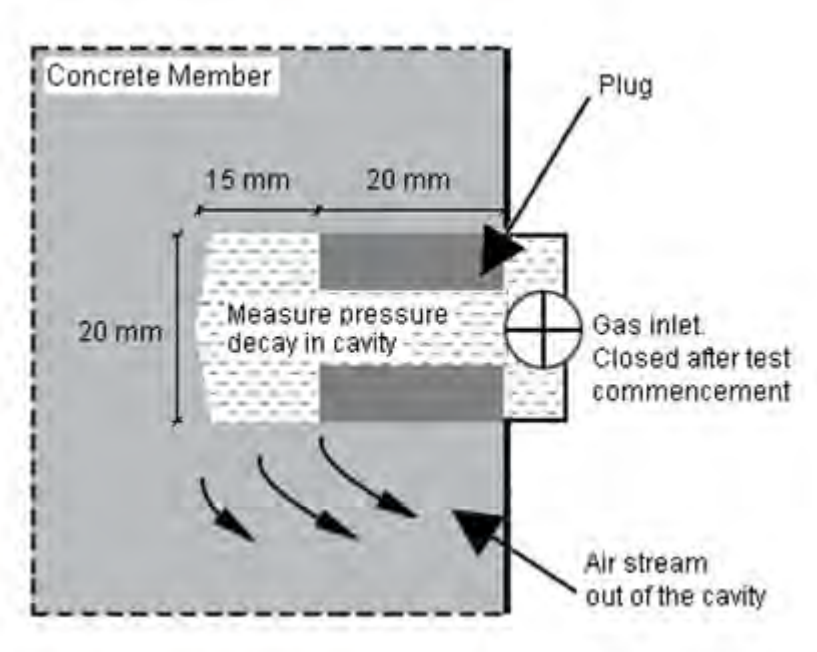

Figure 2.9 Schematic of Hong-Parrot test set-up

- ***Autoclam air permeability test***

The Autoclam air permeability test is a non-destructive that measures the air and water permeability of concrete. The base ring of the permeameter is mounted to the concrete surface, thus isolating the test area. The decay of an initial pressure of slightly above 0.5 Bars is measured over a 15 minutes period. The air permeability index is calculated as the absolute value of the slope of the linear regression curve between the 5^{th} and 15^{th} minute of the test duration (Torrent *et al.,* 2007). Figure 2.10 illustrates the test set-up for the Autoclam air-permeability test.

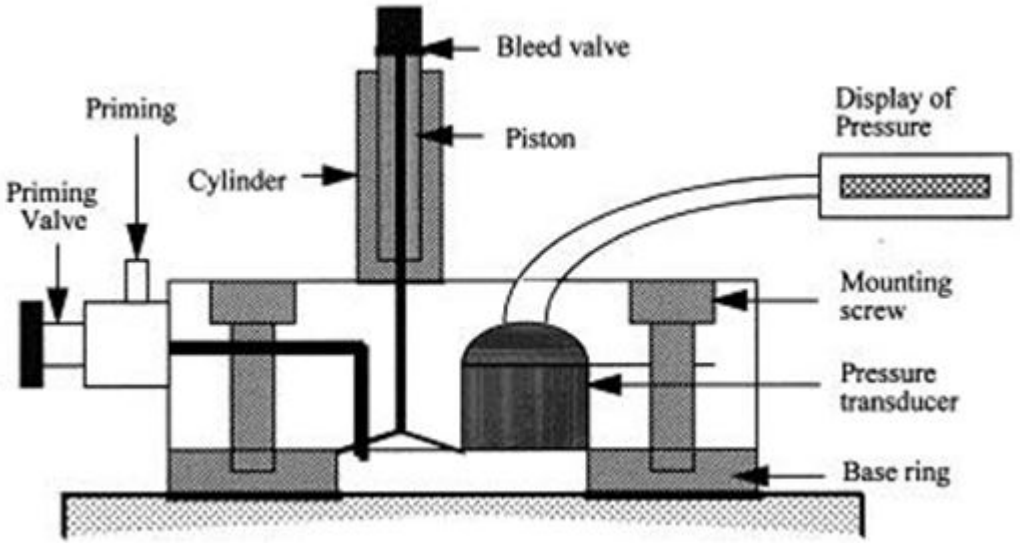

Figure 2.10 Schematic of Autoclam test set-up

- ***Accelerated carbonation test***

This test directly assesses a concretes resistance to the ingress of carbon dioxide, to measure the rate of carbonation that takes place within the concrete. Accelerated carbonation tests are carried out according to fib bulletin 34: Model Code for Service Life Design (100 years). Concrete specimens are placed in chamber with a controlled temperature and relative humidity. The chamber exposes the concrete to an accelerated carbon dioxide concentration over a chosen period of time. Papadakis ***et al.,*** (1989) proposed the following relationship exists between accelerated carbonation conditions and the natural carbonation environment:

$$\frac{X_{accelerated}}{X_{natural}} = \sqrt{\frac{[CO_2]_{accelerated}}{[CO_2]_{natural}}} \qquad \textbf{Equation 2.17}$$

The amount of carbonatable material and diffusion coefficient will be constant for both natural and accelerated conditions given the same RH, temperature and concrete, and can thus be equated. If the carbon dioxide concentration is kept below 3%, the above equation is applicable as proposed by Castellote ***et al.,*** (2009).

2.7.2 International test methods for Cl^- ingress

In the case of chloride ingress, diffusion is generally a slow process and conventional test methods are time consuming, and often take months to years to obtain test reasonable results (Feldman, et al., 1999). Accelerated test methods accelerate the process of chloride transport by means of an external electrical field, a concentration chloride solution or an elevated temperature (Pfeifer ***et al.,*** 1994). The tests methods are briefly discussed below.

2.7.3 Immersion tests

The Nordtest method (1995) requires specimen surfaces to be sealed, except one surface to prevent multi-directional penetration. After being pre-saturated, the specimens are immersed in a solution containing 165 g of NaCl per litre for at least 35 days. This test method is based on natural diffusion under a very high chloride concentration. After certain periods of

immersion, the chloride contents at discrete points are determined as a function of depth, this produces a typical chloride profile.

The non-steady state apparent diffusion coefficient is then obtained by curving-fitting the chloride profile to one of the solutions of Fick's second law. Crank's error function solution (also referred to as Gauss error function) can be stated as:

$$C_{x,t} = C_s\left[1 - erf\left(\frac{x}{2\sqrt{D_a t}}\right)\right] \quad \textbf{Equation 2.18}$$

where: $C_{x,t}$= Chloride concentration at depth x at a given time t

C_s= Surface chloride concentration (g/m^3)

D_a= Apparent chloride diffusion coefficient

t = Time of exposure

erf= Error function

Under the assumption that there is no chloride binding, Equation 2.18 can be used to determine the diffusion coefficient by curve-fitting the chloride profile to the equation.

$$C_{x,t} = C_{s-}(C_s - C_{ti}) \cdot \mathbf{erf}\left(\frac{x}{2\sqrt{D_a \cdot t}}\right) \quad \textbf{Equation 2.19}$$

where: C_t = Initial content of total chloride by weight of material

C_{ti} = Initial content of chloride

C_s = Content of total chloride at the surface of the concrete

Values of the diffusion coefficient can vary from 10^{-13} to 10^{-11} m^2/s depending on the binder type and water/binder ratio utilised. The diffusion coefficient that is obtained based on the concrete properties is utilised as the main parameter to describe the rate of chloride penetration. The chloride profile can, to a limited extent, be extrapolated to longer time periods with the use of Equation 2.19 and the surface content value. This test is laborious and can take relatively long (at least 35 days) to perform.

2.7.3.1 Rapid chloride permeability test (RCPT))

This test method was developed by Whiting, (1981), and has been modified and adopted by various organisations which include AASHTO T277 and ASTM C1202. These test methods specify the rating of chloride permeability of concrete based on the charge passed through the specimen during six hours of testing period (Feldman *et al.*, 1994).

The test consists of placing a 50 mm diameter specimen between two cells with an electrode in each cell. A potential of 60 V is the applied across the specimen, with the chloride cell containing the chloride ions. The electrical current is monitored during the first six hours of

the test. The test result is then expressed as the Coulomb value which is determined from the current data using the following equation:

$$Q = 900\ (I_0 + 2I_{30} + 2I_{60} + \ldots + 2I_t) \qquad \textbf{Equation 2.20}$$

where: Q = Charge passed (coulombs)

I_0 = current directly after the current was applied (ampere)

I_t = current at t time after voltage is applied (ampere)

The qualitative chloride ion penetrability can be estimated using the criteria listed in Table 2:4. A charge value of less than 700 to 1000 coulombs is typically specified, which is characterized as very low chloride permeability based on the rating in Table 2.4

Table 2.2 Chloride ion penetrability based on the charge passed (C1202, 2010)

Charge passed (Coulomb)	Chloride ion penetrability
>4000	High
2000-4000	Moderate
1000-2000	Low
100-1000	Very low
<100	Negligible

The RCPT charge passed has been found to be a good indicator of the chloride resistance of concrete (Khatri *et al.,* 1997; Sherman *et al.,* 1996). The test gives an indication of the conductivity of the pore solution, which is influenced by the concentration of the ions in the pore solution, and the concentration of these ions can vary between binder types (Page *et al.,* 1983). The test accounts for the total current (Whiting, 1981) which does not specifically correspond to the chloride flux. The test is relatively fast and simple to carry out.

2.7.3.2 Steady-state migration test

The first standard procedure that was developed for the steady-state migration test is the Nordic Test method NT BUILD 355, (1997). In this test method, the chloride flux is determined by measuring the change in conductivity in the downstream solution. A 12 V external potential is imposed across a concrete specimen of 100 mm diameter and 20 mm thickness. The test surface is exposed to NaCl solution (upstream cell) and the opposite surface to demineralised water (downstream cell). The conductivity in the downstream solution is measured at time intervals, and converted to a chloride concentration, until a constant increase in conductivity is reached. The test can take from a few days up to 2 weeks depending on the quality of the concrete. The steady state migration coefficient is calculated from the slope of the constant portion of the concentration-time curve (the constant flux) (Luping *et al*., 2012).

2.7.3.3 Non-steady state migration test

In this test method, the specimen of 100 mm diameter by 50 mm is placed in a rubber sleeve as seen in Figure 2.11. This forms a cell containing the electrolyte (3.0 M NaOH) and the anode (stainless steel plate).

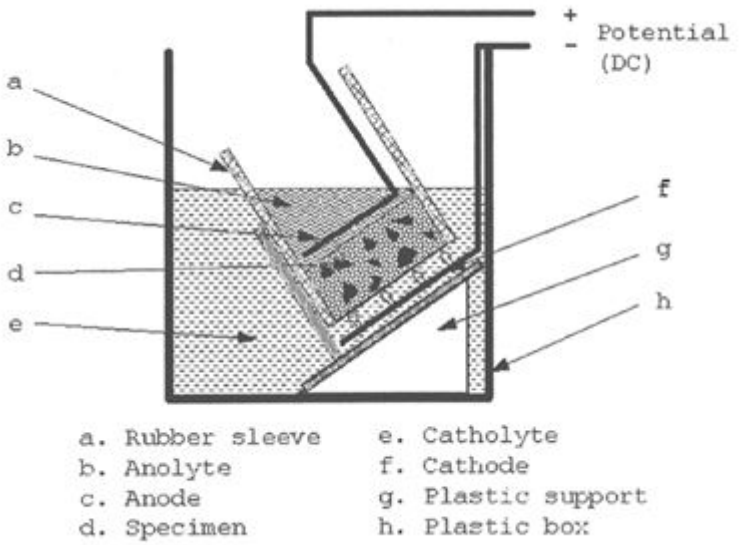

Figure 2.11 Schematic of the experimental arrangement for RCM tests (Luping *et al.*, 2012)

The rubber sleeve containing the specimen is placed above the cathode (stainless steel plate) in a migration box containing chloride solution (10%NaCl in saturated limewater). The specimen is titled to ensure that the gas bubbles at the cathode can escape easily. An external potential of 10-60 V depending on the quality of the concrete is applied across the specimen normally for a 24 hour duration. After the test, the specimen is split into two, and a 0.1N silver nitrate solution is sprayed onto the newly exposed surface. The average penetration depth is then determined, from measurements taken at five different locations using a colorimetric technique (Castellote *et al.,* 1970). The chloride migration coefficient (D_{nssm}) is calculated from the measured penetration depth (x_d), using the following equation:

$$\boldsymbol{D_{nssm} = \frac{RTL}{zFL} \cdot \frac{x_d - \alpha\sqrt{x_d}}{t}} \qquad \textbf{Equation 2.21}$$

where α can be taken as a laboratory constant,

$$\boldsymbol{\alpha = 2\sqrt{\frac{RTL}{zFU}} \cdot \; erf^{-1}\left(1 - \frac{2C_d}{C_o}\right)} \qquad \textbf{Equation 2.22}$$

where: R = Gas constant 8.314 J/(mol K)

T = Absolute temperature (K)

L = Thickness of specimen (m)

z = ion valence

F =Faraday constant 96500 J/(V mol)

U = Electrical potential difference

C_d = Concentration of free chloride at which the colour change when using the colorimetric method to measure the chloride penetration depth ($kg_{cl}/m^3_{solution}$)

C_o = Concentration of free chloride in a bulk solution or an upstream diffusion cell ($kg_{cl}/m^3_{solution}$)

2.7.3.4 Resistivity test

The resistivity test has been used as a measure of the transport property of concrete, since it is known that resistivity is inversely proportional to the conductivity (Andrade ***et al.,*** 1993; Polder, 1997; Gulikers, 2005).

The test has the advantage that it is easy and quick to conduct, and can be performed on specimens of any dimensions. The specimen is saturated with distilled water, artificial pore solution, or very concentrated NaCl solution. Figure 2.12 shows a four-point resistivity meter. As seen on the schematic, the equipment uses four equally spaced probes. A 25 V is applied through the concrete specimen between the outer pair of probes. The equipment measures the current flowing between the outer probes and the potential difference between the inner probes, obtaining the ratio of voltage to current.

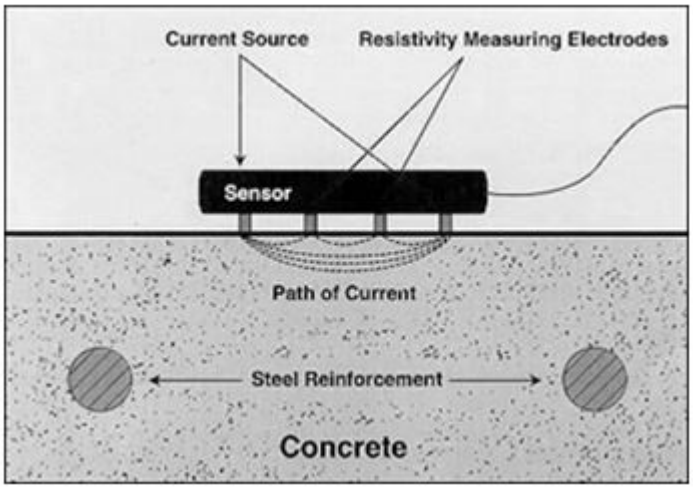

Figure 2.12 Schematic of Resistivity equipment test set-up (Broomfield, 2007)

The resistivity of the concrete is then calculated by using following equation:

$$\rho = \frac{A}{L} \cdot \frac{U_{s+sp} - U_{sp}}{I} \qquad \textbf{Equation 2.23}$$

where: ρ = Resistivity of concrete (ohm)

A = Cross-sectional area of specimen (m^2)

L = Thickness of specimen (m)

A = Applied current (amperes)

U_{s+sp}, U_{sp} = Potential between two probes measured with and without the specimen respectively

The conductivity (i.e. inverse of resistivity) of concrete is dependent on both the water content and the porosity of the concrete is saturated and on the type of ions in and the ionic concentration of the pore solution. The diffusion coefficient can be calculated using Nernst-equation:

$$\boldsymbol{D_{eff} = \frac{RT}{z_i F^2} \cdot t_i \sigma = \frac{RT}{z_i F^2} \cdot \frac{t_i}{\rho}} \qquad \textbf{Equation 2.24}$$

where: σ = Conductivity of the concrete

t_i = Transference number of the i^{th} ion

2.8 South African Durability Index (DI) Tests

The South African Durability Index (DI) approach was developed as a method to measure the durability of the cover layer in terms of quantifiable engineering parameters. The tests are applicable to both in-situ and laboratory-made concrete. The DI approach consists of three tests to be conducted out to characterise the durability of the cover concrete (Alexander ***et al.*** 2008):

1. Oxygen permeability index (OPI) test,
2. Water sorptivity index (WSI) test and
3. Chloride conductivity index (CCI) test.

Each test is designed to measure a specific transport-related property of fluids or ions through the concrete cover layer, typically covering the main mechanisms related to deterioration (Ballim ***et al.,*** 2009). The approach has diverse range of applications: it can be used for material characterisation, for drafting durability specifications on a performance basis, as a means of site quality control, and as a basis for long-term service life predictions (Beushausen ***et al.,*** 2008).

The testing equipment and procedures are well documented in literature, hence a brief outline of the principles of the three Durability Index Tests is provided below.

2.8.1 Oxygen Permeability Index (OPI) test

The basis of the OPI test is to measure the pressure decay passing through a concrete disc 30 ± 2 mm thick and 68 ± 2 mm in diameter, placed in falling head permeameter (Mackechnie ***et al.,*** 2001a). The cell is pressurised to 100 ± 5 kPa before being isolated, after which the pressure decay is monitored over a period of six hours. The Darcy's coefficient of permeability (k) can then be calculated using Equation 2.25:

$$k = \frac{\omega V g d}{R A \theta t} \ln \frac{P_o}{P}$$ **Equation 2.25**

where k = Coefficient of permeability (m/s)

ω = Molecular mass of permeating gas (kg/mol)

V = Volume of pressure cylinder (m^3)

g = Acceleration due to gravity (m/s^2)

d = Specimen thickness (m)

R = Universal gas constant (Nm/Kmol)

A = Cross-sectional area of specimen (m^2)

θ = Absolute temperature (K)

t = Time (s)

Po, P = Pressure at start of test and at time t, respectively

The oxygen permeability index is then calculated and defined as:

$$Oxygen\ Permeability\ Index = -\log(k)$$ **Equation 2.26**

The results give an indication of the gas permeation properties of concrete. The OPI values for concrete typically range from 8 to 11, the higher the index the less permeable (higher quality) the concrete (Ballim *et al.,* 2009). The test provides an assessment of the macro- and microstructure of the concrete and is particularly sensitive to volume and quantity of large pores and voids in the concrete. The state of compaction, presence of bleed voids and channels, and the interconnectivity of the pore structure can also be analysed (Mackechnie *et al.,* 2001a).

2.8.2 Water Sorptivity Test

The water sorptivity test measures the potential of uni-directional absorption of water into one face of a pre-conditioned concrete disc 30 ± 2 mm thick and a diameter of 68 ± 2 mm, by means of capillary suction (Ballim *et al.,* 2009). The concrete discs are sealed in order to ensure that water is only be absorbed from the bottom, when placed in a shallow layer of water. Sorptivity (S) is determined from the plot of mass of water absorbed against the square root of the predetermined time intervals using the Equation 2.270:

$$S = \frac{\Delta M_t}{t^{\frac{1}{2}}} \frac{d}{M_{sat} - M_0}$$ **Equation 2.27**

where ΔM_t = Change of mass with respect to dry mass (g)

M_{sat} & M_0 = Dry and saturated mass of concrete respectively (g)

t = Period of absorption (hr)

d =Thickness of specimen (mm)

The lower the water sorptivity index value, the better is potential durability of the concrete. Typical sorptivity value range from 5 mm/√h for a well-cured Grade 30-50 concrete to 20 mm√h for a poorly cured Grade 20 concrete (Ballim *et al.,* 2009). The test is an assessment of the microstructural porosity of the near surface concrete and distinguishes from bulk absorption effects. It is consequently sensitive to curing and early age dying effects on concrete hence it is used for checking construction quality.

2.8.3 Chloride Conductivity Index (CCI) Test

In this test the CCI measures the conductive ionic flux through a concrete disc, 30 ± 2 mm thick and a diameter of 68 ± 2 mm, under a potential difference. The specimens are pre-conditioned a 5 M NaCl solution before testing. A potential difference of 10 V is applied across the ends of the specimen that are placed in a two-cell conduction rig. The conductivity is determined using the equation below:

$$\sigma = \frac{I \cdot t}{V \cdot A} \qquad \textbf{Equation 2.28}$$

where σ = Chloride conductivity (mS/cm)

I = Measured current (mA)

V = Voltage (V)

t = Specimen thickness (cm)

A = Cross-sectional area (cm^2)

The test is a rapid assessment of the resistance of concrete to ingress of chlorides. Lower conductivity values indicate concrete that exhibits higher resistance to chloride ingress. The test is sensitive to binder types with blended binders such as fly ash illustrating higher resistance to chloride ingress (Ballim *et al.,* 2009).

2.9 Using the Durability indices to make service life predictions of RC structures

Two correlations have been established using early-aged results of the OPI and CCI tests and durability performance results. Theses correlations are based on empirical relationships that exist and serve as the basis from which the service life prediction was developed (Mackechnie *et al.,* 2002). Since the durability tests are based on transport mechanisms associated with deterioration, the indices obtained can be used for durability predictions. Authorities such as South African National Road Agency Limited (SANRAL) make use of the indices for the assessment of existing structures as well as recently built ones.

2.9.1 Using the OPI for carbonation-based service life prediction

A good correlation has been found between the OPI value at 28 days and carbonation depths after exposure. Figure 2.13 shows the correlation for concrete that has been exposed for four years.

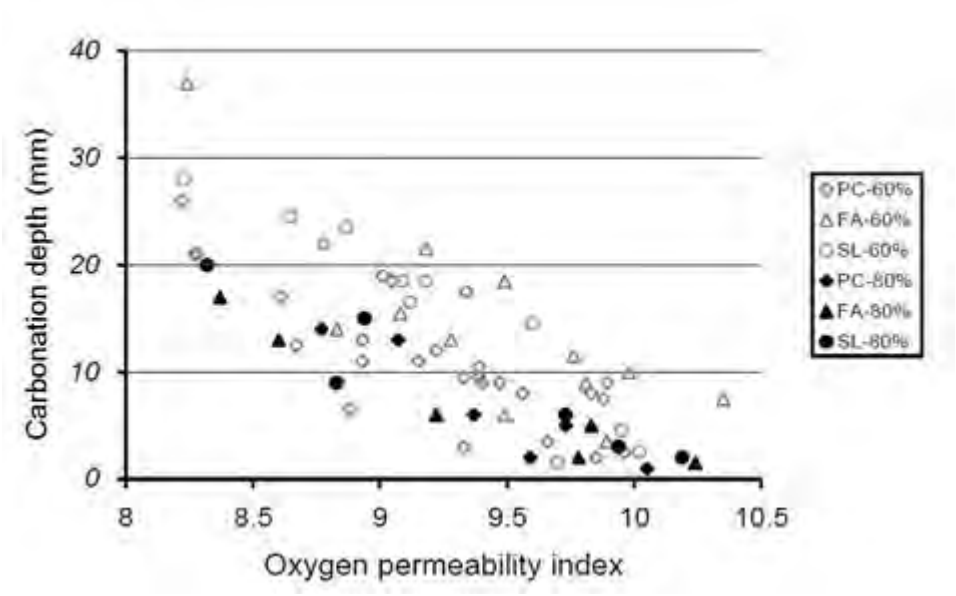

Figure 2.13 Determining the carbonation depth using OPI (Mackechnie *et al.*, 2002)

Using the established correlation, an empirical prediction model for carbonation was therefore formulated using the oxygen permeability test. Using this method a 50 year carbonation depth can be predicted for different exposure environments. The service life prediction model based on the OPI value uses this correlation to predict the carbonation depth. The model accounts for the environmental exposure and the binder type used. Figure 2.14 shows a typical interface of the carbonation prediction model based on the OPI value, binder type and exposure environment.

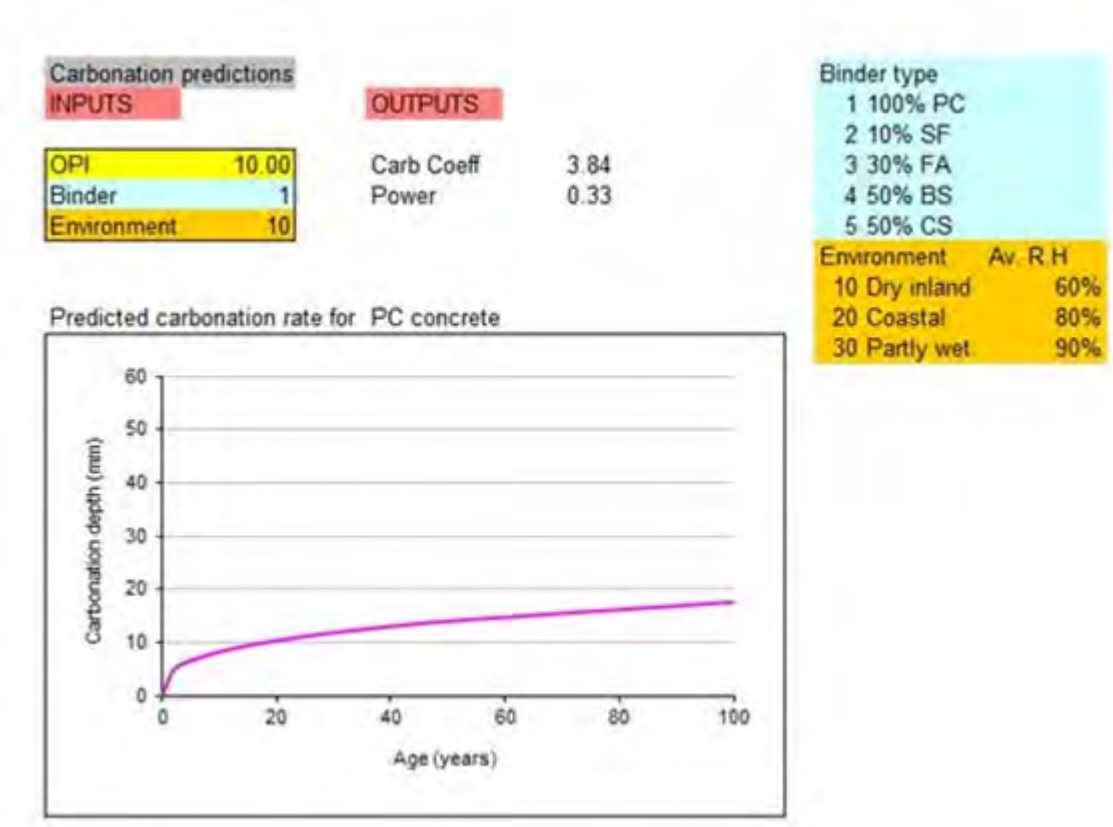

Figure 2.14 Typical plot of the carbonation prediction mode based on the OPI value, binder type and exposure environment

2.9.2 Using the CCI for chloride-induced service life predictions

Mackechnie *et al.,* (2001) established that the CCI (from the chloride conductivity test) can be utilized to predict the chloride ingress into structures by correlating it to the diffusion coefficient. The correlation was established by relating the apparent diffusion coefficient at 2-years (D_a) to the 28-day chloride conductivity value. The conductivity (σ)of saturated materials is linearly related to steady state diffusivity, while apparent diffusivity is a function of steady state diffusivity and the chloride binding capacity (Streicher, 1997).

Figure 2.15 illustrates how the CCI is utilized along with the binder type and exposure environment to determine the corresponding diffusion coefficient.

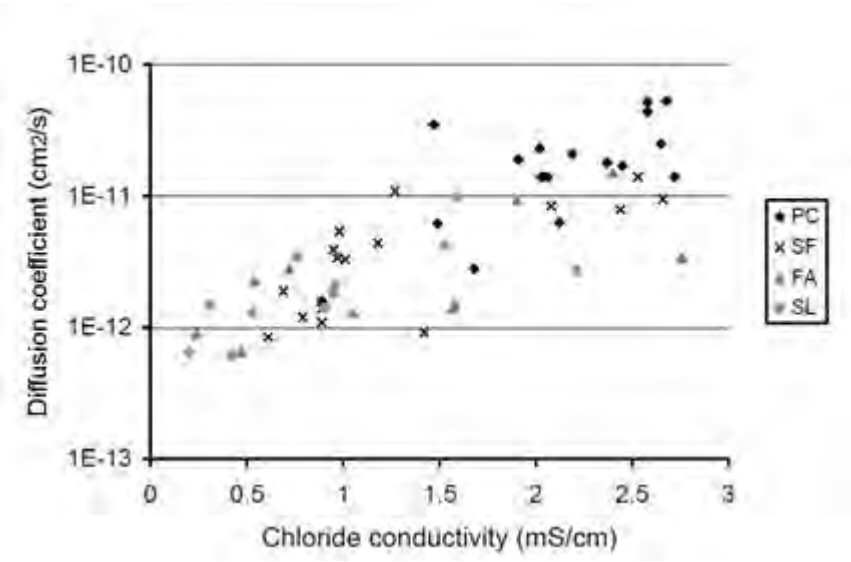

Figure 2.15 Typical plot showing correlation between CCI and diffusion coefficient (Mackechnie J., 2001)

The service life prediction model uses the established CCI correlation to predict the chloride ingress for a given concrete. The model also takes into account the environmental exposure, the binder type and the age of concrete at testing. Figure 2.165 shows the interface of the DI prediction model used to predict diffusion coefficient based on a given CCI value.

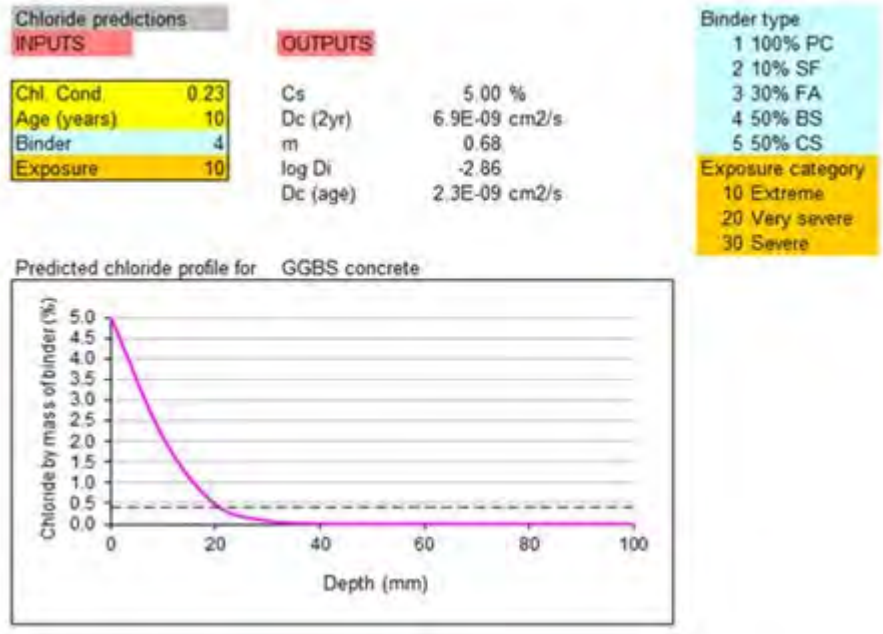

Figure 2.16 Typical plot of the chloride ingress prediction mode based on the CCI value, binder type and exposure environment

2.10 Limitations of Durability Index (DI) Testing Approach

The three DI tests are carried out on specimens that are 30 ± 2 mm think and have a diameter of 68 ± 2 mm. Due to the manner in which the test methods and apparatus were developed; consideration has to be taken to ensure that the concrete specimen is not extracted from a region that contains cracks. Caution has to be exercised further during the coring and cutting of the specimen to prevent additional damage to the specimen.

The concern with this procedure is that it only encourages the selection of sound concrete for testing. Even if the structure shows signs of cracking on the surface, this area of concrete cannot be selected for testing.

The implications of such a procedure are illustrated here using the OPI test. When sound concrete specimens are tested, a high OPI value is obtained. This indicates a high degree of impermeability of the concrete. However when a cracked concrete specimen are tested, a low OPI value is obtained. This indicates a high of permeability relative to the sound concrete specimen. The test as mentioned earlier is sensitive to large pores and voids. The presence of cracks creates a passage for the gas to permeate through the concrete pore structure of the specimen, indicating that the concrete has a high permeability.

When the two OPI values are used for service life predictions, they represent two extreme scenarios. In the case of the sound concrete, the high OPI value will imply that hardly any carbonation will take place. In contrast to the cracked concrete, the low OPI value will indicate that severe carbonation will take place in the cracked regions. One scenario depicts an ideal case with regards to service life prediction while the other depicts a real case situation.

Due to the disparity in the results when uncracked specimens and cracked specimens are tested, this research aims to try and bridge this gap by incorporating the influence of cracks in the Durability Index test method. If this approach proves to be unsuccessful, modifying the DI results in service life predictions could be considered as an alternative to account for the presence of cracks in RC structures.

2.11 Example of use of the DI tests in South Africa - South African National Road Agency Limited (SANRAL)

SANRAL has adopted durability limits which are based on the South African Durability Index approach. These limits are prescribed in order to ensure the service life of the structure is achieved. Values are based on research performed by the Universities of Cape Town and the Witwatersrand that have been published in various monographs, giving required DI values for a 100 year service life based on service life models.

Two sets of limits have been prescribed based on environments where carbonation or chloride induced corrosion may occur on structural concrete. Table 2.5 & 2.6 illustrate a condensed version of the prescribed limits.

Table 2.3 Concrete Durability Specification Targets - Carbonation Induced Corrosion

In-situ DI Value for various Cover Depths - 100 Year Life

Designation	Cover Depth (mm)	OPI (log scale)	Sorptivity (mm/h)
		Recommended value	Recommended value
XC1a	40	n/a	10.0
XC1b	40	9.20	10.0
	50	9.00	10.0
	60	n/a	n/a
XC2	40	9.40	10.0
	50	9.10	10.0
	60*	9.00	10.0
	70*	n/a	n/a
XC3	40	9.40	10.0
	50	9.10	10.0
	60*	9.00	10.0
	70*	n/a	n/a
XC4	40	9.60	10.0
	50	9.30	10.0
	60*	9.10	10.0
	70*	9.00	10.0

Table 2.4 Concrete Durability Specification Targets - Chloride Induced Corrosion

Designation	Cover Depth (mm)	In-situ Durability Index for various Cover Depths - 100 Year Life				
		Recommended CCI (mS/cm)				Sorptivity
		Typical Binder Blends				(mm/h)
		70:30	50:50	50:50	90:10	Recommended
XS1	40	1.50	1.60	2.10	0.40	10.0
	50	2.10	2.20	2.80	0.50	10.0
	60	2.60	2.70	3.40	0.65	10.0
XS2a	40	1.00	1.10	1.40	0.30	10.0
	50	1.40	1.60	2.00	0.40	10.0
	60	1.80	2.10	2.50	0.50	10.0
XS2b	60	1.45	1.70	2.00	0.40	10.0
XS2b	40	0.65	0.85	1.00	0.25	10.0
	50	1.10	1.35	1.45	0.35	10.0
	60	1.10	1.30	1.55	0.30	10.0

In the case of existing RC structures, these adopted limits are used as criteria when assessing concrete structures in carbonation or chloride induced environments. However, it can be seen that the limits make no consideration for the presence of cracks on RC structures. This can result in a misleading assessment and service life prediction of the RC structure in question. Consequently, these decisions can have a significant impact on the infrastructure in South Africa that are assessed and maintained using this adopted approach.

Section B: Influence of crack width on transport properties of concrete

2.12 Origin and presence of cracks in concrete on a microscopic level

A crack may be defined according to ACI 201-2R (2001) as a complete or incomplete separation of concrete or masonry, into two or more parts, produced by breaking or fracturing. According to Metha (2006) it is important to understand, the origin and growth of cracks in concrete as they play a key factor in determining the permeability and durability of in-service RC.

Concrete is a heterogeneous, multiphase material. It is usually considered as a three phase material consisting of hardened cement paste (HCP), aggregate and an interfacial transition zone (ITZ) between the HCP and aggregate (Richardson, 2002). The ITZ is typically 10 to 50 μm thick and forms a thin shell around the large aggregate and is generally (in normal concrete) the weakest of the three components. However the ITZ has a significant influence on the mechanical behaviour of concrete, with regards to the development of cracks (Alexander, 1993).

In the freshly mixed and compacted concrete, water film is absorbed around the aggregate particles. The presence of a water film increases the water-to-cement ratio of the paste close to the aggregate surface compared with the bulk paste. In the ITZ between a course aggregate particle and cement mortar, the spaces with the high water-to-cement ratio become filled with a porous framework of large, plate-like, oriented, and non-adhesive crystal of calcium hydroxide. This in turns causes the interface zone in the hardened state to be characterised by high capillary porosity, relatively large calcium hydroxide crystals, ettringite crystals and very little calcium silicate hydrate (CSH). This consequently leads to the paste-aggregate interface being the weakest link in conventional concrete mixes (Roy & Idorn, 1993). The interface strength is influenced by a number of factors such as: the water-to-cement ratio of the paste, age of concrete, amount of bleed of the fresh concrete, type of cementitious material, amount of ultrafines in aggregate, surface texture of aggregate and presence of absorbent aggregates (Richardson, 2002).

Metha (2006) stated that tensile stresses that are generated by differential movements between the HCP and the aggregate are relieved by the formation of microcracks in the ITZ. This implies that ordinary concrete will contain microcracks in the ITZ even before the structure is loaded. The amount of microcracks present depends on numerous parameters including the size, and grading of aggregate, cement content, water content, degree of consolidation, curing conditions, humidity and temperature gradients to which fresh concrete had been exposed.

There are two general terms that are utilised to characteristic cracks that develop in concrete from a size perspective; micro- and macro-cracks. Fine cracks, known as microcracks develop on the concrete surface are too small to be visible and quantified by the naked eye, and therefore are ignored in the structural design and construction practice. A microcrack is defined as a crack with a width of ≤ 10 μm (Reinhardt, 2007). Microcracks that are caused by settlement, shrinkage, and accidental overloads do not have any adverse effect on the static

behaviour of concrete structures. It is important to note that even though microcracks may not be visible to the naked eye, they can nevertheless influence transport properties of concrete such as permeability (Samacha & Hover, 1992).

Microcracks are further divided into bond cracks and mortar cracks. Bond cracks exist at the interface between course aggregates and mortar while mortar cracks exist within the mortar. Bond cracks predominate over mortar cracks for most loading ranges (concrete subjected to compressive forces). Mortar cracks almost always bridge between nearby bond cracks, and usually where the distance between particles of course aggregate are relatively small. Furthermore mortar cracks tend to bridge between bond cracks of large particles of aggregate in preference to those on small particles (Bisschop & Van Mier, 1999).

The details mentioned above provide an overview on the origin of microcracks in concrete. The focus however, of this study is on the impact of macrocracks on transport properties in concrete, and not microcracks. It is however still crucial to understand the development of microcracks in concrete as macrocracks are inherently microcracks that have propagated to a greater extent.

2.13 Different crack types in concrete

There are several influences which can lead to the development of cracks on RC structures. It is necessary to be able to distinguish between the different crack types that occur on a structure in order to assess the severity of damage and choose the appropriate repair option (if necessary).The range of cracks that occur in concrete can be subsequently be characterized into two different categories as shown in Figure 2.17, cracks that form before the hardening of concrete, in its fresh state, and the cracks that form after the concrete has hardened. Commonly observed crack types will be discussed below to give the reader a general idea of the range (with respect to the cause) of cracks that develop on RC structures.

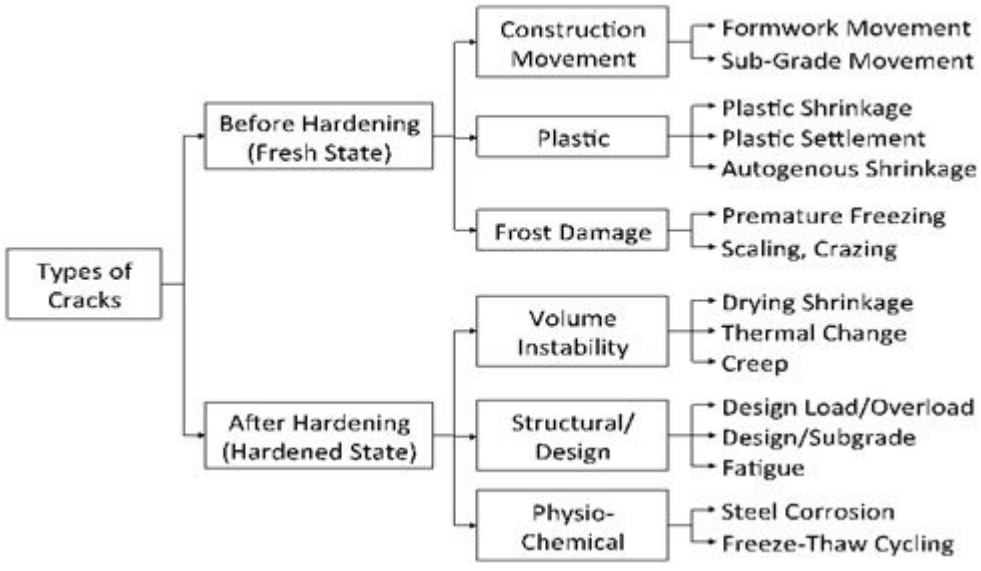

Figure 2.17 Types of cracks in concrete structures (Adapted from Transportion Research Board, 2006)

2.13.1 Different cracks formed prior to concrete hardening

Plastic cracks refer to cracks that occur before hardening, in the concrete fresh state. Their occurrence is predominantly a result of excessive evaporation of water, settlement and construction movements.

i. Plastic shrinkage cracks

Shrinkage is defined as the volumetric change of concrete due to a loss in moisture. Plastic shrinkage occurs typically within the first three hours of placing the concrete, in its fresh state. The rapid removal of the water from the surface of the concrete is a consequence of the rate of evaporation exceeding the rate of bleeding. This induces surface tension as the surface contracts but it is restrained by the underlying concrete. When the stresses exceed that of the tensile stress of the concrete, the cracks begin to develop (Day & Clarke, 2003).

ii. Plastic settlement cracks

Plastic settlement refers to concrete in its fresh state that is, after compaction has taken place. The solid particles have the tendency to settle, displacing the mixing water, which as a result rises to the surface. Cracking in this instance develops in the restrained sections of the concrete, typically by the top reinforcement bars in beams or slabs, stirrups and changes in the sections dimensions. (Woodson, 2009)

2.13.2 Cracks formed in the hardened concrete state

This refers to cracks that develop after the concrete has hardened. This typically occurs a day after the concrete was placed, vibrated and finished.

i. Drying shrinkage cracks

Depending on the relative humidity, ambient temperature, water/binder ratio and the surface area of the concrete that is exposed, moisture will be lost from the concrete surface to the atmosphere. Initially, this water is drawn from the large capillary pores. This does not cause a substantial volume change, however if evaporation continues to occur, moisture will be drawn from the smaller capillary pores and the gel pores. Tensile forces are thus created in the capillary water due to the reduction in vapour pressure in the capillary pores. These tensile forces are then balanced by compressive forces in the surrounding concrete, resulting in shrinkage in the concrete (Brooks, 2003).

ii. Thermal cracking

Thermally induced cracks develop predominately as a result of the non-uniform temperature gradient that is created in the hardening concrete. This is caused by the hydration reactions that occur during curing. Thermally induced stresses are directly affected by the degree of restraint due to thermal expansion or contraction. The concrete element can either be internally or externally restrained (Day & Clarke, 2003).

iii. Structural cracks

A majority of structural cracks can occur as a result of design deficiency, construction deficiency, settlement or heaving of soil or reinforcement corrosion. These cracks develop at the core or frame that form the structure. Structural cracks in residential foundations usually result from settlement or horizontal loading. Most (but not all) structural cracks resulting from applied loads are nearly horizontal (parallel to the floor) and occur 16" to 48" from the top of the wall. They are much more prevalent concrete block construction. They can be brought about by hydrostatic pressure or heavy equipment next to the foundation. Diagonal cracks that extend nearly the full height of the wall are often an indication of settlement (Grantham, 2003).

iv. Freeze & thaw cracks

The natural accumulation of water under pavements in the base and sub-base layers, may result in the aggregate eventually become saturated. Then with freezing and thawing cycles, cracking of the concrete starts in the saturated aggregate at the bottom of the slab and progresses upward until it reaches the wearing surface (Grantham, 2003). This type of cracking is referred to as D-cracking, it is defined by a characteristic crack pattern that appears at the wearing surface of the pavement as a series of closely spaced fine cracks adjacent and generally parallel to transverse and longitudinal joints and cracks and to the free edges of the pavement.

v. Corrosion cracks

Once corrosion of the reinforcing steel is initiated, the formation of corrosion products is expansive resulting in a build-up of tensile forces around the reinforcement. Splitting cracks start to develop along with a loss in bond strength between the steel and the concrete. The depth of the cracking is proportional to the cover depth of the concrete. These cracks commonly extend to the concrete surface, resulting in spalling (Grantham, 2003).

It must be noted that not all cracking causes concern. Cracks caused by freezing and thawing of saturated concrete, alkali- aggregate reactivity, sulphate attack, or corrosion of reinforcing steel may not appear on structures for years. Therefore, the cause of cracking should be carefully identified to determine which cracks are common and acceptable and which cracks require repair and/or further investigation (Transportation Research Board, October 2006).

2.14 Crack characteristics

Irrespective of the cause of the crack, quantitative investigation of cracks can provide substantial insight into the deterioration of in-service cracked concrete infrastructure. Cracks are not simple geometrically and range in size from several microns to several millimetres**.** There are several parameters that are used to quantify cracks in concrete some of the predominant characteristics are mentioned below. Some of the crack characteristics have

been mentioned with respect to corrosion (initiation or corrosion rate) which is has been used as a measure to highlight the significance of each characteristic in view of RC deterioration.

- *Crack width*

A threshold crack width value of 0.4 mm is generally proposed in structural design codes. Crack widths up to this value been stated to have a small influence on the corrosion rate of steel (ACI 224R-01). However work done by Otieno ***et al.,*** (2010) has shown that it is not possible to determine a universal crack width for corrosion initiation, since corrosion is dependent on numerous factors such as the concrete properties (w/b ratio and binder type) of each concrete composition. Work done by Schiessl & Raupach, (1997) has shown that wider crack widths results in earlier corrosion initiation but are also in agreement with Otieno's conclusion in that parameters such as binder type and water/binder ratio influence corrosion much more significantly when compared to crack width.

- *Crack frequency*

Work done by Arya & Ofori-Darko (1996), illustrated that the smaller the frequency of cracks (number of cracks per unit length) the lower the amount of corrosion. A higher crack frequency significantly increases the permeability of concrete resulting in increased penetration of aggressive species.

- *Crack orientation*

The orientation of cracks has a significant effect on corrosion. Longitudinal cracks that develop along the reinforcement allow a higher access of aggressive species to the surface of steel and therefore result in higher corrosion rates. In contrast, transverse cracks that expose a single or several parts of the steel surface and depassivation only occur at those points along the reinforcing steel hence result in lower corrosion rates (Wilkins & Lawrence, 1983).

- *Self-healing of cracks*

Cracks are capable of self-healing in certain circumstances; this process is termed ***autogenous or self-healing***. The process can be caused by the precipitation of calcium carbonate in the crack which can be attributed to the reaction between unhydrated cement and carbon dioxide dissolved in water. This can lead to clogging of the crack and preventing further ingress of harmful species (Victor & Yang, 2008). The flow of aggressive species can also be blocked by the water impurities or from concrete particles that have broken off from cracking.

- *Active/Dormant cracks*

Dormant cracks are characterised as having constant crack parameters (e.g. width) over time as compared to active cracks, which have varying parameters over time. Dormant cracks may be caused in cases where applied loads are constant over the time while active cracks would be expected in cases where the applied load is varying. Active cracks may also develop in the instance where there are fluctuating environment conditions such as thermal cycling. Dormant cracks are therefore more amenable to self healing than active cracks but may be reactivated (re-opened) by the application of load (Edvardsen, 1999).

It can be seen that based on the some of the crack characterises mentioned above, cracks can be fairly difficult to analyse and understand. As a result this complicates the modelling of cracks in concrete when having to account for the influence of these numerous parameters when trying to investigate cracked transport properties in concrete (particularly with respect to their effect on corrosion and service life predictions).

2.15 Quantification of crack characteristic in concrete

In order to investigate the influence of cracks, a basis of observing and measuring cracks need to be established. There are two aspects that need to be considered in order to characterise cracks: firstly observation and secondly a technique to quantify the analysis. Many different techniques have been specially developed for the analysis of cracking in concrete and other cement type materials. Radiography, impregnation, acoustic emission, ultra sound, laser holography and interferometry are some of the techniques that have revealed quantitative information about cracks in concrete. There are two widely used techniques used for 2D observation of cracks in concrete: scanning electron microscopy and optical microscopy (Litorowicz, 2006). Fluorescent microscopy and confocal laser microscopy are alternative techniques that have also been used. For 3D observation, the neutron radiography (Samaha & Hover, 1992) and computerised microtomography (Landis et al., 2007) have been used.

The techniques mentioned above require costly specialised equipment in order to characterise cracks. However practical, quick and relatively cheaper methods have been established to analysis cracks in concrete.

One method to detect cracks involves using strips of electro-conductive paint that are applied to the surface of RC structure. A crack is indicated by the interruption of the circuit owning to a temperature rise followed by burning of the paint. Crack as small as 0.1 μm can be detected using this technique. Another method involves the use of a crack gauge card. A transparent card containing lines of varies crack widths ranging from 1 mm to 10 mm, is printed along the card's edge in black ink. The card is placed over the crack and aligned with the black ink to determine the approximate crack width.

The type of method used determines the quality of information that can be obtained about the crack. This can, in some cases, limit the work that can be done following the characterisation. Once a suitable method for observing cracks has been established, the reader can then attempt to analysis the transport mechanisms in cracked concrete.

2.16 Techniques for inducing artificial cracks in concrete

In order to investigate the ingress of species into cracks in concrete, reliable methods for cracking specimens in the laboratory are needed. Different methods have been proposed in the literature such as sawing cracks (Marsavina *et al.*, 2009) or putting a plate as a mould of the crack into the cast concrete to create artificial cracks (Yoon *et al.,* 2007). However new techniques have been developed to produce more natural cracks, these methods include three-four point bending, Brazilian splitting, expansive cores, and wedge splitting. The advantage

of these techniques is that more natural cracks are achieved by loading the concrete. Below is a brief description of some of the commonly used techniques:

- ***Three/four-point bending***

Centrally notched beam specimens are subjected to loading using either a three or four point loading setup (Gowriplanan *et al.,* 2000; Win *et al.,* 2004). This technique involves placing the specimen on two parallel supporting pins (Figure 2.18) while the loading force is applied in the middle.

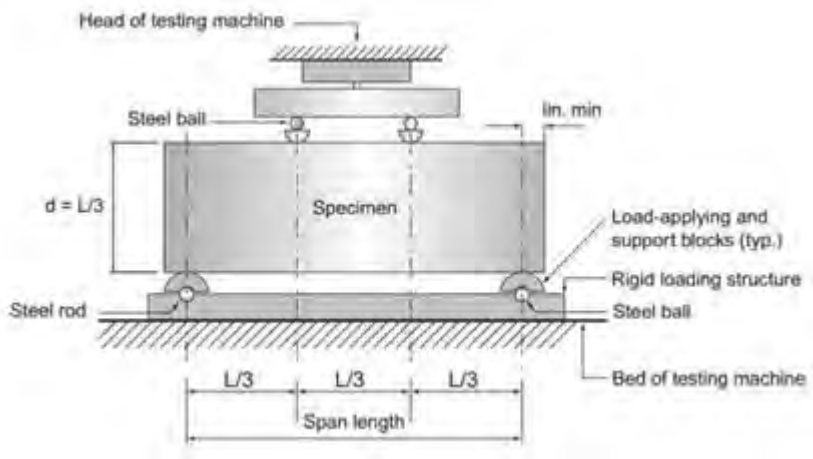

Figure 2.18 Schematic of a four-point bending set-up

The stresses that are generated in the specimens tend to exceed its tensile strength which as a result causes cracks to propagate in the specimen.

- ***Brazilian splitting***

The Brazilian or the indirect tension test is a popular method (ASTM C-496) of characterizing the tensile strength of concrete. The main advantage of this splitting tensile test is that only external compressive loads are required. In general, a cylinder or disc is subjected to compressive loading along two diametrically opposite generators so that a uniform tensile stress is induced in the loading plane as seen in Figure 2.19. Two steel strips are usually placed between the loading platens and the specimens to prevent failure in compression and distribute the load evenly.

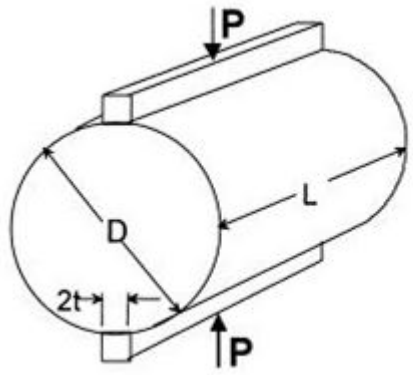

Figure 2.19 Schematic of Brazilian splitting

- ***Expansive cores***

The specimens are subjected to control tensile cracking using a mechanical expansive core and external steel confinement rings. The expansive core, which is inserted into the specimen hub, consists of a conical hardened-steel cylinder that slides within a set of six conical hardened-steel petals. A high-strength steel nut and bolt are used to force the conical cylinders against the petals. This process causes the PVC jacket to expand, which induces deformation in the internal diameter of the specimen. This technique was used by Ismail ***et al.***, (2004) to control the cracking of brick disc.

- ***Wedge splitting***

The wedge splitting approach was developed in an attempt to study the fracture mechanics of concrete. The specimen is prepared by casting or sawing a notch in the concrete. The procedure is illustrated in Figure 2.20.

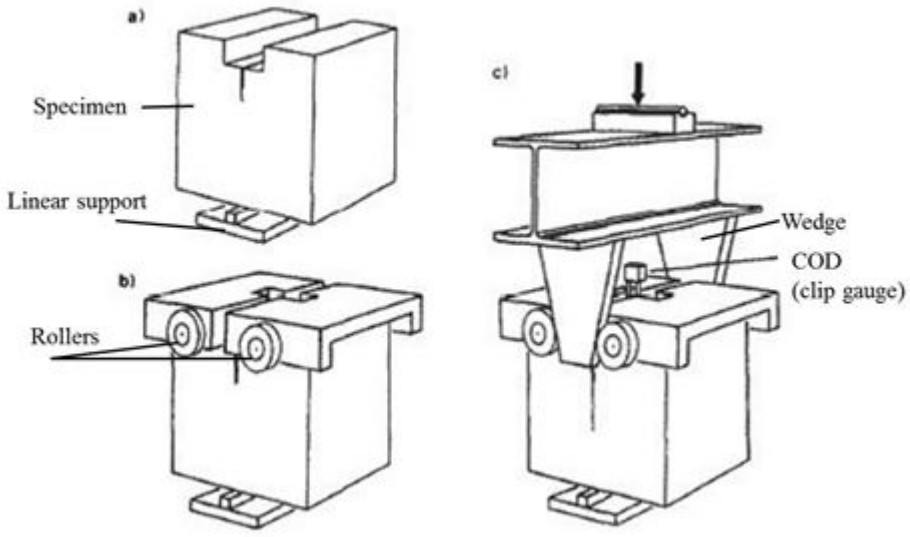

Figure 2.20 Set-up of Wedge splitting test (Bruwhiler & Whittmann, 1990)

Referring to Figure 2.20 the specimen is firstly placed on a linear support (a). Two rollers and a wedge are then used to transfer the vertical load into horizontal load (b). A crack opening displacement (COD) clip gauge is placed at the bottom of the notch, and the values obtained are used to feed back to the machine (c). In this manner that crack width is controlled (Bruwhiler & Whittmann, 1990 & Walter *et al.,* 2005)

Selecting the appropriate technique for generating cracks in concrete is based on first, the objectives which a researcher aims to achieve with regards to cracked concrete. Secondly, the availability of apparatus/equipment also needs to be taken into account.

2.17 Quantifying the ingress of ions and gases in cracked concrete

Due to the gap in knowledge regarding the influence of cracks on transport properties in concrete, various researchers have made attempts to understand and quantify the influence of cracks on diffusion and permeation properties, which will be illustrated below.

It must be noted that numerous investigations (Sugiyama *et al.*, 1996; Ammouche *et al.*, 2001; Choinska *et al.*, 2007; Hoseini *et al.*, 2009) have been carried out trying to relate the fracture mechanics of cracking concrete to the transport properties in concrete. However due to the different loading types such as tension, compression, flexure which can be applied to the concrete, different crack characteristics develop in the concrete. It is difficult to obtain a quantitative relationship between loading levels, tensile stress or tensile strain and the transport properties. Hence research has shifted to directly relate crack width to transport properties since this is one of the distinct features of cracked concrete. Attempts have been made to try correlating other crack characteristics such as crack frequency and cracking orientation with the transport mechanism in concrete (Mu *et al.,* 2013). However in this study, the focus is solely on the influence of crack width on transport mechanisms in cracked concrete.

The research studies listed below highlight various researchers' attempts to try quantify the influence of cracks (specifically using the crack width) on diffusion and permeation properties in cracked concrete.

2.17.1 Chloride ingress in cracked concrete

Pa Pa et al. (2004)

The penetration of chlorides into cracked concrete was investigated by Pa Pa *et al.,* (2004). Beam specimens were cracked to form single or multicrack as test parameters. Three water/binder ratios of 0.25, 0.45, and 0.65 were used. The specimens were left for three months prior to being exposed to two NaCl solutions of 3% and 8%. The electron probe microanalysis (EPMA) tests for Cl^- concentration as well as penetration depth were conducted after seven days and one month duration.

The EPMA test images below illustrate the concentration of chloride ions that are present in the concrete specimen, using a colour scale to indicate various concentrations of chlorides. Once the specimens were exposed to the chloride solution, it was noted that the bulk

movement of solution containing Cl^- ions occurred along the crack and reached the crack tip within a very short time. While the capillary suction flow of the bulk movement of the solution within the crack is taking place during exposure, a secondary movement of moisture containing Cl^- ions around the crack that is perpendicular to the crack direction also took place as seen in Figure 2.21.

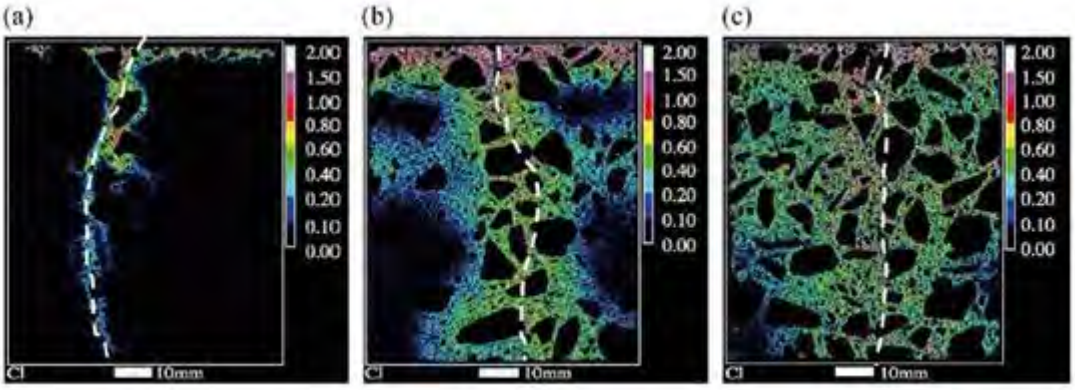

Figure 2.21 EPMA images of Cl- ion concentration for a given w/b ratios (a)0.25, (b)0.45 and (c)0.65 after one mont

The EPMA images above highlight the effect of w/b ratio on chloride ingress in cracked concrete. The complete black area marks the concrete area that has no chlorides present. The left most image (a) illustrates the presence of low chloride concentration, shown by the vast amount of black shaded area around the dashed line, that represents the crack that was formed in the concrete. The right most figure (c) illustrates a substantly higher presence of chlorides for the 0.65 w/b ratio cracked concrete. This is evident on the image by the distribution of colour around the crack in both a longitudinal and tranverse direction.

The results from the EMPA indicated a clear trend that the higher w/b ratio for a given Cl^- concentration, the higher the concentration of Cl^- over the depth of the specimen due to the presence of cracks. The quality of concrete with respective to the ingress of aggressive species, has a great influence on the penetration process, in both the cracked and uncracked concrete. Furthermore, chloride penetration depths were also determined on the cracked beams after seven days and one month. The results have been plotted as percentage of chloride concentration against the depth into concrete specimen and are shown in Figure 2.22. A general trend can be seen in both figures, that increased w/b ratio results in increased chloride concentration for a given depth in the cracked concrete for all three w/b ratios tested. Considering the cracked and uncracked specimens at seven days, both the 0.25 cracked and uncracked w/b ratio specimens showed similar over lapping chloride profiles. Whereas the 0.45 cracked and uncracked w/b ratio specimens exhibit completely different chloride profiles, highlighting the influence that cracks have on chloride ingress after seven days of exposure. The percentage of chlorides in the 0.45 cracked profile is much greater than the 0.45 uncracked profile.

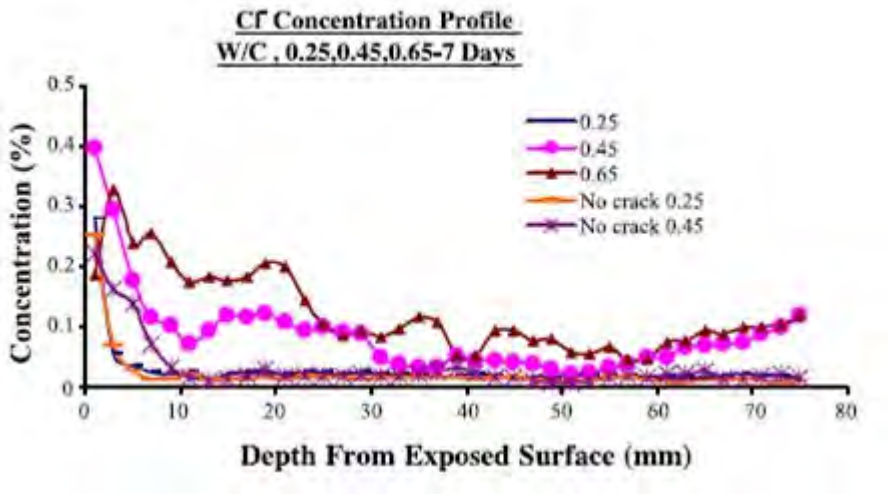

*

Figure 2.22 Chloride profile for 7 day for uncracked and cracked specimens (Pa Pa *et al.*, 2004)

Lastly, the ingress of chlorides in cracked concrete does not follow an decreasing exponential trend with regards to the percentage of chlorides in the concrete that can be seen in the uncracked concrete profiles. All three cracked profiles in Figure 2.23 illustrate chloride concentration that decrease with depth into the specimens, however the data points fluctuate and does not follow a constant trend. Hence it can be concluded that cracks do influence the penetration of chlorides into concrete and can increase the amount of chlorides present in the concrete as compared to uncracked concrete. As the quality of concrete decreases (with respect to increasing w/b ratio) the influence of cracks on chloride penetration is more prominent.

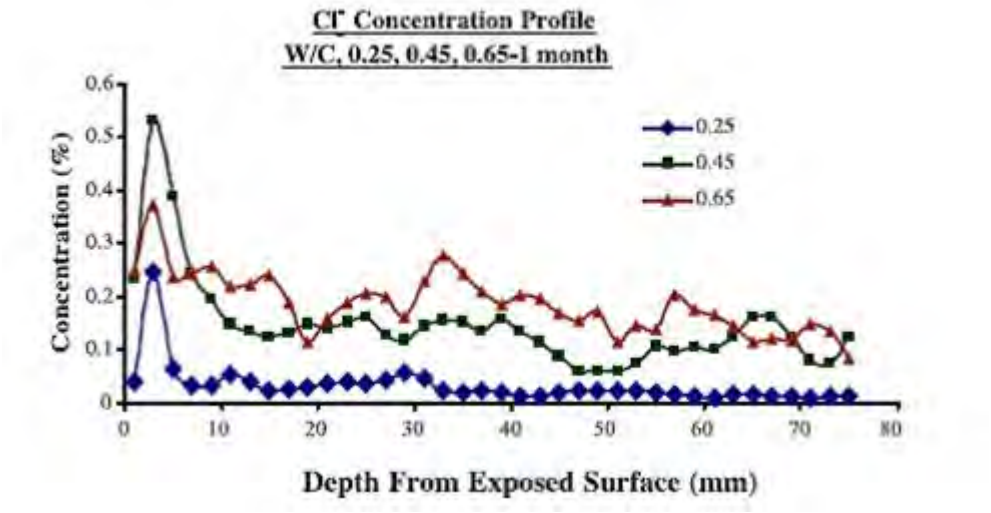

Figure 2.23 Chloride profile for one month for cracked specimens (Pa Pa *et al.*, 2004)

Schlangen et al. (2007)

Schangen et al., (2007) investigated the effect of crack widths on chloride ingress in cracked concrete. Concrete was cast using a w/b ratio of 0.5 and contained 370 kg/m^3 of Portland cement. After 28 days since casting and making the crack in the specimens, they were tested using Rapid Chloride Migration (RCM) and the chloride diffusion coefficient was obtained. The diffusion coefficient for un-cracked (D_1) and cracked concrete (D_T), were calculated by measuring the diffusion coefficient at distinct regions on cracked specimens as shown in Figure 2.24:

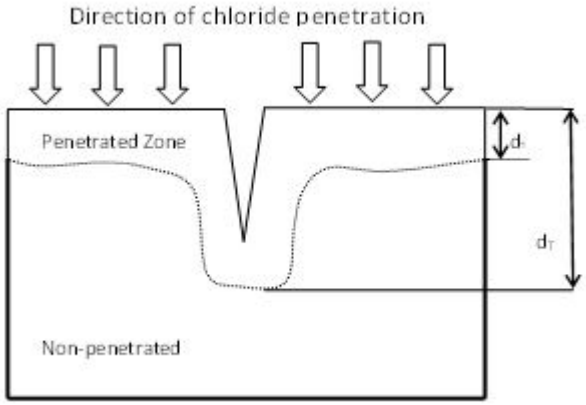

Figure 2.24 Schematic of location where cracked and uncracked measures were taken from specimen (Schangen *et al.*, 2007)

Figure 2.25, illustrates the results of chloride diffusion coefficient that was obtained for the crack mean opening displacement (CMOD):

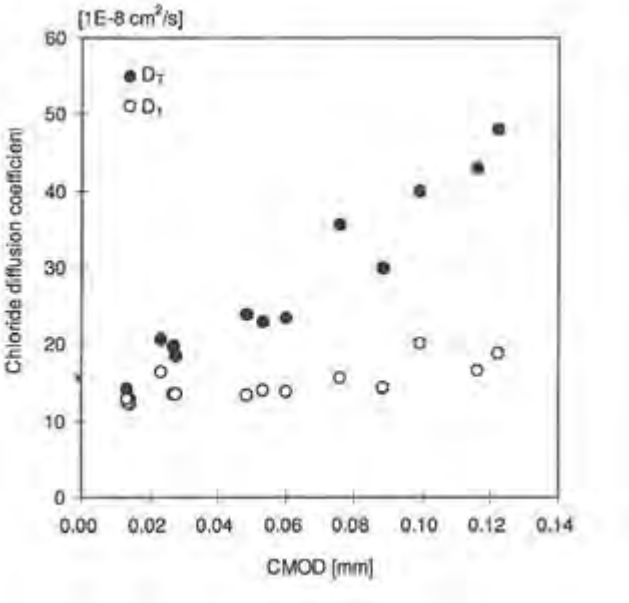

Figure 2.25 D_T and D_1 versus CMOD

Initially it can be seen that the diffusion coefficient for both the crack and uncracked regions are low for small CMOD of 0.01. However, the diffusion coefficient for un-cracked part of the specimen is a fairly constant value as the CMOD increases, which implies it is independent of the crack width. In contrast to the diffusion coefficient for the area where the crack has been made D_T, increases linearly with increasing CMOD. Hence it can be seen that due to the presence of the cracks the diffusion coefficient was modified, indicating the significant influence that cracks have on modifying transport properties.

Zhang et al. (2011)

A study was recently conducted by Zhang ***et al.***, (2011) to investigate the influence of flexual crack widths on chloride penetration in concrete. A single concrete mixture was used, consisting a water/binder ratio of 0.43 and Portland cement. Five RC beams, 150×180×1000 mm, were manufactured with the uniform cover thickness of 30 mm. The configuration of the reinforcement in the beams are shown in Figure 2.26. The 12 mm diameter bolts were tightened to produce the required crack width in the beams.

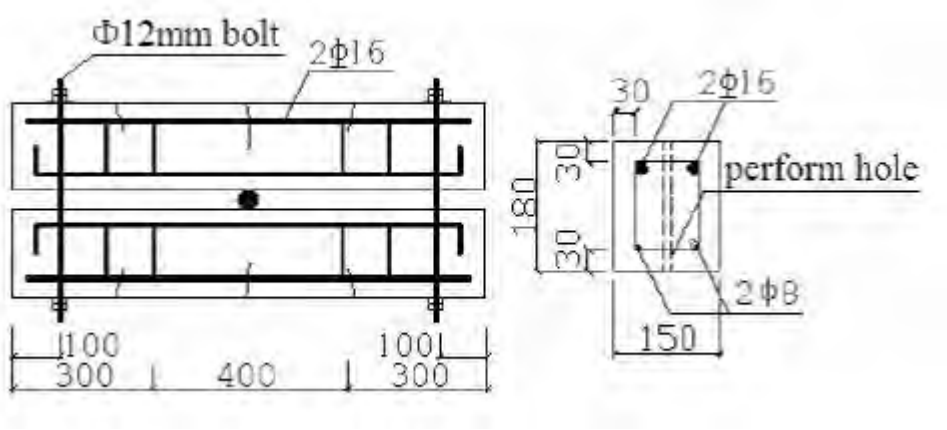

Figure 2.26 Layout of reinforcement in beams (Zhang *et al.*, 2011)

After 28 days the specimens were immersed in 5% NaCl solution after 15 cycles of one week dry and one week wet, rapid chloride tests were conducted on the cracked sections.Four broad crack widths ranges were investigated: 0.1-0.2 mm, 0.2-0.3 mm, 0.6-0.4 mm and 0.4-0.5 mm. The results of the influence of the chloirde ingress on this crack ranges are shown in Figure 2.27:

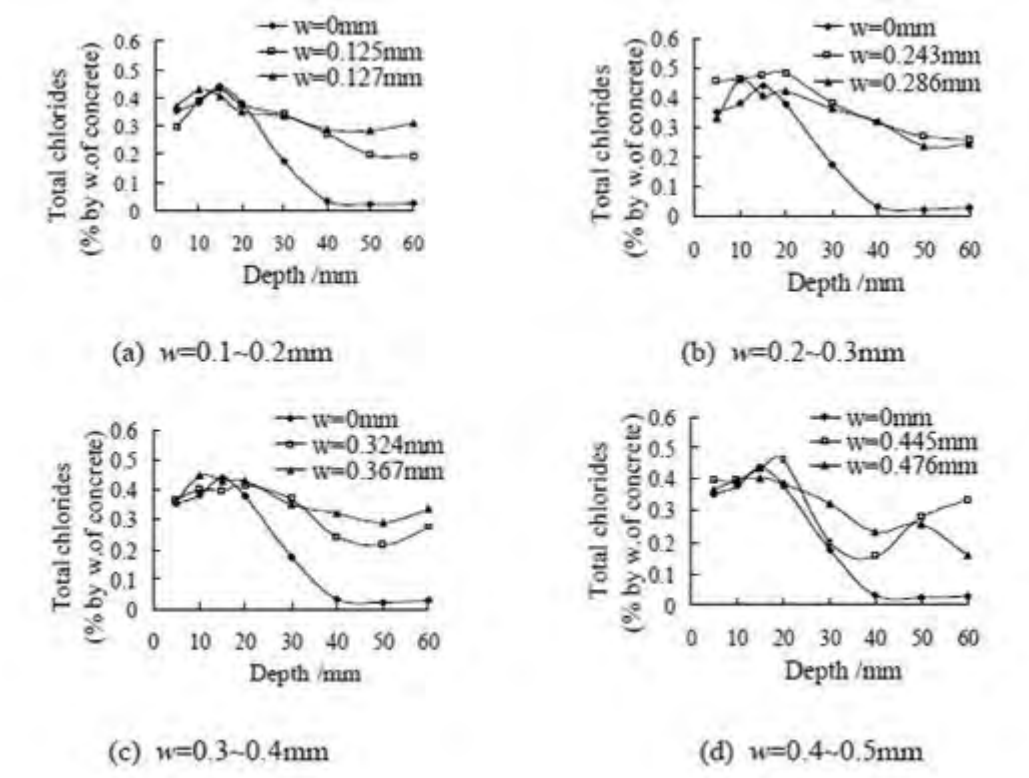

Figure 2.27 Chloride profile of cracked and uncracked concrete with various crack widths (Zhang *et al.*, 2011)

In each of the graphs in Figure 2.27, it is clear that is an effect of crack width on chloride ingress for uncracked concrete in comparision to various crack widths. The uncracked concrete in all four graphs follows a general trend of a deceasing exponential chloride profile. However it can be seen that the cracked specimens chloride profile follow a similar trend however at around 30 mm into the depth of the concrete they exhibit much higher chloride concentrations and start to deviate from the uncracked concrete trend. The cracked chloride profiles in Figure 2.11(a), (b) and (c) show a small deviation between the two cracked chloride profiles however in graph (d) there is a large scatter in the two cracked chloride profiles. The data points are scattered and there is no specfic relationship that can be fit to the data points except that there is considerably higher chloride concentration at the depth of 60 mm into the concrete as compared to the uncracked concrete.

Jang et al. (2011)

Jang *et al.*, (2011) investigated the diffusion characteristics of cracked concrete according to the crack width. The main test variable in this study was the crack width at unloaded state. The effect of concrete strength, addition of fly ash, and maximum aggregate size on the diffusion of cracked concrete was also investigated. W/b ratios of 0.40, 0.53 and 0.64 were investigated using 100 % portland cement mix and blend of 80/20 % portland cement/fly ash mix. The target compressive strengths of concrete were 15 MPa, 21 Mpa, 30 MPa, respectively. The maximum aggregate size was 25 mm. The crack widths were selected ranging from 0 to 200 μm. The cracks were induced using the set-up illustrated in Figure 2.28.

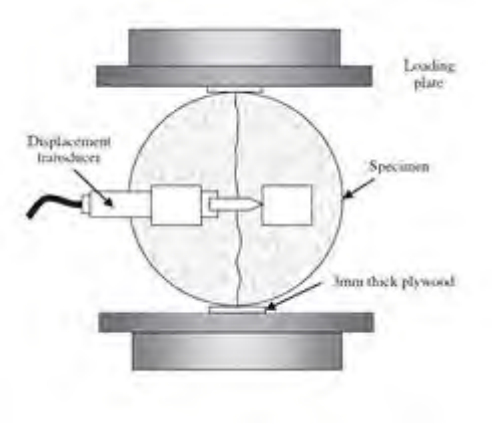

Figure 2.28 Schematic of loading set-up to induce crack in concrete specimens (Jang, et al., 2011)

The results indicated that as the concrete strength increases and the addition of fly ash decreased, the bulk diffusion coefficient decreased in the cracked concrete. The maximum size of the aggregate was found to have no influence on the bulk diffusion of cracked concrete. They found that the diffusion coefficient does not increase with crack width up to 80 μm. However, over 80 μm the diffusion coefficients start to increase. Hence 80 μm was proposed as being a possible threshold value for diffusion.

The results indicated that as the concrete strength increases and the addition of fly ash decreased, the bulk diffusion coefficient decreased in the cracked concrete. The maximum size of the aggregate was found to have no influence on the bulk diffusion of cracked concrete. They found that the diffusion coefficient does not increase with crack width up to 80 μm. However, over 80 μm the diffusion coefficients start to increase. Hence 80 μm was proposed as a possible threshold value for diffusion.

2.17.2 Influence of chloride penetration in cracked concrete on chloride - induced corrosion

A few studies have been conducted by various researches to directly measure the link between crack widths and its effect on chloride-corrosion initiation in cracked concrete, which reduces the service life of RC structures. Examples of a few of these studies are illustrated below:

Raupach (1996)

Raupach (1996), looked at the influence of chloride attack on the formation of macrocell under certain conditions. Various parameters that influence the corrosion rate in steel such as crack width, concrete cover and water/ binder ratio were investigated. Figure 2.29 below illustrates the mass loss that was recorded over a 2 year period by measuring the electrical current between the reinforcing steel electrodes in the concrete specimens.

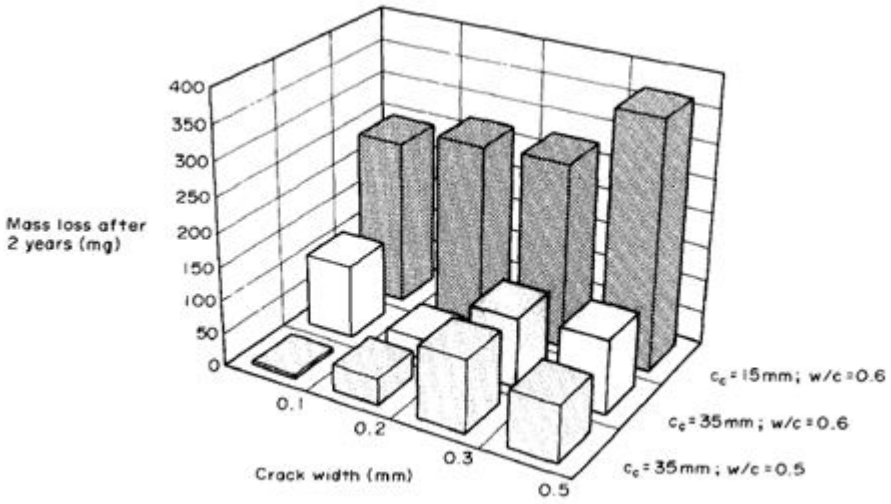

Figure 2.29 The influence of crack width, concrete cover and water binder ratio on mass of steel lost over 2 years (Raupach, 1996)

The graph indicates that corrosion currents usually increase with growing crack width under the selected test conditions and observation periods, but it is also evident that concrete cover and composition have a much greater influence than crack width. Raupach also concluded that the reinforcement in the crack zone acts as an anode, the reinforcement between the cracks set up to a distance of several decimetres as a cathode, often leading to extremely high measured corrosion rates in the crack zone.

Raupach (1996) stated that in the area of cracks, the anodes and cathodes can be formed side by side. In this instance, ratio between cathodically and anodically acting steel surface areas can be quite high, resulting in high corrosion rates and consequently in high losses in cross-section. Macrocell corrosion is of great concern because the local dissolution of the rebar. The resulting local loss in cross-section has dangerous implications for the structural safety if the corroded bars are located in a zone of high tensile or shear stresses.

Otieno et al. (2010)

An experimental study by Otieno ***et al.,*** (2010) illustrated the influence of crack width, concrete quality on corrosion rate. Beam specimens were cracked and subjected to a 3-day wetting (with 5% NaCl) cycle and 4-day air drying under laboratory conditions (16-24 °C) for a period of 32 weeks. Two w/b ratios (0.4 and 0.55) and two binder types (100% PC CEM I (PC) and 50/50% PC/Corex slag (SL)) were utilised in the concrete mixes. The results are shown in Figure 2.30.

It can be seen that crack width clearly influence the rate of corrosion. However it was pointed out that the extent of significance of the cracks depends on the interaction between crack width, concrete quality and the concrete resistivity. It was also concluded that the initiation phase may be shortened depending on the crack width and concrete properties.

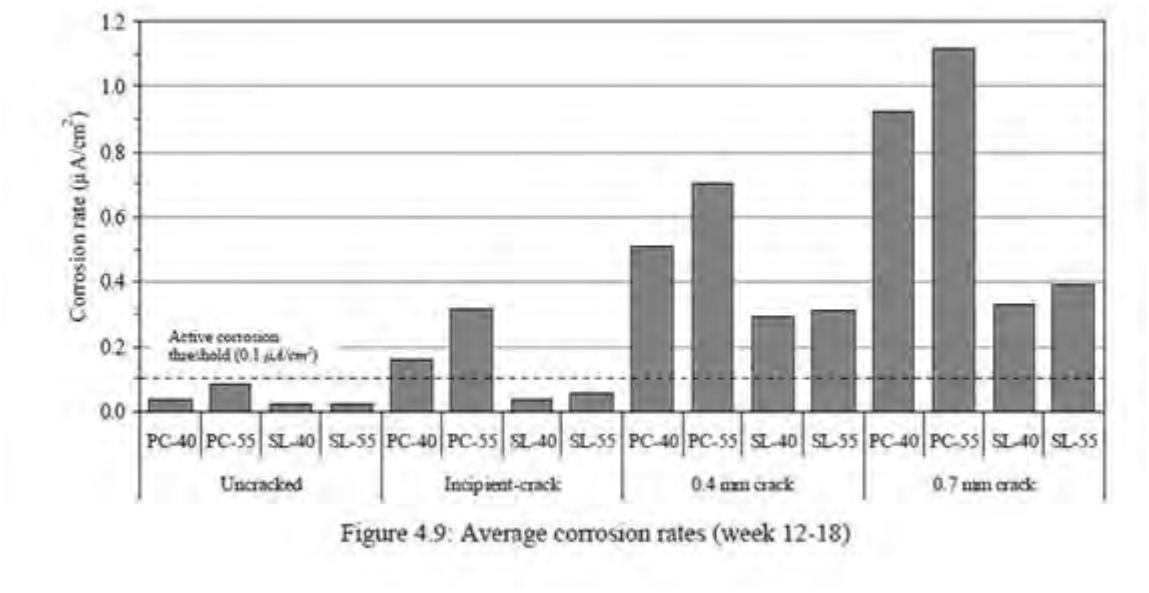

Figure 2.30 Effect of crack width on chloride-induced corrosion (Otieno *et al.,* 2010)

2.17.3 Permeability of gases and liquids in cracked concrete

Wang et al. (1997)

Wang *et al.,* (1997) related the water permeability directly to the crack width. In Wang's study, the influence of different cracks on permeability was investigated for a single concrete mixture containing a w/b ratio of 0.41. Concrete specimens used were 25 mm thick slices, cut from 100 mm x 200 mm. cylinders. Different crack widths were generated using feedback controlled splitting tests and two LVDTs were used to control average crack opening displacement. Specimens were loaded to have a crack opening displacement of 25, 50, 80, 110, 140, 180, 350, or 550 microns, and then unloaded. It was also noticed that after complete unloading, the crack opening displacement was reduced, i.e., the crack partially closed or recovered due to the material elasticity.

Water permeability tests were performed on the cracked specimens under two conditions, under loading and after loading. Figure 2.31 highlights the influence of increasing crack width on water flow for different crack opening displacement (COD) under load. It is clear that larger COD values result in greater flow of water. In the case of a COD of 180 μm there is a significant increase in water flow as a result of increase permeability in the concrete specimen.

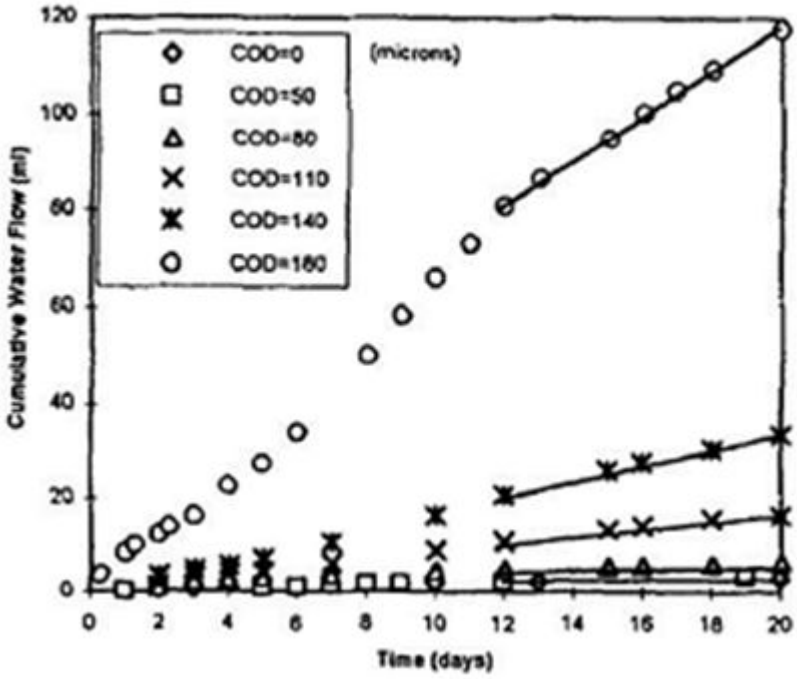

Figure 2.31 Water flow for concrete with different crack width (Wang *et al.,* 1997)

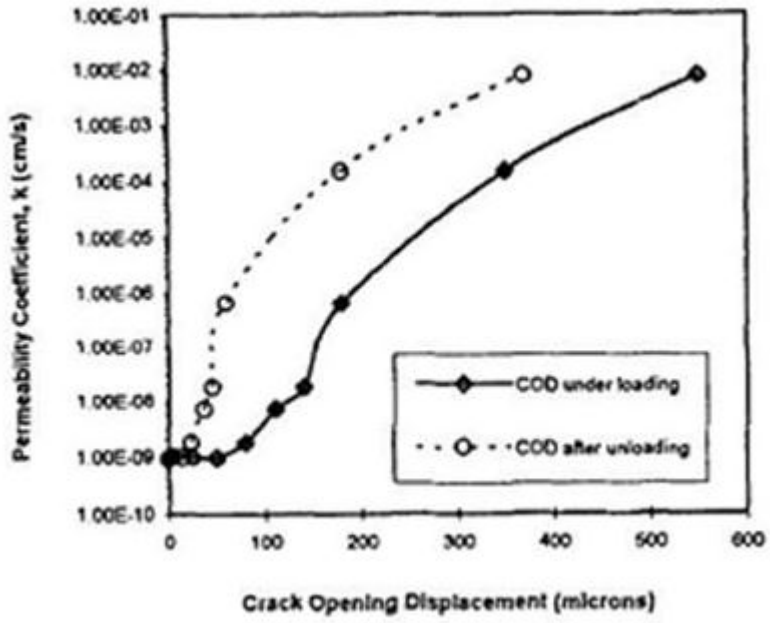

Figure 2.32 Relationship between crack widths and water permeability coefficients (Wang *et al.*, 1997)

Whereas Figure 2.32, illustrates the relationship between water permeability coefficient and crack opening displacement for both the loading scenarios.

Based on Figure 2.32 the permeability curve after unloading illustrates a reduced permeability compared to the under loading curve, this can be explained by the cracks closing due to the elastic of the material. Wang further concluded that a crack opening displacement (COD) of less than 50 μm under loading rarely affected the permeability. When the COD was in the range of 50 μm to 200 μm under load, the permeability increased rapidly. Over 200 μm under load, the permeability increased steadily. Generally the results indicated that increasing crack widths increase the permeability of concrete and result in accelerated water flow in concrete.

Wittmann et al. (2011)

Wittman *et al.,* (2011), illustrated the use of Neutron radiography to study the moisture movement in cracked and uncracked concrete. The study investigated the influence of predefined crack widths on the moisture movement of water into concrete specimens, since absorption is the most effective manner by which chloride ions are transported into concrete (Luping, *et al.,* 2012). The results shown below in Figure 2.33 pertained to an artificial crack width of 0.35 mm. The three images illustrate the moisture distribution in the cracked region after a 1, 30 and 60 minute duration of the concrete being in contact with water.

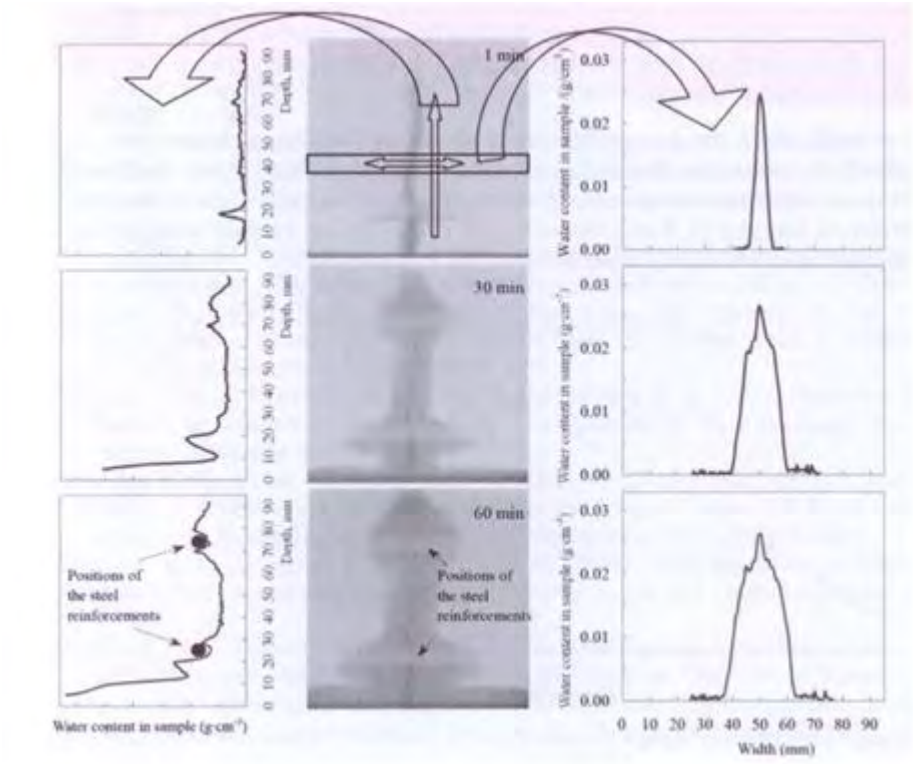

Figure 2.33 Schematic of moisture movement in cracked concrete Wittman *et al.,* (2011)

The results were quantified by placing two axes along the centre image; the axes measure the water content against the depth of the concrete specimen in both the vertical and horizontal direction. The central images visually illustrate the moisture movement within the cracked specimen (in darker grey shade) of after a certain duration The three images along the left-side indicate the water content that was determined in the specimen with regards to moisture penetrating perpendicular to the crack. In comparison to the three images on the right-side that indicate the water content that was determined in each specimen with regards to moisture penetration parallel to the crack width.

It can be seen on the top centre image in Figure 2.33 that after 1 minute, the artificial crack is filled with moisture, indicated by the darker grey outline. In addition, it can be seen that

ahead of the real crack tip a fracture process zone has been created. Hence water also can penetrate easily into this damaged area. The porosity of the fractured zone was increased by micro-crack formation. Water penetrated from the crack into the adjacent material following a square root of time law.

Yi et al. (2011)

Yi *et al.(2011),* investigate water permeability and how it is affected by hydraulic pressure and crack widths in cracked concrete. The test variables were hydraulic pressure and crack width. The crack widths were 30, 50, and 100 μm and the hydraulic pressures applied were 0.01, 0.025, 0.05, 0.1, and 0.2 MPa. 150 mm diameter by 300 mm height cylinders was used and the cracks were induced using a method that involves applying only a pure tensile force. For each crack and pressure condition, three specimens were tested.

The water permeability the setup was composed of applying the target hydraulic pressure to the upper part of the specimen and measuring water flow contents collected through the lower part of the specimen. As the water passed the crack of the specimen, it was collected. A weight of water collected in the reservoir was measured to obtain flowing water contents per time. The permeability coefficient (K_e) was the determined for the various crack widths as seen in Table 2.5 and Table 2.6. Table 2.5 shows the K_e values with hydraulic pressure and crack width at an initial stage after 30 minutes. From this table, it is noted that the K_e values increase as the crack width increases regardless of the pressure.

Table 2.5 Initial K_e values (x 10^{-3}) (Yi *et al.*, 2011)

	0.01 MPa	0.025 MPa	0.05 MPa	0.1 MPa	0.2 MPa
30 μm	2.31	3.62	3.18	11.3	2.39
50 μm	9.60	3.91	3.64	8.56	21.8
100 μm	147	271	208	154	113

Table 2.5 shows the K_e values with hydraulic pressures and crack widths summarized at stabilized and final stages. Similarly with the initial K_e values, the final K_e values increase as the crack width increases.

Table 2.6 Final K_e values (x 10^{-5}) (Yi *et al.*, 2011)

	0.01 MPa	0.025 MPa	0.05 MPa	0.1 MPa	0.2 MPa
30 μm	20.0	8.09	4.74	1.08	2.25
50 μm	36.5	4.02	4.50	3.84	3.68
100 μm	69.1	13 000	14 100	11 700	8910

It was concluded that due to the influence of autogenous healing, the final K_e value was smaller than the initial K_e value and increased as crack width increased. However, the influence of crack widths on the final K_e value compared to the initial K_e value was small.

Park et al. (2012)

Park *et al.,* (2012) showed evidence that crack widths have a marked influence on water permeability of cracked concrete. Cylindrical concrete specimens (10 by 20 cm) are prepared based on a single concrete mixture, with a 0.44 w/b ratio. The cylindrical specimens are cut into four disk shapes of the same thickness (50 mm) to induce a crack in the concrete specimens, and a splitting test is conducted.

The results indicated that crack widths of 0.1 mm have up to 2.9 times greater influence on water permeability when compared to sound concrete. Crack width of 0.2 mm, 0.3 mm and 0.4 mm were also investigated, and the coefficient of permeability determined for each scenario. Figure 2.34 illustrates results observed for permeability coefficient for each of the predefined crack widths which were determined over a period of 30 days.

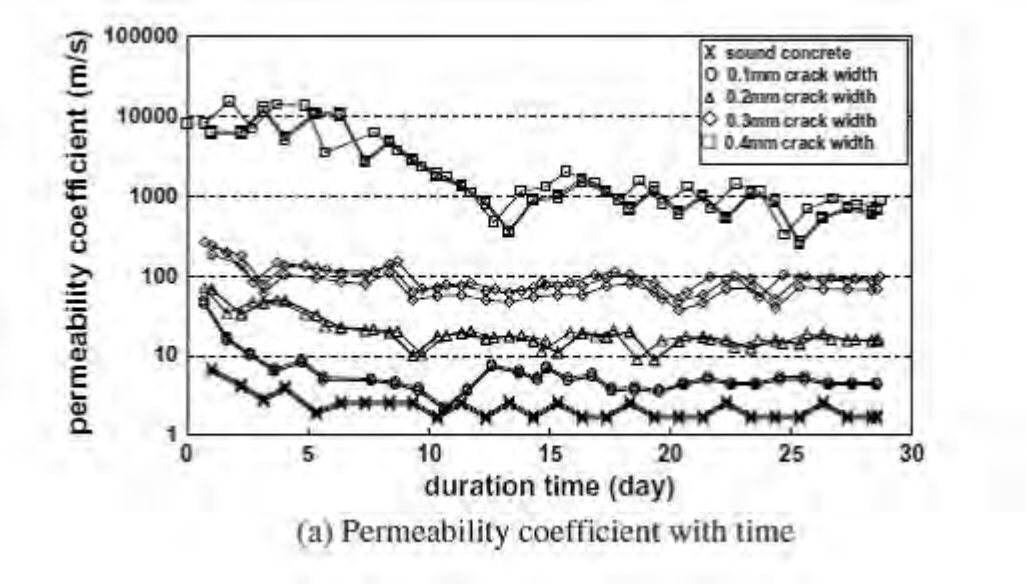

Figure 2.34 Influence of crack widths on permeability coefficient (Park *et al.*, 2012)

Initially, the permeability coefficient is higher for all cases, due to the fact that the water permeability test starts off in a non-steady condition as the specimen is not saturated, the permeability coefficient only stabilizes after 3-4 days. It is evident that the permeability significantly increases for crack widths above 0.2 mm. When comparing the cracked concrete permeability coefficient to sound concrete, 0.2mm, 0.3 mm and 0.4 mm crack width were 20.0, 52.2, 1004.7 times greater than the sound concrete, respectively.

2.17.4 Influence of cracking on carbonation

Few studies have been conducted to directly relate crack widths to carbonation-induced corrosion as shown below.

Song et al. (2006)

Song et al., (2006), developed an analytical technique to predict carbonation in both sound and cracked concrete and verified the results with experimental testing. Cylindrical concrete specimens of size 10 cm diameter and 20 cm height with different w/b ratios (0.45, 0.55, and 0.65) were cast for accelerated carbonation test. For carbonation in cracked concrete, the cracks are induced into the specimens by splitting test. In Figure 2.35 are the results of the carbonation depths for sound and the three cracked three w/b ratio tested.

The figure clearly shows that the carbonation process is faster with higher w/b ratios and larger crack width. It is also observed that, as the crack width increases the carbonation depth also increases with increase in w/b ratio and exposure period. It is known that as the crack width increases, atmospheric (gaseous and dissolved) CO_2 enters through the crack and it deteriorates the concrete in terms of carbonation by forming $CaCO_3$ and reducing the alkalinity of the concrete, which reduces the durability of concrete.

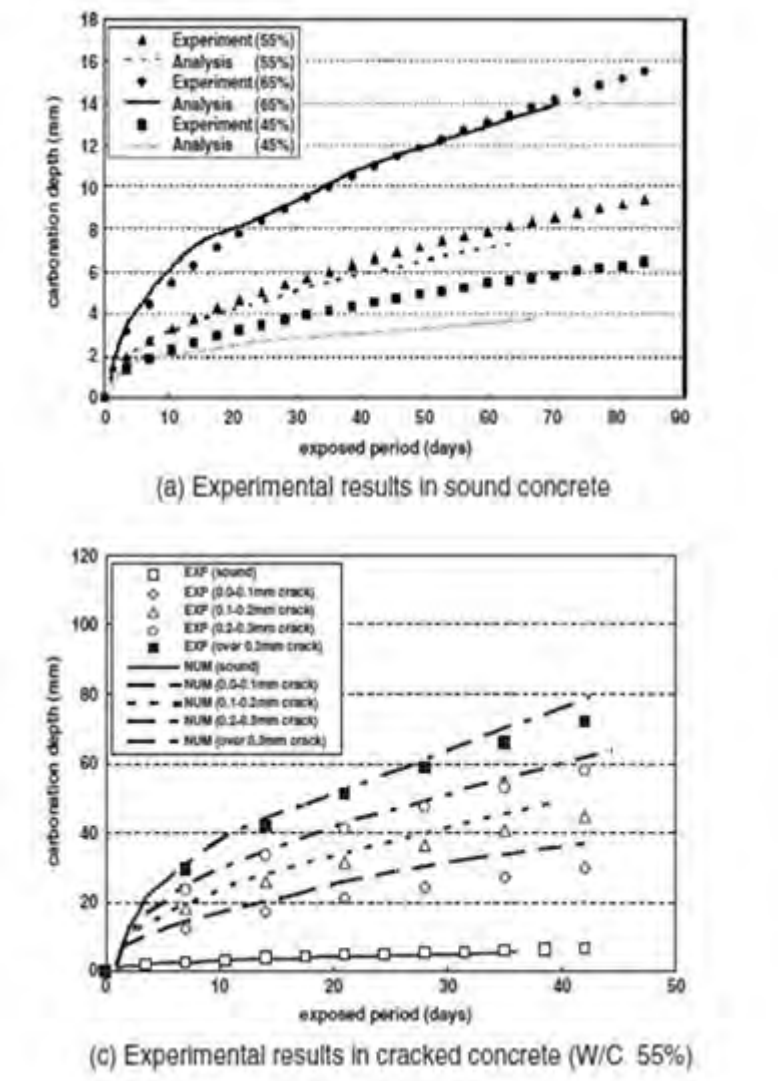

Figure 2.35 Carbonation depth for sound and cracked concrete specimens for both the numerical technique and experimental tests

2.18 Relevance of the Influence of cracks on transport properties in concrete

Literature has shown that extensive research has been conducted to investigate methods to generate cracks in concrete and measure the influence of these cracks on fluid transport in concrete. Most research has focused on assessing and modelling the fluid and ion transport in uncracked cementitious materials. Difficulties in generating desirable crack patterns in concrete specimens and the availability of appropriate tests methods for concrete has further limited the number of studies that have been conducted on cracked concrete.

However from the studies reviewed in the preceding sections, it is clear that crack width have a marked influence on the transport properties in cracked concrete. It can also be seen that many different approaches have been utilised in an attempt to quantify the influence of cracks on the transport properties in concrete. The advancement of technology has provided a means of better analysing cracks in concrete. However, there is not enough research that had been conducted to reach a consensus on the accurate effects of cracks on the durability of concrete. For example, there is conflicting data that has been published on the relationship between corrosion and crack width (Schiessl & Raupach, 1997; Ayra & Ofori-darka, 1996; Vida, Castel, & Francois, 2004).

Attempts have been made by researchers to modify existing equations based on uncracked concrete to describe the transport properties in cracked concrete. It is debatable whether completely new equations should be derived, since modifying existing ones is still based on the premise of uncracked concrete.

Trying to understand the influence of cracks on transport mechanisms in concrete is crucial in understanding the durability of RC structures. Accurate knowledge and means of quantifying the transport properties of cracked concrete is still lacking. This knowledge is essential for predicting the realistic durability of a structure, since the deterioration mechanisms are related to the ingress of aggressive species through the porous body.

2.19 Closure

It be seen that the presence of cracks in concrete has a marked influence on transport mechanism that govern the durability of RC structures. The incorporation of the influence of cracks in DI approach is currently an area where there is still room for investigation to further improve this testing approach. The degree of impact that cracks have will indicate what to what extent a modification needs to be made to incorporate the influence of cracks in the prediction model output. This will led to a more realistic prediction model that will account for parameters such as cracks in RC structures.

The incorporation of the influence of cracking in service life models is vital in providing realistic predictions of RC infrastructure. It is seen that in-service life models that have been developed such as the Duracrete, only the influence of corrosion induced cracks are considered in the analysis of service life prediction. Cracks that are presence prior to corrosion are mentioned in the report and the influences of these cracks are discussed but no attempt is made to account for their presence in the service life prediction model. When the effects of cracks that occur prior to the onset of corrosion are not considered in the durability predictions, the performance and service life of RC structures may be overestimated and may lead to an unexpected premature failure.

3 EXPERIMENTAL DETAILS

3.1 Introduction

This chapter outlines the experimental set-up that was used in order to investigate the influence of cracks on the transport properties of chlorides and carbon dioxide in cracked and uncracked concrete. It discusses the rationale for the choices made with regard to the project variables, materials, mix designs and the tests conducted. A brief schematic of the experimental methodology is presented in Figure 3.1.

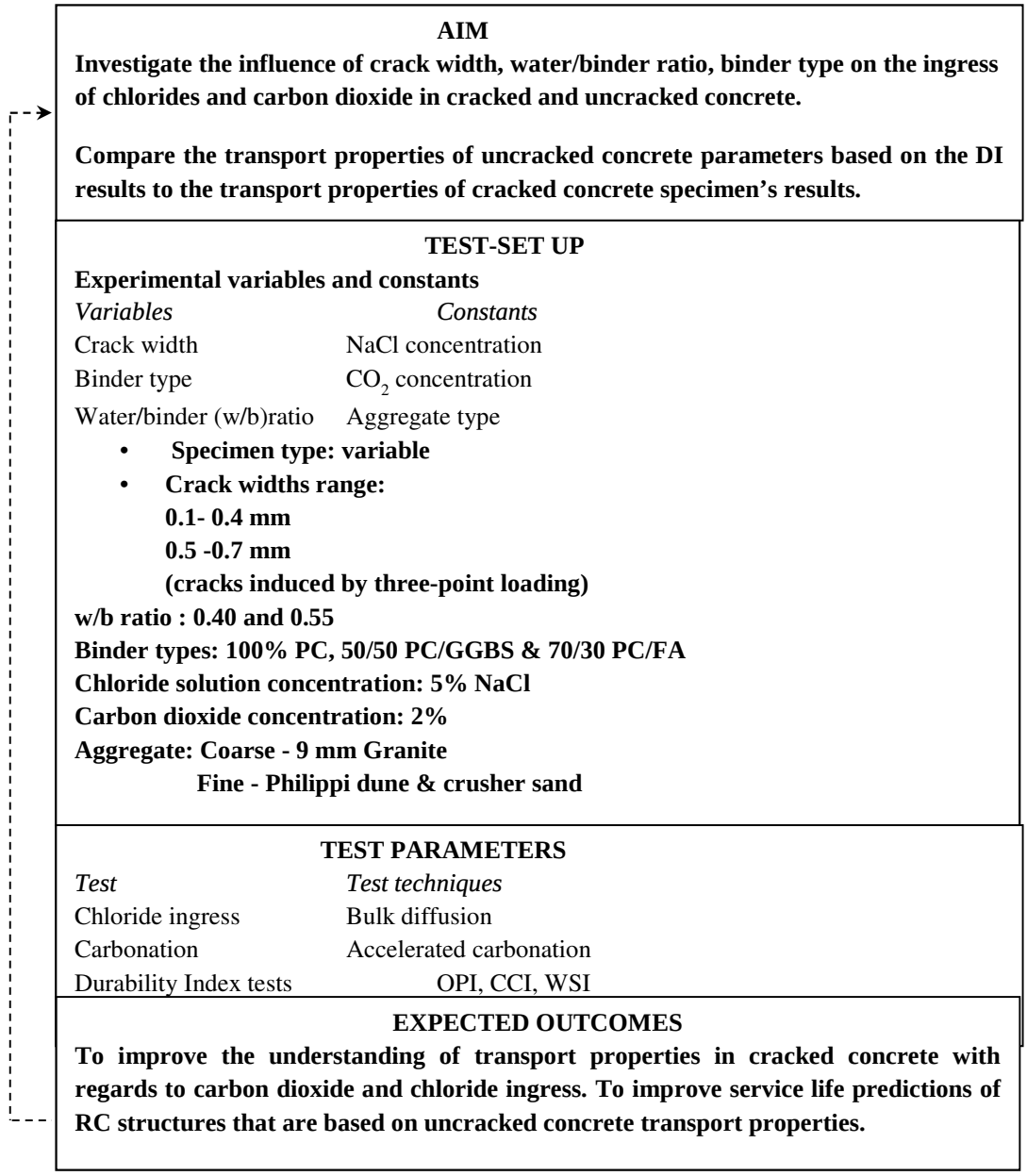

Figure 3.1 Schematic overview of the testing methodology for this study

3.2 Scope of testing

Three sets of tests were performed to provide an understanding of the influence of cracks on transport properties of chlorides and carbon dioxide in cracked and uncracked concrete:

a) South African Durability Index tests
b) ASTM C1556 - Standard test method for determining the apparent chloride diffusion coefficient of cementitious mixtures by bulk diffusion
c) Accelerated carbonation tests

The results from the penetration of chlorides and carbon dioxide into cracked and uncracked concrete were used to improve the understanding of the influence of cracks on transport properties in concrete.

3.2.1 Durability Index tests

The Durability Index (DI) tests provide an understanding of the transport properties in uncracked concrete. Three DI tests were performed (chloride conductivity, water sorptivity and oxygen permeability) (Alexander *et al.,* 1999). These tests characterise the quality of the cover concrete as affected by choice of material and mix proportions, placing, compaction and curing.

3.2.2 ASTM C1556 - Standard Test Method for Determining the Apparent Chloride Diffusion Coefficient of Cementitious Mixtures by Bulk Diffusion

This test technique was chosen to investigate the resistance of concrete to chloride ingress. Furthermore, this testing procedure was chosen as it allowed for the ingress of chlorides to be measured in cracked and uncracked concrete specimens. The results from this test can be correlated to chloride conductivity test results, to compare the transport properties of chlorides in cracked and uncracked concrete using the respective diffusion coefficients obtained.

3.2.3 Accelerated carbonation test

This technique was chosen to investigate the rate of carbonation in concrete. The test procedure allowed for the cracked and uncracked concrete specimens to be tested and the depth of carbonation measured. Furthermore the test results of the accelerated carbonation tests can be correlated with the oxygen permeability test results, to compare the rate of carbonation in cracked and uncracked concrete using the respective carbonation coefficients obtained.

3.3 Experimental variables

The influences of the following variables on the penetration of aggressive species were considered significant in determining the durability performance of uncracked and cracked concrete for each of the tests chosen:

I. Water/binder ratio
II. Binder type
III. Crack width

3.3.1 Water/binder Ratio

Two water/binder ratios (w/b) of 0.40 and 0.55 were utilized. A w/b ratio has a large influence on the strength and permeability properties of paste made with a given combination of Portland cement and extender (Grieve, 2009). The lower w/b ratio 0.40 was chosen to investigate the influence of cracks on concrete which is less permeable to the ingress of aggressive species. The higher w/b ratio of 0.55 was used so as to attain a conventional concrete mix (Grieve, 2009).

- **Binder type**

Three binder types were used in this study. Literature has shown that the use of supplementary cementitious materials such as fly ash and blast-furnace slag has beneficial factors which include reduced concrete production cost, energy and resource conservation, reduced environmental pollution impact (Yang ***et al.,*** 2007). Furthermore the use of these supplementary binders in concrete increases the resistance of chloride ingress (Yang, 2002).

- ***Portland Cement (PC)***

CEM I 52.5N was obtained from the Riebeek West PCC factory in the Western Cape Province, South Africa. All the cement used was sourced from the same factory. The typical oxide composition of the PC is given in Table 3.1.

- ***Fly Ash (FA)***

The fly ash utilised in this investigation was obtained from Ash Resources' Lethabo plant in Mpumalanga, South Africa. The fly ash product that was utilised is commercially referred to as DuraPozz, and it complies with SANS 1491 Part 2. A 70/30 blend of PC/FA was adopted in this study and the typical oxide composition of FA is given in Table 3.1.

- ***Ground Granulated Blastfurnace Slag (GGBS)***

The ground granulated blast-furnace slag utilized in this investigation was obtained from the Mittal Vanderbijl Park steel plant in Gauteng, South Africa. A 50/50 PC/GGBS blend was used. The typical oxide composition of the GGBS is given in Table 3.1.

Table 3.1 Typical oxide analysis of PC, FA and GGBS (Alexander *et al.*, 2012)

Constituents in PC	**SiO_2**	**Al_2O_3**	**Fe_2O_3**	**CaO**	**MgO**	**K_2O**	**SO_3**	**Na_2O**			
% composition	21.10	4.00	3.35	65.80	0.87	0.70	2.30	0.10			
Constituents in FA	**SiO_2**	**Al_2O_3**	**Fe_2O_3**	**CaO**	**MgO**	**K_2O**	**TiO_2**	**Na_2O**	**Mn_2O_3**	**P_2O_5**	**SO_3**
% composition	54.63	30.04	2.75	5.82	1.91	0.76	1.74	0.60	0.02	0.85	0.3
Constituents in GGBS	**SiO_2**	**Al_2O_3**	**Fe**	**CaO**	**MgO**	**K_2O**	**TiO_2**	**MnO**	**SO_3**		
% composition	39.45	12.84	0.36	38.89	7.34	0.92	0.58	0.47	0.48		

3.3.2 Crack Width

Two crack width ranges were investigated in this study; 0.1 - 0.4 mm and 0.5 - 0.8 mm. Crack ranges were utilized due to the difficulty of obtaining a single pre-defined crack width when subjecting the concrete specimen to a flexural load. The first range was limited to maximum of 0.4 mm as it is conventionally considered the threshold crack width below which steel corrosion proceeds similar to that in uncracked concrete (ACI 224R-01). The upper limit for the second range was 0.8 mm, which simulates unfavourable crack widths, which may pose severe corrosion threats to RC structures.

3.4 Experimental Parameters

3.4.1 Aggregate

9 mm granite stone was chosen as the coarse aggregate and a 50/50 mix by mass of greywacke crusher sand and Philippi dune sand were used as fine aggregate for the concrete mixes. The grading analysis was performed according to SANS3001-PR5 (2011).

a) Coarse aggregate

Granite is an igneous rock consisting mainly of quartz, mica, and feldspar. The measured grading curve for Cape Granite is given in Figure 3.2:

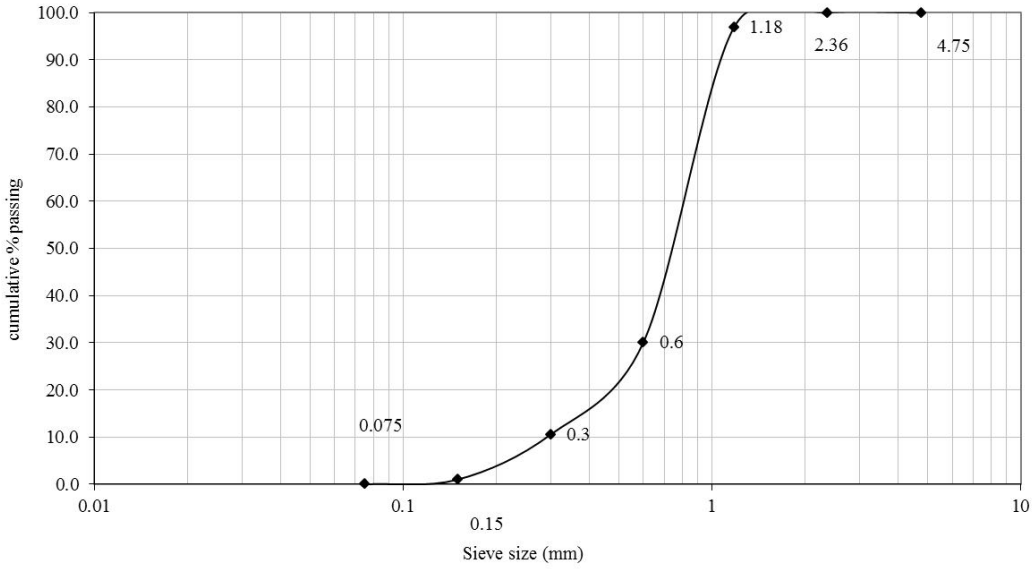

Figure 3.2 Grading curve of 9 mm Granite stone

a) Fine Aggregate

Philippi dune sand is a shell-bearing sand with a shell content of approximately 25 to 30%. The sand was obtained from the Cape flats in Cape Town, South Africa. Because of their well-rounded grains, they produce concrete with low to medium standard water requirement of about 200 l/m^3 (Grieve, 2009). The measured grading curve for Philippi dune sand is given in Figure 3.3:

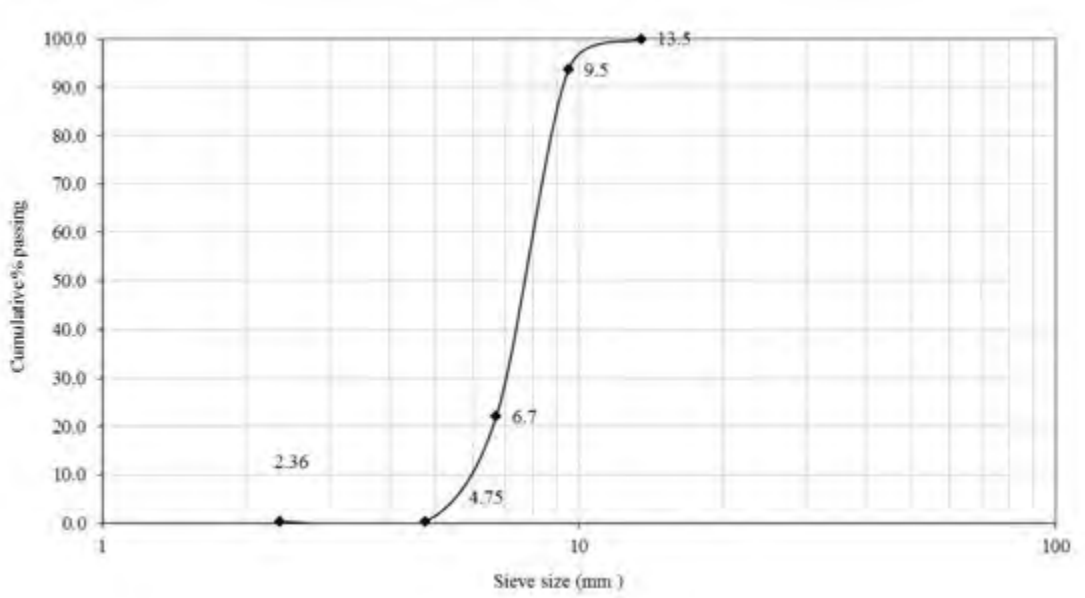

Figure 3.3 Grading curve of Philippi dune sand

Greywacke, developed by thermal metamorphism of argillaceous rocks of the Malmesbury group, and commonly referred to as Malmesbury shale in the Western Cape Province, South Africa, was used. The measured grading curve for Greywacke crusher sand is given in Figure 3.4.

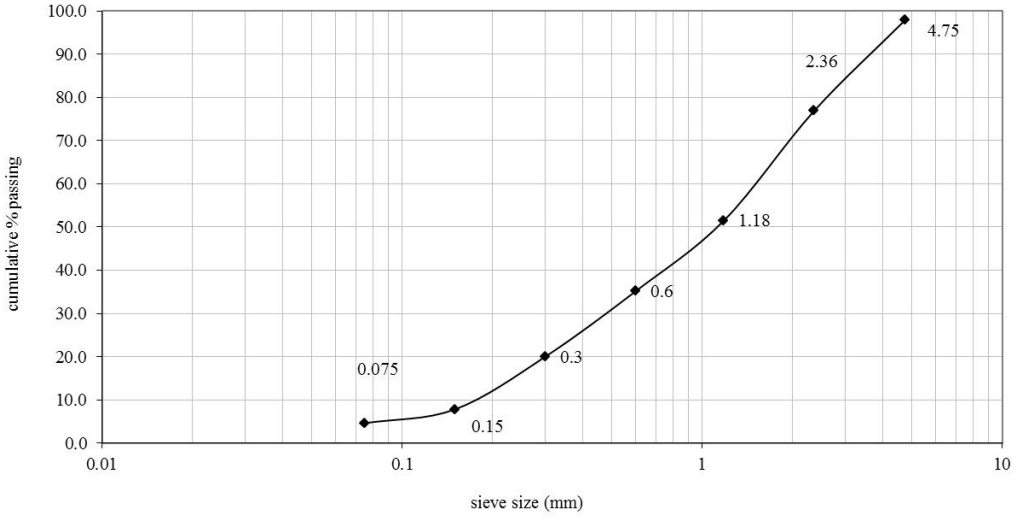

Figure 3.4 Grading curve of Greywacke crusher sand

Prior to using the aggregates, they were dried in an oven at 50°C for 48 hours and then cooled to room temperature for 24 hours.

3.4.2 Concrete mix design and mix proportions

For the purpose of comparison of results, the mix proportions that were used have been adopted from Otieno ***et al.,*** (2010). This was done to allow the data obtained in this study to be easily correlated (or compatible) with previous ones and to check the validity of the data obtained.

Table 3.2 Concrete mix proportions and selected concrete properties, (Otieno *et al.*, 2010).

	100 PC		70/30 PC/FA		50/50 PC/GGBS	
Materials (kg/m^3)						
Water/binder ratio	0.40	0.55	0.40	0.55	0.40	0.55
PC CEM I 52.5N	500	364	324	236	213	168
Fly Ash	-	-	139	101	-	-
Ground Blastfurnace Slag	-	-	-	-	213	168
Greywacke Crusher Sand	265	435	375	428	375	428
Phili Dune Sand 2 mm max.	265	435	375	428	375	428
Granite 9 mm max.	960	960	1040	1040	1040	1040
Water content	200	200	185	185	185	185
28 day strength (MPa)	60.0	45.7	57.9	35.6	56.2	39.5

3.5 Experimental programme timeline

The experimental programme for this study was conducted over a period of 24 weeks. The outline for the experimental programme is shown below:

Table 3.3 Timeline used for experimental programme

Week 0	Casting of beam specimens 100 x 100 x 500 mm
Week 1	Removed specimens from water-curing tank after seven days Induced cracks in beams by 3-point flexural loading
Week 7	Specimen preparation: - Cutting off of cracked section from beam - Applying epoxy on surface of cracked specimen
Week 8	Placed cracked specimens in either: carbonation chamber or sodium chloride solution
Week 16	Conducted 1st set of tests (durability index tests, chloride profiling, measuring carbonation depth)
Week 24	Conducted 2nd set of tests (durability index tests, chloride profiling, measuring carbonation depth)

3.6 Specimen size, casting and specimen preparation

3.6.1 Number of specimens

For a given binder type, water/binder ratio and crack range, six 100 x 100 x 500 mm long beams were cast. A total of 72 beams were cast.

3.6.2 Casting of specimens

The available wooden beam moulds were modified to facilitate one 10 mm diameter deformed steel bar to be embedded in the concrete. This was done to allow the reinforcement to carry the tensile stresses that would develop in the beam, ensuring that the beam remained intact as a single specimen during and after being subjected to a flexural load. Two specially designed PVC blocks were fixed at the ends of the mould to hold the steel bar in place during casting. Before placing the bars in the mould, they were cleaned and de-greased using acetone. In order to force the crack to propagate at mid-span of the beam, a 1.0 mm thick PVC sheet was cast into the beam. The PVC sheet extends 1.0 mm into the depth of the beam. Casting of concrete was done in accordance with SANS5861-2 (1994).

After the placement of concrete in the beam moulds, compaction was done on a vibrating table for 30 seconds.

3.6.3 Curing of specimens

After casting the specimens were covered with polythene sheets for 24 hours at room temperature 22 ± 2 °C to prevent any moisture loss from the concrete. The beams were then demoulded and placed in a water bath at 23 ± 2 °C for seven days. This time period allowed the concrete to gain adequate strength prior to loading the beam specimens to induce cracks.

3.6.4 Generation of cracks in concrete

After seven days, the beams were removed from the curing tank and subjected to three-point flexural loading. The PVC sheet that was casted-in at mid-span of the beam, was removed from the beam which created a notch in the longitudinal centre of the beam. When the concrete beam was subjected to the bending load, the tensile forces were generated at the mid-span, which forced a crack to propagate from the notch tip into the beam, inducing a crack. A schematic of the layout of the propagation of a crack in the beam is shown in Figure 3.5.

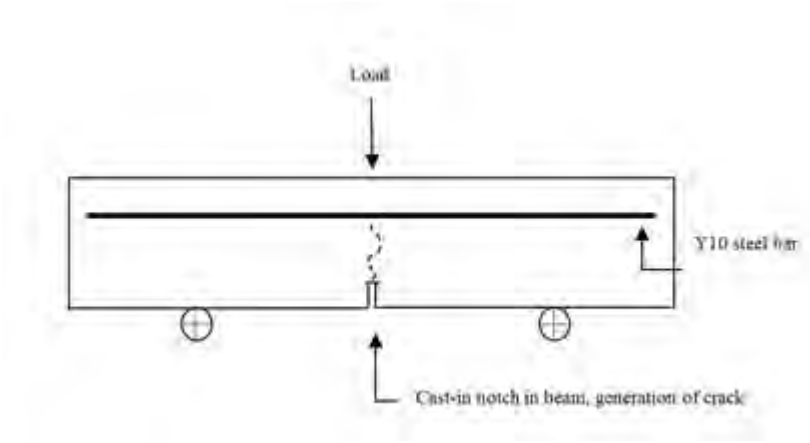

Figure 3.5 Schematic of loading of beam using a three-point beam set-up

A feeler gauge and crack width gauge with 0.1 mm accuracy were utilised to determine if the appropriate crack width range was achieved. Once the crack width was obtained, 20mm by 10mm stainless steel spacers were inserted into the crack to keep the crack open at a given crack width range as seen in Figure 3.6. Two stainless steel plate thicknesses of 0.3 mm and 0.7 mm were used to accommodate the two different crack width ranges. Once this was done, the flexural loading was released.

3.6.5 Specimen preparation

The central portion of the beam with the induced crack was sawed off from the rest of the beam using a diamond-tipped blade (Figure 3.6).

The exterior faces of the cracked section were then labelled A and B. A crack profile of each face was then mapped. This involved measuring the crack width reduction along the depth of the specimen at 10 mm intervals. The concrete specimens were then coated with Sikafloor 261A Epoxy resin. All surfaces of the concrete specimens were coated except the top surface, which contained the crack to allow for a unidirectional ingress of carbon dioxide or chlorides into the concrete.

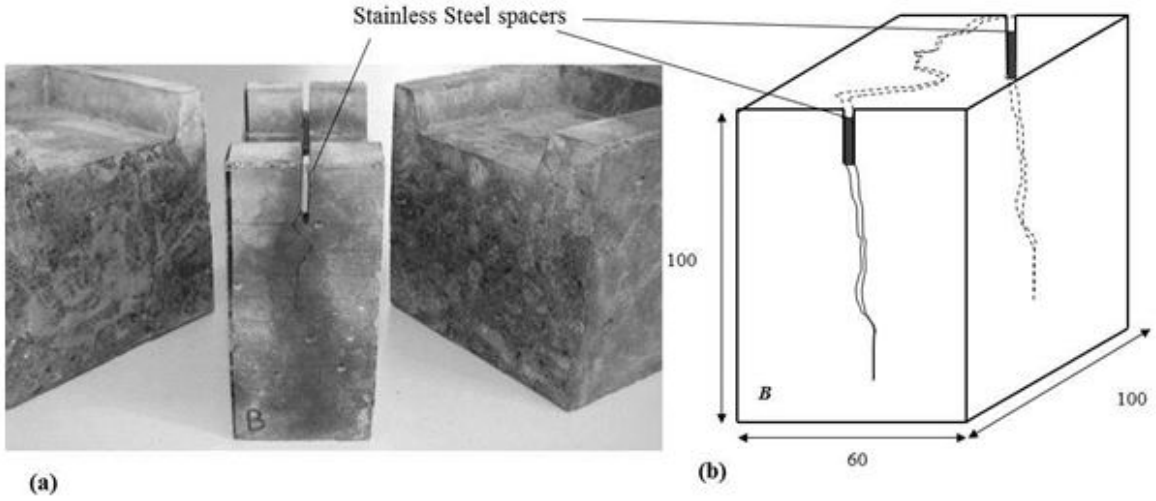

Figure 3.6 Photograph of a typical central portion of a beam cut from rest of the beam, illustrating a cracked section of beam.

3.7 Testing procedure

For statistical purposes, each test was performed on three specimens. This was done to account for variability in test results.

3.7.1 Compressive strength

The 28-day compressive strength of the concretes was determined in accordance with SANS 5863. 100 mm cubes were used.

3.7.2 Accelerated carbonation tests

A 150 litre carbonation chamber (LEEC GA2010) that was utilized to carry out the carbonation tests. The chamber can control the carbon dioxide concentration from 0 to 20 % ± 0.1%. The temperature was maintained at 20 °C ± 2 °C. Silicon crystals were used in the chamber to control relative humidity. Initially, the relative humidity varied due to temperature fluctuations, however once the desired relative humidity was attained the chamber successfully maintained the humidity. The relative humidity was kept within the range of 65 ± 5%. In summary, the accelerated carbonation was performed at 20 °C ± 2 °C, 65 ± 5% and CO_2 concentration of 2% ± 0.1%, as specified by the *fib bulletin 34: Model code for service life design*.

A total of 36 cracked concrete specimens (Figure 3.7 (a)) were conditioned to 65 % humidity prior to being placed in the carbonation chamber. A CO_2 gas meter with an inbuilt capability to measure relative humidity was used to monitor carbon dioxide concentration and relative humidity. The specimens were left in the chamber for a period of 8 weeks. Once the specimens were removed, a 20 mm thick slice of concrete was sawn off from each specimen to expose the concealed concrete (Figure 3.7 (b).

The two freshly exposed faces of concrete were then left to dry for 24 hours in a controlled temperature room 22 ± 2 °C. The specimens were then sprayed with phenolphthalein

indicator to measure the depth of carbonation (Figure 3.7 (c)). Once the carbonation depth measurements were taken, the thicker sections of concrete specimens (i.e. not the 20 mm thick slices) were then recoated with epoxy resin (Figure 3.7 (d)) and placed back in the carbonation chamber for a further 8 week period. The same procedure was followed to measure for carbonated depth in the concrete after 16 weeks of exposure.

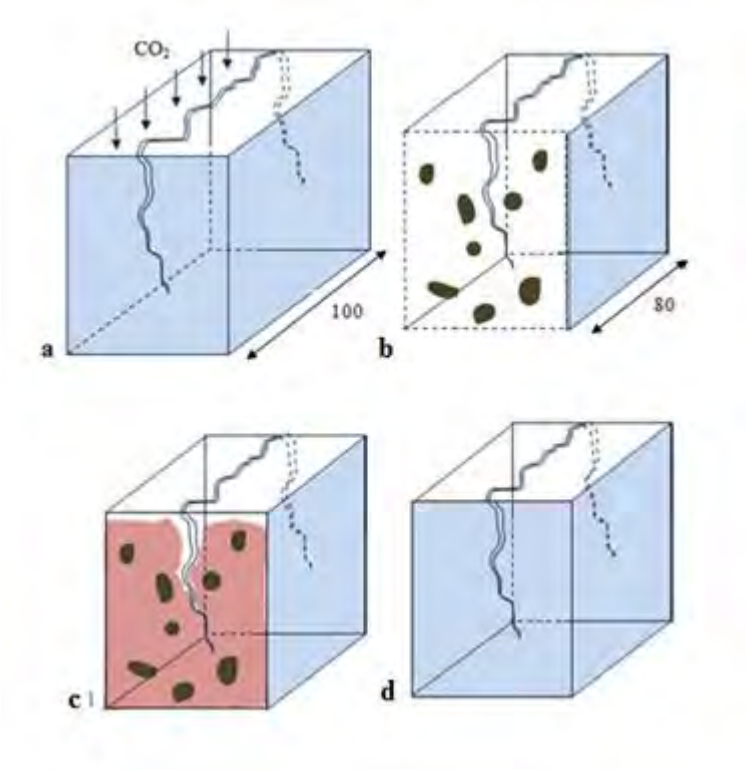

Figure 3.7 Schematic of the procedure followed to measure carbonation front on cracked specimens

Two sets of carbonation depth readings were obtained from the phenolphthalein-sprayed concrete specimens. Figure 3.8 illustrates the region where the uncracked (*yellow arrows*) carbonation readings and the cracked (*blue arrow*) carbonation readings were taken. Figure 3.8 further illustrates an example where carbonation has taken place on the concrete specimen on the left, which is highlighted in a red dashed line as compared to another concrete specimen on the right of the image where no carbonation has taken place.

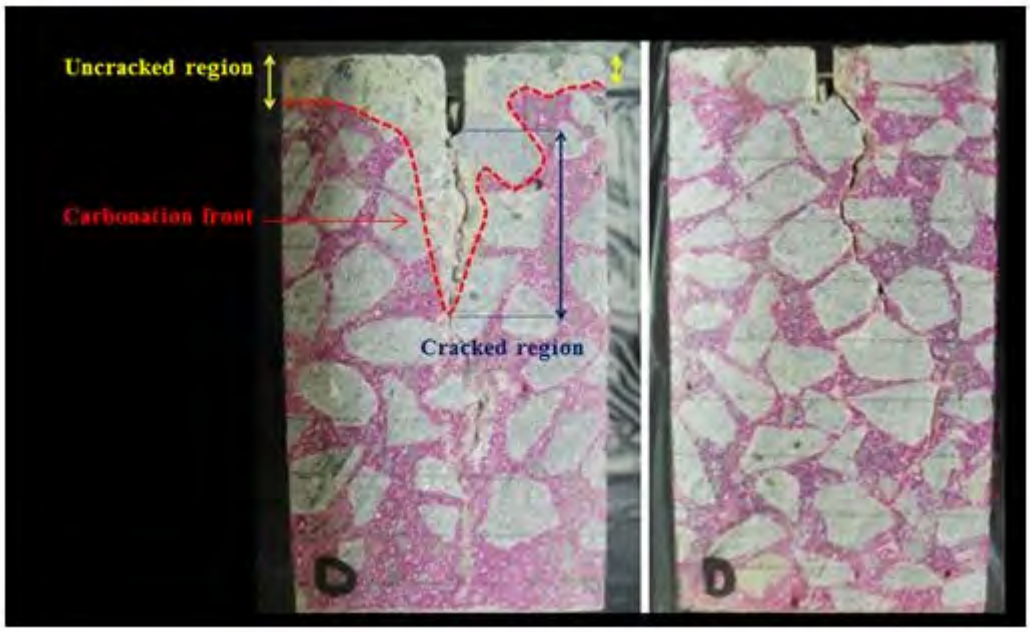

Figure 3.8 Image displaying where the carbonation front was measured in the cracked and uncracked regions in the various concrete specimens

3.7.3 Bulk diffusion Tests

The bulk diffusion test was performed according to ASTM C1556 procedure.

36 cracked concrete specimens were submerged in a 5% sodium chloride solution (Figure 3.9 (a)). Industrial NaCl salt and portable water was used to prepare the solution. The concrete specimens were initially exposed to the chloride solution for a period of 8 weeks.

Thereafter the specimens were removed from the sodium chloride solution and a 20 mm thick slice of concrete sawed off from one of the exterior sides of each specimen (Figure (b) & (c)). 10 mm intervals were then drawn using a lead-tipped pencil on the freshly exposed face as seen in (Figure 3.9 (d)). Crack profiles illustrating the reduction of crack width along the depth of the specimen were also recorded at 10 mm intervals as shown in Figure 3.10.

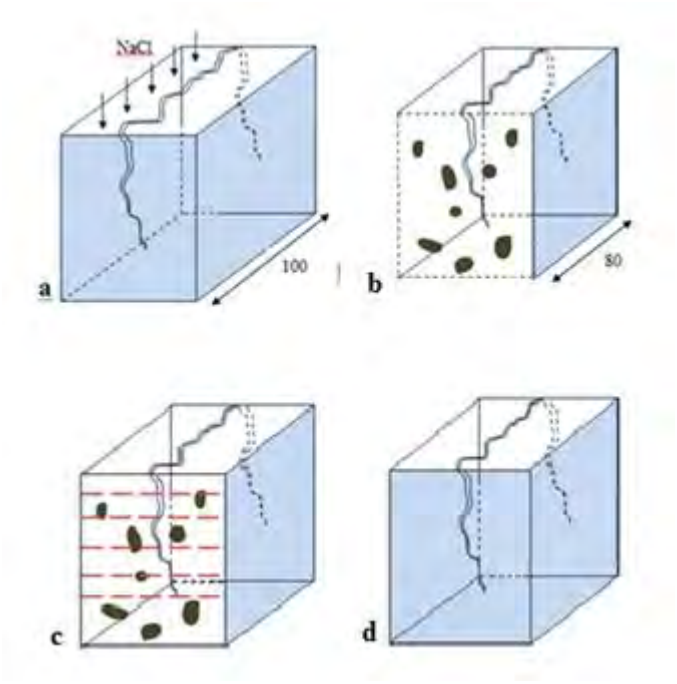

Figure 3.9 Schematic of procedure used to obtain chloride profile from bulk diffusion concrete specimens

Figure 3.10 illustrates two regions that were identified on each sawed specimen depending on the orientation of the crack. The uncracked region is seen outlined by the *yellow dashed box* and the cracked region is outlined in the *dark blue dashed box*. If the crack was skewed to the left or right of the specimen (i.e. the crack did not lie approximately in the centre of the specimen), the uncracked region selected was on the extreme right or left of the concrete face to avoid the cracked area.

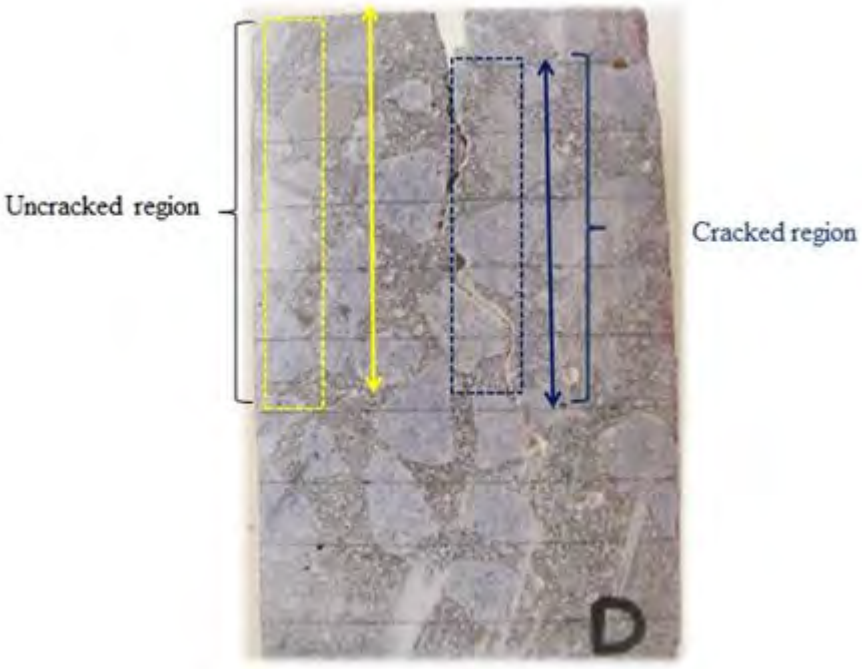

Figure 3.10 Image illustrating the cracked and uncracked region used when conducting the chloride profiles

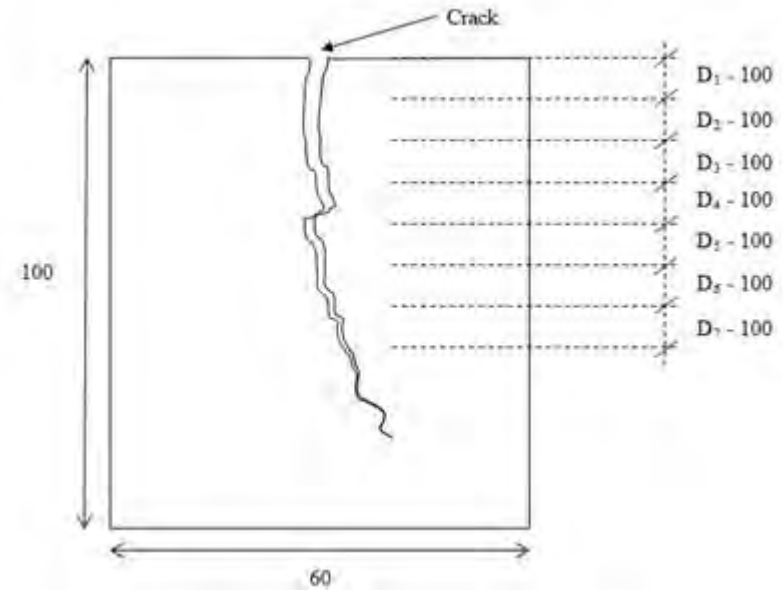

Figure 3.11 Schematic of the 10 mm depth intervals of a chloride specimen (dimensions in mm)

Chloride profiles were then obtained for a particular concrete for both the cracked and uncracked regions at six 10 mm intervals. The cracked region was cut off from the uncracked region. Using the notation in Figure 3.11, D_1 represented the face of concrete that was exposed to the solution. D_2 represented the next 10 mm interval depth of concrete below D_1. For the cracked specimen, 10 mm thick slices were cut to represent the various depth intervals D_1 to D_6. These slices were then pulverized into fine powder using a mechanical crushing machine. The powder was then acid-titrated using a Mettler Toledo DL 50 titration machine to determine the chloride content of the concrete at the various depths. The same procedure was followed to determine the diffusion coefficient of the uncracked concrete.

3.7.4 Durability Index tests

The three durability index tests were conducted according to the Durability Index Manual (Alexander *et al.,* 2009). Two 100 mm cores were removed from the remaining outer section of the beam specimens as shown in the Figure 3.12 below:

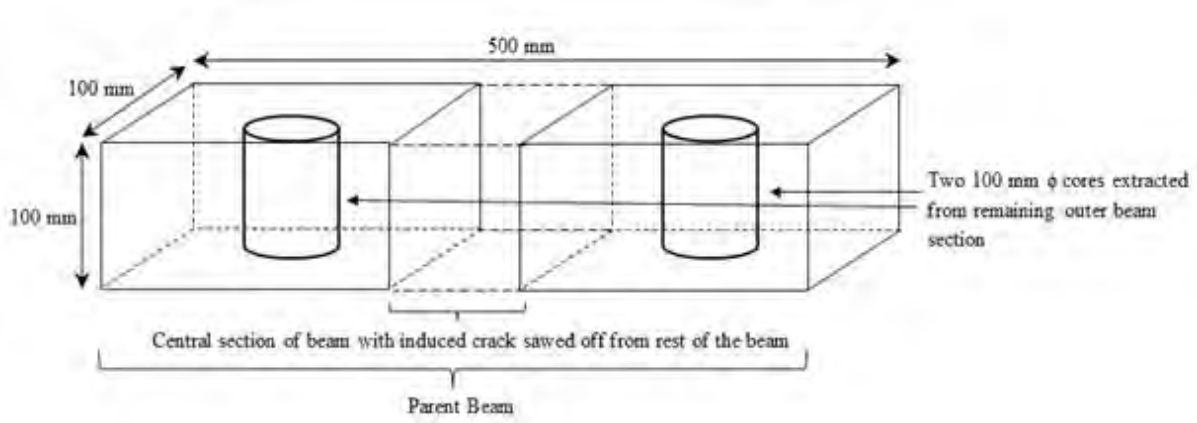

Figure 3.12 Schematic of cores that were obtained from the concrete beams for the DI testing.

For detailed information regarding the durability index testing procedure refer to Appendix A.

4 RESULTS & DISCUSSION

4.1 Introduction

This chapter presents, discusses and draws insights from the results, observations and trends from the tests that were outlined in Chapter 3. These tests include the Durability Index (DI) tests, accelerated carbonation tests and the chloride bulk diffusion tests.

The chloride profiling and carbonation depth measurements were conducted at two ages of 8 and 16 weeks after either being placed in a carbonation chamber or in 5% NaCl solution. The results presented in this chapter are based on the 16 week exposure period. These results provided a more defined representation of the transport properties in the cracked concrete than the results from short exposure (8 week).

The Durability Index tests are conventionally conducted after 28 days of the concrete being cast as stipulated in the Durability Index Testing Manual. However, in this study the tests were conducted after 8 and 16 weeks, corresponding to the same testing age as the chloride profiling and carbonation depth measurements. This was to ensure that the durability parameters that were obtained in the uncracked concrete specimens at a later age were a more realistic characterization of the concrete properties and could be compared with the durability parameters that were obtained in the cracked concrete specimens at the same age of the concrete. The latter testing age further allowed for the beneficial pozzolanic effects of supplementary cementitious materials to develop in the concrete and their influence on durability properties to be measured.

A 95% confidence interval was used to present the variability for all sets of results. Grubb's outlier test was used to identify and remove any outliers (refer to Appendix B for further details). Furthermore ANOVA's were conducted as a statistical method to determine the respective p-values and highlight the statistical significance of the data obtained (Underhill & Bradfield, 2007). The complete set of as-measured test results can be found in Appendix C through to Appendix F.

4.2 Durability Index Test Results

4.2.1 Oxygen permeability Index

The coefficient of oxygen permeability (k) was determined for each concrete and converted to an OPI value by taking the negative logarithm of the oxygen permeability value as seen in Table 4.1. High OPI values indicate less permeable (higher quality) concrete with regards to oxygen ingress, whereas low OPI values indicate a more permeable concrete.

Table 4.1Summary of oxygen permeability coefficient (k) and OPI results at week 16

Mix	Coefficient of oxygen Permeability, k (m/s) x 10^{-11}	OPI (-Log k)	Mix	Coefficient of oxygen Permeability, k (m/s) x 10^{-11}	OPI (-Log k)
PC-0.40	15.20	9.82	PC-0.55	16.32	9.79
PC/FA-0.40	6.68	10.18	PC/FA-0.55	12.53	9.90
PC/GGBS-0.40	11.00	9.96	PC/GGBS-0.55	14.30	9.84

Prior to interpreting of the OPI results, it is important to note that the OPI scale is a logarithmic one.

Influence of w/b ratio on oxygen permeability

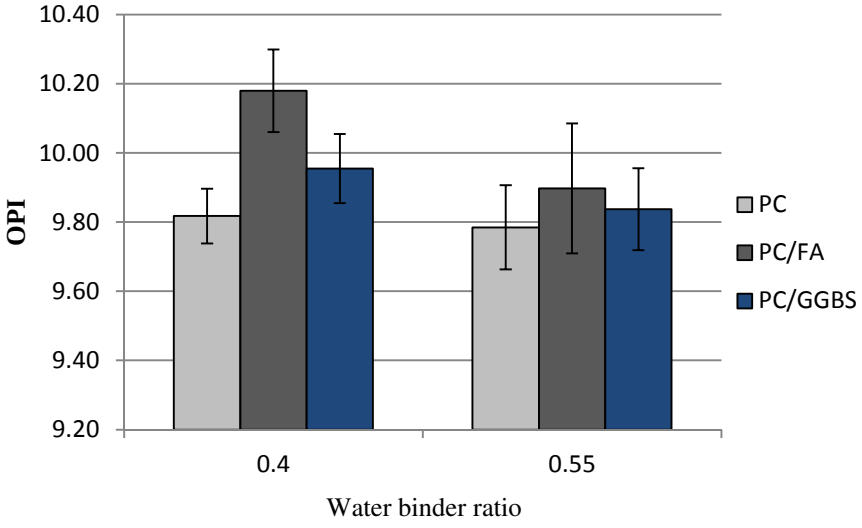

Figure 4.1 Summary of OPI results at week 16

When evaluating the influence of the w/b ratio's on the OPI results, the 0.40 w/b mixes yielded higher OPI values than the 0.55 w/b ratio mixes (Figure 4.1). This trend was observed for all three binders investigated. This result was expected from literature (Ballim *et al.,* 2009), and is explained by an increase in porosity of the concrete as a result of increasing capillary porosity within the concrete matrix when using higher w/b ratios. This concept has been well documented in literature (Mackechnie., 1996; Alexander *et al.,* 1999; Ballim *et al.,* 2009).

The 0.40 and 0.55 PC concrete obtained mean OPI values of 9.82 and 9.79 respectively. An analysis of the PC concrete means using an ANOVA test produced a corresponding p-value of 0.001, this indicated a statictically signifincant difference between the two mean OPI values obtained. The 0.40 PC concrete produces a 7% less permeable concrete when compared to the 0.55 PC concrete.

In the case of the PC/FA concrete, the 0.40 and 0.55 mean OPI value obtained were 10.10 and 9.90 respectively. The corrsponding p-value for this set of data was 0.004, this result illustrated a statistical significant difference in the two means obtained. The 0.40 PC/FA concrete produced a substantial 47% less permeable concrete when compared to the 0.55 PC/FA concrete.

Lastly, the 0.40 and 0.55 PC/GGBS concrete obtained mean OPI values of 9.69 and 9.84 respectively. The corresponding p-value was 0.084 for this data set. In contrast to the other p-values obtained for the PC and PC/FA mix, this value was greater than 0.05, implying that there was no statistically significant difference in the mean OPI values obtained for the PC/GGBS concretes. However it must be noted that although the 0.40 PC/GGBS concrete produced a 23% less permeable concrete as compared to the 0.55 PC/GGBS concrete, there was no statistical significant effect of the w/b ratio on the OPI value obtained for this type of concrete mix.

It can be seen that for all three binders investigated, the lower w/b ratio of 0.40 produced greater OPI values when compared to the 0.55 OPI values, indictative of less permeable, higher quality concrete.

Influence of binder types on oxygen permeability

When comparing the influence of binder type, the results illustrated that the replacement of PC with 30% and 50% of FA and GGBS respectively improved durability properties of the concrete. The supplementary binders refine the pore structure which inherently reduces the permeability by decreasing the interconnectivity of the pores (Ramezanianpour ***et al.,*** 1995).

It must be noted by the reader that for both sets of w/b ratios (0.40 & 0.55) investigated the OPI values generally increased in the following order: FA > GGBS > PC. It can be seen that the effect of using of supplementary binders on OPI values was more prominent for the 0.40 concrete mixes than in the 0.55 concrete mixes. When comparing the mean OPI values obtained for the 0.40 mixes, the p-value obtained was 0.0006. This result showed strong statistical evidence that there is a significant difference between the means OPI values obtained. However, in the case of the 0.55 mixes, a p-value of 0.469 (greater than 0.05) was obtained showed that there was no statistical difference when comparing the mean OPI values for the different concrete mixes.

It can be seen that the partial replacement of PC with 30% fly ash, significantly improved the concrete's permeability compared to both the PC and GGBS (0.40 & 0.55 w/b) mixes. For the 0.40 w/b ratio concrete, the PC/FA concrete was 57% and 40% less permeable when

compared to the PC and PC/GGBS concretes respectively. In the case of the 0.55 w/b ratio concrete, the PC/FA concrete was 24% and 13% less permeable compared to the PC and PC/GGBS concrete respectively. Similar results were illustrated in work done by Hassan *et al,.* (2000), which showed that the inclusion of FA (30% by replacement) lead to relatively poor permeability characteristics at 28 days however after a long period (one year) produces improved concrete permeability properties compared to PC concrete.

The FA concretes performed better possibly due to the microstructural modification caused by FA as a supplementary binder (Swamy, 1997). Firstly, literature has shown that during the hydration process, large spaces between the cement grains are filled with hydration products. Over time the pozzolanic reaction of fly ash with water and calcium hydroxide continues to produce more impermeable products that increase the density of the concrete matrix leading to pore refinement (Thomas & Matthews, 1992). Secondly, soluble calcium hydroxide that is present in the concrete is converted to cementitious compounds that decrease bleed channels, capillary channels and void spaces and thereby reduce permeability with time (Young , 1988). Lastly, according to Isaia *et al.,* (2003) the reduced permeability can be attributed to the fine FA particles which act like micro-aggregate that fill voids in the concrete.

Similarly it can be seen that the partial replacement of PC with 50% GGBS also increased the permeability of the concrete in comparison to the PC mixes. A 28% and 13% permeability increase was observed in the 0.40 and 0.55 PC/GGBS concrete mixes respectively in comparison to the PC concrete mixes; however the increase was not as pronounced as that in the FA mixes. GGBS concrete increased permeability according to Swamy (1997) is due to the hydraulic activity when it reacts with water and PC. During hydration, GGBS reacts with calcium silicate to produce additional calcium-silicate-hydrate. This leads to large pores in the matrix being filled with CSH gels and producing a denser cement paste. This inherently reduced the permeability of the concrete matrix (Regourd, 1980; Malhotra, 1987).

4.2.2 Chloride conductivity test

This test measures the penetrability of chlorides in concrete by recording the current that pass though each specimen and using Equation 2.31 to determine the equivalent chloride conductivity index value. Low CCI values are indicative of a concrete's resistance to ionic ingress, whereas high CCI values are indicative of reduced resistance to chloride ion transport (Mackechnie., 1996). Table 4.2 shows a summary of the chloride conductivity results that were obtained for all six concrete mixes.

Table 4.2 Summary of chloride conductivity results at week 16

Mix	Chloride Conductivity, σ (mS/cm)	Mix	Chloride Conductivity, σ (mS/cm)
PC-0.40	0.92	PC-0.55	1.29
PC/FA-0.40	0.72	PC/FA-0.55	1.25
PC/GGBS-0.40	0.24	PC/GGBS-0.55	0.51

Influence of w/b ratios on chloride conductivity

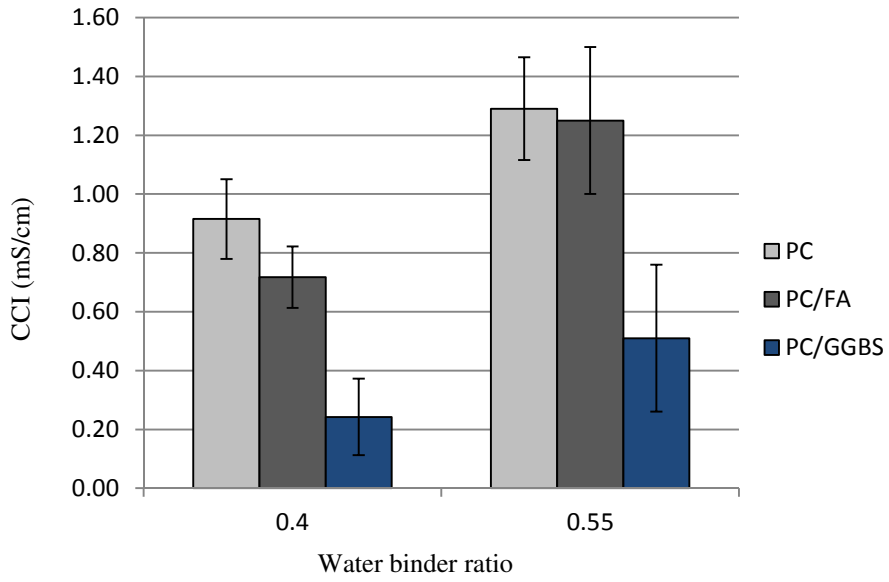

Figure 4.2 Summary of CCI results at week 16

From Figure 4.2 the use of higher w/b ratio of 0.55 resulted in higher CCI values (for each all three binders investigated) in contrast to the 0.40 concretes. This can be explained by the decrease in the overall capillary porosity of the concrete as the w/b ratio increases, which has been well documented in literature. This inherently permits the diffusion of ionic species into the concrete which can alter the chemical composition of the concrete (Sutter *et al.,* 2008).

The statistical analysis of the effect w/b ratio (0.40 & 0.55) on the mean CCI values obtained produced p-values of 1.3E-09 and 4.6E-07 for the PC and PC/FA mix respectively, hence there was a statistical difference in the mean CCI values. When comparing the influence of w/b ratios (0.40 and 0.55)on CCI values, the results indicated a 29.0% and 42.6 % decrease comparing the PC and PC/FA mix respectively. In the case of the PC/GGBS mix, a 52.5% decrease in mean CCI value was attained when comparing the 0.40 and 0.55 results. However, the p-value of 0.13 indicated that there was no statically significant difference for the mean CCI values obtained for the 0.40 and 0.55 PC/GGBS mixes.

Hence it can be seen that for all three concretes investigated that the lower w/b ratio of 0.40 produced lower CCI values in comparison the 0.55 concrete mixes. This can be attributed to denser concrete matrix in the 0.40 concrete mixes characterised by lower capillary porosity, which subsequently reduced the diffusion of ions in the concrete.

Influence of Binder Type on chloride conductivity

The results show that the inclusion of supplementary binders (FA and GGBS) significantly reduced the CCI values for a given w/b ratios (0.40 and 0.55). The mean CCI values generally decreased in the following order: GGBS > FA > PC. The p-value when comparing the different binders of the 0.40 and 0.55 mixes were 4.3E-06 and 7.8E-05 respectively. This implied that there was a statistical significant difference between the different mean CCI values obtained for a given w/b ratios.

It can be seen that the use of supplementary binders was most prominent in the PC/GGBS mixes. The 0.40 PC/GGBS mix showed a 73.5% and 66.2% decrease in CCI value when compared to the PC and PC/FA mix respectively. A similar trend was observed for the 0.55 PC/GGBS mix, with a 60.4% and 59.2% decrease in CCI value when compared to the PC and PC/FA mix respectively. The trend of attaining low CCI values may be attributed to the refined pore structure of GGBS concrete and its inherent low electrical conductivity. The results agree well with those documented in literature which have shown a reduction in CCI value due to the inclusion of supplementary binders (Mackechnie, 1996; Ballim *et al.,* 2009).

Furthermore the use of FA showed a significant improvement in CCI values obtained, however the influence was not as substantial when compared to the PC/GGBS mixes. The 0.40 PC/FA mix showed a 21.5% decrease in CCI value compared to the 0.40 PC mix. Whereas the 0.55 PC/FA showed a 3.1 % decrease compared to the 0.55 PC mix. This effect can be related to the beneficial effect of pore refinement in the paste fraction of the concrete, which reduces the rate of diffusion of species into the concrete (Nikam & Tambvekar, 2003).

4.2.3 Water Sorptivity test

This test assesses the potential of concrete to absorb and transmit water by capillary suction. The test gives an indication of the possible macroscopic pore structure changes as a measurement of the changes in mass for partially submerged specimens. Table 4.3 shows a summary of the sorptivity as well as the porosity result for all the concrete mixes investigated.

Table 4.3 Summary of sorptivity test results at week 16

Mix	Sorptivity ($mm/hr^{0.5}$)	Porosity (%)	Mix	Sorptivity ($mm/hr^{0.5}$)	Porosity (%)
PC-0.40	9.9	10.8	PC-0.55	11.35	10.3
PC/FA-0.40	11.6	8.5	PC/FA-0.55	9.75	11.0
PC/GGBS-0.40	8.5	8.1	PC/GGBS-0.55	10.9	9.3

Influence of w/b ratios on sorptivity

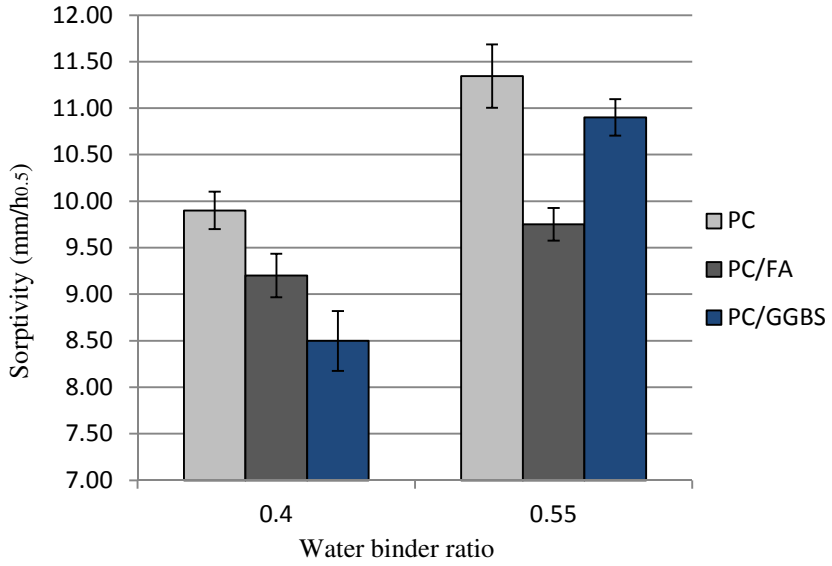

Figure 4.3 Summary of WSI results at week 16

When evaluating the influence of w/b ratio on sorptivity, it can be seen from Figure 4.3 that for all three concretes investigated (PC, PC/FA & PC/GGBS), the sorptivity properties of the concretes increased with increasing w/b ratio. This result implied that concretes with higher w/b ratios will experience greater rates of water absorption into the concrete through capillary action. Similar results have been documented by Parrot (1992), Dhir *et al.,* (2004) and Kolias & Gerorgiou (2005) and have been attributed to the increased pore refinement as the w/b ratio decreases.

P-values of 6.6E-09, 2.0E-12 and 4.1E-07 were attained when carrying out a statistical analysis comparing the 0.40 mixes to the 0.55 mixes for the PC, PC/FA and PC/GGBs mixes respectively. The results indicated that the mean WSI values that were obtained were statistically difference for the two w/b ratios that were being compared for all three concretes. There was a 12.7%, 5.7% and 22.0% increase in WSP index value when comparing the 0.40 and 0.55 WSI values for the PC, PC/FA and PC/GGBS mix respectively.

Influence of binder types on sorptivity

A comparison of the results showed that the use of FA and GGBS is very beneficial in decreasing the sorptivity properties of the concrete specimens when compared to PC concrete. In the case of the 0.40 mixes, the WSP index generally decreased in the following order: PC > FA > GGBS. In contrast to the 0.55 mixes, where the WSP index decreased in the following order: PC > GGBS > FA. P-values of 2.9E-05 and 6.1E-06 were obtained when comparing the different binders (PC, PC/FA and PC/GGBS) for a particular w/b ratio (0.40 and 0.55). This denoted that there was a statistical difference between the WSI values that were obtained.

Figure 4.3 illustrates that sorptivity of the concrete decreases with the addition of fly ash. The reason of lower sorptivity of FA concrete (compared to PC and GBBS concrete) can be attributed to the pozzolanic reaction (Gopalan, 1996; Joseph & Ramamurthy, 2009). Uysal & Akyuncu (2012) stated that during hydration, fly ash reacts with free lime to produce bermorite gels in addition to the silicate gels of the cement. Capillary pores of fly ash concrete are thus filled in this manner, lowering the sorptivity. Furthermore, the fine-filler effects of fly ash, results in better packing arrangement of particles in the system (Yahia ***et al.,*** 2005). Hence an denser adequate concrete interface is achieved to reduce sorptivity behaviour.

It can also be seen that the sorptivity decreases for concretes that contain GGBS relative to the PC concretes. The reason can be explained by the refined pore structure of the concrete matrix due to the formation of the secondary CSH gel from the pozzolanic reaction of slag (Hadjsadok ***et al.,*** 2012). This has been confirmed by other researchers, particularly for mixes that contain higher than 50% GGBS content (Guneyisi ***et al.,*** 2008).

It must be noted that the water sorptivity results do not match the oxygen permeability results, which one might expect. One possible explanation is that the water sorptivity and oxygen permeability measure two different characterises of the pore structure of concrete. The influence of tortuosity and the interfacial zone on water sorptivity is different to that of oxygen permeability (Elahi ***et al.,*** 2010).

4.3 Accelerated Carbonation Tests Results

4.3.1 General Observations

Figure 4.4 shows a summary of the accelerated carbonation depth measurements on the concretes specimens after 16 weeks of exposure in the carbonation chamber. The errors bars indicate the standard deviation for each set of carbonation depth readings taken. From Figure 4.4, the general trend noted was that of an increasing carbonation depth was obtained with an increasing w/b ratio for all three binders investigated. This trend was also present in both the uncracked region of the concrete and the cracked region (w_{cr1} (0.1-0.4mm) and w_{cr2} (0.5-0.8mm) crack width) of the concrete specimens (for all three binders investigated).

This trend can be attributed to the effect of increasing w/b ratio on the permeability of concrete, which resulted in higher porosity of the concrete. Consequently, the more porous structure of the concrete permitted greater ingress of carbon dioxide, which led to the increased rate of carbonation exhibited by the increased carbonation depth results in the cracked concrete specimens (Song & Kwon, 2007).

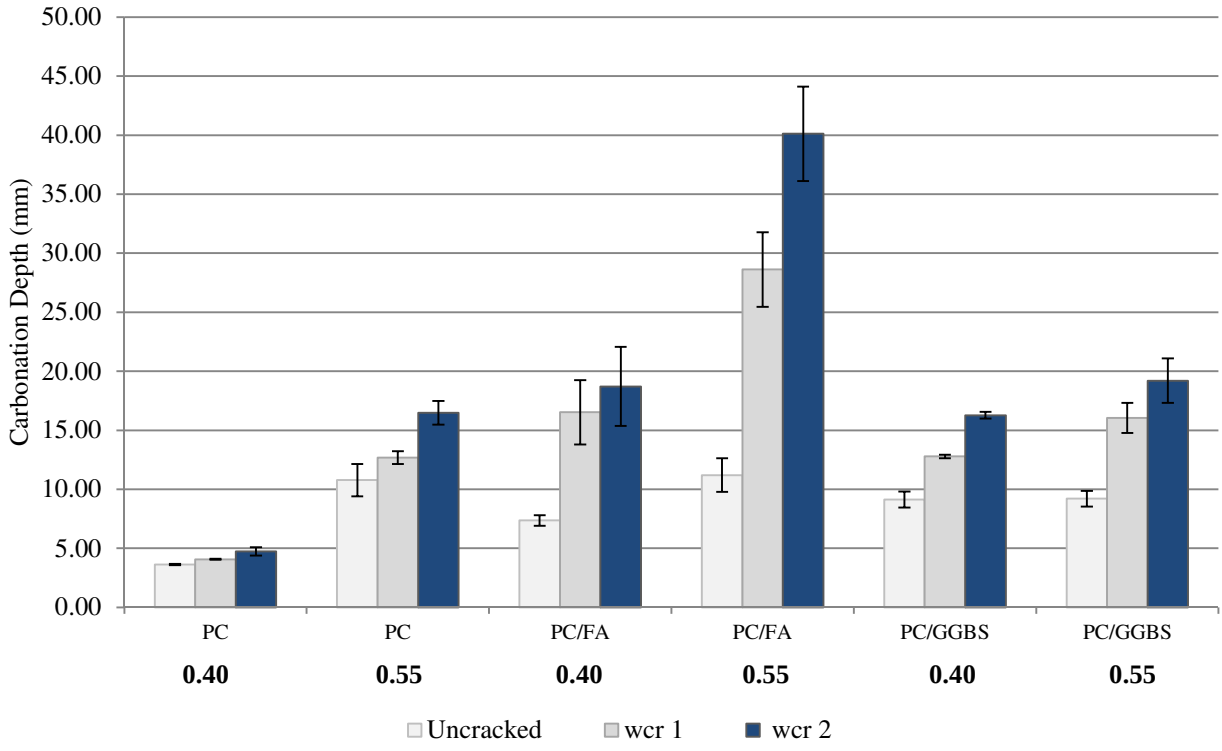

Figure 4.4 Summary of carbonation depths (mm) readings after 16 weeks of exposure in the carbonation chamber

4.3.2 Effect of cracks on carbonation depth

Figure 4.4 illustrated the average carbonation depths recorded for the uncracked region of the specimen and cracked width regions (w_{cr1} & w_{cr2}), for a given binder type. The influence of w/b ratio (0.40 & 0.55) on concrete carbonation can also be observed

The general trend expressed in Figure 4.4, is that the specimens with the greater the crack width range (w_{cr2}) exhibited higher carbonation depths compared to those with small crack width range (w_{cr1}) and the uncracked concrete specimens. This trend could possibly be explained by the increased surface area of the exposed concrete face (as a result of the induced crack) in contact with carbon dioxide gas. This increased surface area in the cracked concrete specimen led to greater carbonation taking place in specimens as a result of more carbon dioxide being allowed to diffuse into the concrete matrix, noted by the increased carbonation depths recorded.

However in the PC mixes the presence of cracks for both crack width ranges (w_{cr1} & w_{cr2}), did not show a significant increase in the carbonation depth for the cracked specimens as compared to the uncracked specimens. It can be seen that this results did not fit the general trend of increasing crack width leading to increase carbonation depth (as seen in PC/FA & PC/GGBS mixes), this result was noted and taken into consideration when carrying out further analysis using this data. One possible reason can be attributed to the cracks exposing unhydrated cment particle leading to self healing and crack closure. It would be recommended that further investigation be conducted, to determine the crack width range at which carbonation particularly in cracked PC concrete significantly differs to that in carbonation in uncracked PC concrete.

It is notable that for both the uncracked and cracked PC-0.40 specimens (Figure 4.4) little carbonation (less than 5 mm depth) occurred after 16 weeks. The influence of cracks on carbonation was slightly more pronounced in the PC-0.55 specimens. The carbonation depth in the uncracked concrete specimens measured 10.8 mm as compared to the carbonation depth of 12.7 mm and 16.5 mm for the w_{cr1} and w_{cr2} crack width range specimens respectively.

The influence of crack width on carbonation in the blended PC/FA concretes was more distinct (Figure 4.4) in contrast to the PC concrete. The carbonation depth in the uncracked concretes, 0.40 PC/FA and 0.55 PC/FA, measured 7.4 and 11.2 mm respectively. For the 0.40 PC/FA mix, the w_{cr1} specimens measured carbonation depths of 16.5 mm as compared to 18.7 mm in the w_{cr2} specimens. The difference between carbonation depth in the uncracked and the cracked specimens w_{cr1} and w_{cr2} was in the range of 9.1 mm (1.2 times greater) and 11.3 mm (1.5 times greater) respectively. In the case of the 0.55 PC/FA mix, the $_{wcr}1$ specimens measured 28.6 mm as compared to 40.1 mm in the w_{cr2} specimens. Hence the difference between the uncracked and the cracked specimens $_{wcr}1$ and w_{cr2} was in the range of 17.4 mm (1.6 times greater) and 28.9 mm (2.9 times greater) respectively.

Furthermore Figure 4.4 highlights the influences of cracks width on carbonation depth for blended PC/GGBS concrete specimens. The uncracked PC/GGBS concrete specimens (0.40

& 0.55) had carbonation depths of 9.13 and 10.3 mm. For the 0.4 PC/GGBS mix, the w_{cr1} specimens measured carbonation depths of 12.8 mm as compared to 16.3 mm in the w_{cr2} specimens. Hence the difference between carbonation depth in the uncracked and the cracked specimens w_{cr1} and w_{cr2} was in the range of 3.67 mm (0.4 times greater) and 7.17 mm (0.8 times greater) respectively. In the case of the 0.55 PC/FA mix, the w_{cr1} specimens measured carbonation depths of 16.1 mm as compared to 19.2 mm in the w_{cr2} specimens. Hence the difference between the uncracked and the cracked specimens w_{cr1} and w_{cr2} was in the range of 5.8 mm (0.6 times greater) and 8.9 mm (0.9 times greater) respectively.

It can be seen from all three binder investigated that both the uncracked and cracked 0.55 concrete specimens have exhibited greater carbonation depths than the 0.40 concrete specimens. This trend can be attributed to the increased permeability in the concrete mixes as a result of increasing capillary porosity within the concrete matrix when using higher w/b ratios. Hence, there was greater volume of carbon dioxide that was able to diffuse into the more permeable concrete to facilitate carbonation.

4.3.3 Effect of binder type on carbonation depth

Figure 4.4 furthermore illustrated the influence of binder type (PC, FA & GGBS) on carbonation in uncracked and cracked (w_{cr1} & w_{cr2}) concrete specimens.

Generally, the results show that the use of supplementary binders increased carbonation for the uncracked concrete. This trend was expected from literature for uncracked concrete specimens (Meyer, 1969; Papadakis *et al.,* 1992; Papadakis, 2000) and is explained by the increase percentage of $Ca(OH)_2$ that is present in PC concrete specimens that increased its resistance to carbonation when compared to blended (PC/FA and PC/GGBS) concrete specimens. Similar carbonation depth trends were also observed for the concrete specimens with the two crack width ranges (w_{cr1} & w_{cr2}).

As can be seen in Figure 4.4 the PC mixes have the greatest resistance to carbonation in both (0.40 & 0.55 w/b) uncracked and cracked (w_{cr1} & w_{cr2}) concrete specimen. The 0.40 PC specimens measured 3.6 mm as compared to 7.4 mm and 9.1 mm for the PC/FA and PC/GGBS specimens respectively. The same trend was also observed in the 0.55 PC specimens. According to Meyer (1969) and Papadakis (2000) this can be attributed to the increased volume of $Ca(OH)_2$ (i.e. carbonatable material) that is available for carbonation in PC concrete, and as a result this reduces the progression of carbonation into the concrete. Whereas in concretes with supplementary binders (FA and GGBS) for a given w/b ration less $Ca(OH)_2$ is available hence the rate of carbonation is increased which is agreement with work done by (Parrot, 1987).

Generally, the addition of FA in concrete resulted in increased carbonation when compared to the PC (0.40 & 0.55) and the PC/GGBS (0.40 & 0.55) concretes. This trend was observed in both uncracked and cracked concretes. This result was anticipated for the uncracked concretes as literature (Parrott, 1987) has shown that through the use of FA in concrete, the calcium hydroxide components in the cement paste are reduced. As a result the total amount

of carbonatable material is decreased due to the decrease in total $Ca(OH)_2$ when compared to Portland cement (Papadakis *et al.,* 1992; Papadakis , 2000). Furthermore, the calcium hydroxide that is present in the concrete carbonates as well as the calcium silicate hydrate (CSH), which is the main product of the pozzolanic reaction.

In the case where GGBS was used, carbonation depths were higher when compared to those in PC (0.40 &0.55) concrete. However the effect of slag on carbonation was not as prominent as compared to the carbonation in PC/FA (0.40 & 0.55) concrete. GGBS is known to have as a higher fineness than FA. Hence GGBS concrete is reported (Shi *et al.,* 2009) to produce better penetration resistance, due to a denser concrete matrix. In addition the low calcium hydroxide content resulted in better carbonation resistance in comparison to FA concrete.

4.4 Analysis of carbonation coefficient results for uncracked and cracked concretes based on gaseous diffusion

In order to draw any comparison between the effects of cracks on transport properties (gaseous diffusion of carbon dioxide) in concrete, the carbonation coefficients had to be determined from the oxygen permeability index results (uncracked concrete) and the accelerated carbonation results (cracked concrete). In order to proceed Equation 2.14 (equation used to model carbonation) had to be applied to determine the corresponding carbonation coefficients in the two scenarios. Recalling Equation 2.14 below:

$$\boldsymbol{D = At^n}$$

In the following sections, an explanation will be provided to make the reader aware of how the carbonation coefficient was obtained (in respect of the above equation) in the case of the OPI results and using the accelerated carbonation readings.

OPI - Carbonation coefficient

The OPI results that were obtained (Section 4.2.1) characterised the oxygen permeability of the six concrete mixes with respect to concrete specimens that were uncracked. The DI carbonation prediction model was then used to establish a correlation between the OPI values obtained and carbonation behaviour of the concrete, with respect to the carbonation coefficient for "uncracked concrete". The model also accounted for the environmental influences as well as the various binder types when predicting the carbonation behaviour of a given concrete (Refer to Section 2.14.1 for further details on the DI carbonation prediction model). The carbonation prediction model was used to determine the equivalent carbonation coefficient (A), corresponding power value (n) based on the OPI values obtained with the corresponding binder type and environmental condition.

Table 4.4 shows the input parameters and corresponding outputs that were determined using the DI prediction model for carbonation. Binder input "1", "3" and "4" were used to represent the use of 100% PC, 30% FA and 50 % GGBS respectively which were the various binders types used in the concrete mixes tested. The environmental input "10" was used as opposed to number "20" and "30" as the concrete specimens tested were kept in a control room at

room temperature prior to carrying out the tests; this best simulated a dry inland environmental condition.

Table 4.4 Input and output parameters obtained using OPI values and DI carbonation prediction model

MIX	INPUT			OUTPUT	
	OPI	BINDER*	ENVIRONMENT*	CARBONATION COEFFICIENT	n
PC-0.40	9.82	1	10	5.22	0.33
PC/FA-0.40	10.18	3	10	2.46	0.40
PC/GGBS-0.40	9.96	4	10	4.15	0.33
PC-0.55	9.79	1	10	5.45	0.33
PC/FA-0.55	9.90	3	10	4.61	0.40
PC/GGBS-0.55	9.84	4	10	4.92	0.33

*** Note the following notation was used as per the prediction model to represent the type of binder and environment used:**
Binder: 1 – 100% PC, 2 - 10% SF, 3 - 30% FA, 4 - 50% GGBS, 5 - 50% CS
Environment: 10 – Dry inland (R.H. 60%), 20 – Coastal (R.H. 80%), 30 – Partly wet (R.H. 90%)

Following Table 4.4, it can be seen that carbonation coefficients obtained from the model generally increases in the following order: PC > GGBS > FA. The 0.40 w/b ratio mixes produced lower carbonation coefficients in comparison to the 0.55 w/b ratio mixes. This result was expected due increase in porosity of the concrete as a result of increasing capillary porosity within the concrete matrix when using higher w/b ratios. This in turn increased the ingress of carbon dioxide to into the concrete matrix, promoting a greater rate of carbonation within the concrete.

With respect to the use of different binder types for a given w/b ratio, it can be seen that the carbonation coefficient followed a general trend of increasing from FA < GGBS < PC.

Accelerated carbonation – Carbonation coefficient

In order to determine the carbonation coefficient from the accelerated carbonation results, a few considerations were necessary to account for the difference in accelerated and natural environments. Having considered the carbon dioxide concentrations shown below:

- The carbonation chamber maintained a carbon dioxide concentration of 2.0 %
- The natural atmosphere has a carbon dioxide concentration of 0.039%

It can be seen that the carbon dioxide concentration in the carbonation chamber is approximately 51 times greater than that of the natural atmosphere. This relationship was assumed to be linear based on research conducted by Cui *et al,*.(2015) owing to the low carbon dioxide concentration of 2.0% used in this study. Applying this acceleration factor (51) to the exposure duration of 16 weeks, results in 816 weeks of natural exposure time to

achieve the same rate of carbonation. This equated to approximately 16 years. Equation 2.17 (formula used to model carbonation) was then rewritten with the carbonation coefficient as a function of carbonation depth and exposure period as shown below:

$$D = At^n$$

$$\therefore A = {}^{d}/_{t^n} \qquad \textbf{Equation 4.1}$$

By using Equation 4.1, the carbonation depth (d) results that were obtained for the cracked specimens were used to determine the respective carbonation coefficient, based on the 16 weeks (t) of accelerated exposure. The power exponents (n) that was obtained from the DI prediction model were used, to ensure that the similar conditions are compared. Once this was done, it was then possible to compare the carbonation coefficient from the uncracked (DI) specimens with the cracked specimens.

4.4.1 Verification of carbonation coefficient from OPI and Uncracked carbonation reading

The main focus of this study was to assess the influence of cracks on the transport properties of concrete with a particular focus on the DI testing approach. Hence in order to compare the output from the DI models to the measured carbonation results, the accuracy of the results from the DI testing approach needed to be checked, with respect to its ability to predict carbonation depth within reasonable accuracy. Figure 4.10 illustrates the carbonation coefficients that were obtained from the OPI values (Model), plotted against the actual (measured) accelerated carbonation coefficients.

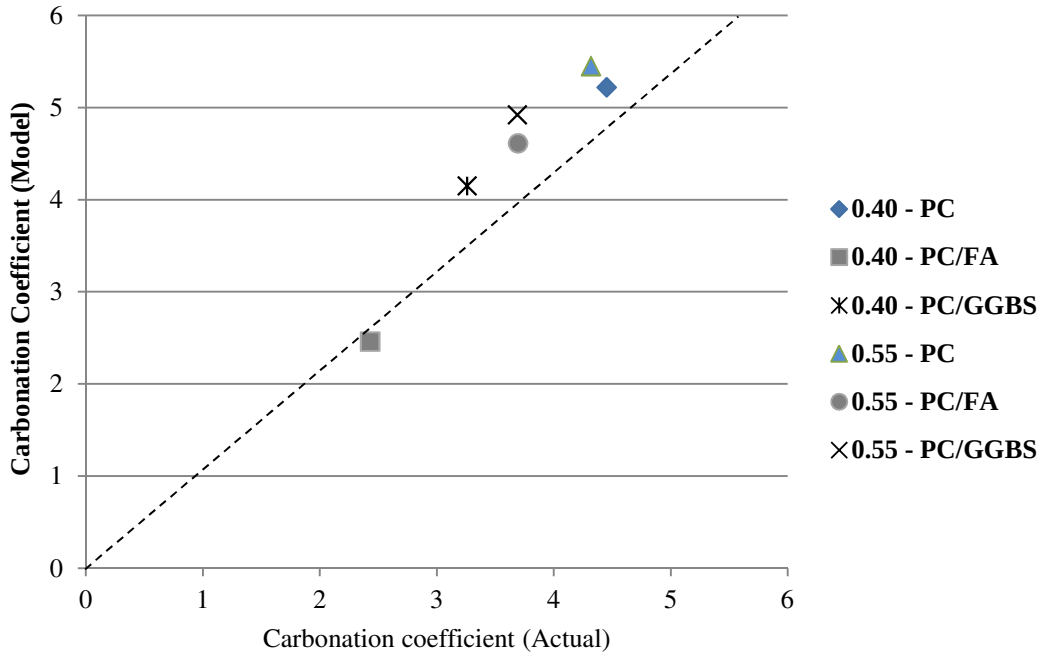

Figure 4.5 Actual carbonation coefficient vs model carbonation coefficient

Figure 4.5 above serves to illustrate the accuracy of the OPI model to predict the carbonation behaviour in concrete, based on the carbonation coefficients that were obtained and compared

with the actual measured carbonation coefficients. Data points that fall on the forty five degree line indicate that the predicted DI carbonation coefficients are the same as the carbonation coefficients obtained from the measured accelerated carbonation results.

A 0.961 product moment correlation coefficient was obtained for the data points (for both w/b ratios (0.40 & 0.55) and the three binders used (PC, FA & GGBS)). It can be seen that all the data points do not lie on the 45 degree line, there was a 0.04 variability present in the results that were obtained. It can also be noted that the carbonation coefficients obtained from the DI prediction model were relatively higher than the measured carbonation coefficient (except for the 0.40 PC/FA mix).

The aim of the study was to not correct or modify the accuracy of the DI prediction model but to note the difference between the predicted model and measured values. Furthermore it ensured that there was not a substantial difference between the two variables as this would not provide an appropriate context to compare results and draw any conclusion.

4.4.2 Comparison of the carbonation coefficients obtained from the OPI results and the cracked carbonated concrete

It is noticeable that the carbonation coefficient (k) obtained is dependent on a number of factors such as environmental conditions (e.g. CO_2 concentration and humidity) and concrete characteristics (e.g. w/c ratio, type of cement). The carbonation coefficient (k) may range from 1 to 12 according to the concrete/environmental conditions of the concrete in question (CEB, 1992).

However in this study, the carbonation coefficients were determined in order to assess the diffusivity of carbon dioxide into uncracked and cracked concrete. Figure 4.6 to Figure 4.8 illustrates the carbonation coefficients that were obtained from the uncracked OPI test, and the carbonation tests (uncracked, w_{cr1} & w_{cr2}) for a given binder type for both w/b ratios (0.40 and 0.55).

A general trend observed from the actual carbonation specimens was that an increased carbonation coefficient was obtained in the cracked concrete specimens as the crack width increased (w_{cr1} & w_{cr2}) for all three concrete mixes investigated. This result was expected as the presence of cracks created paths in the concrete matrix which increased the ease with which carbon dioxide could diffuse into the concrete matrix and thus increase the rate of carbonation. However, it should be noted that the magnitude of the difference between the uncracked and cracked carbonation coefficient was of interest, as this was an indication of the degree to which the transport properties of the concrete were modified as a result of the presence of cracks.

Furthermore, a general trend observed was that the carbonation coefficients obtained from the OPI specimens were greater than that of the actual uncracked carbonation specimens for all three concrete mixes investigated.

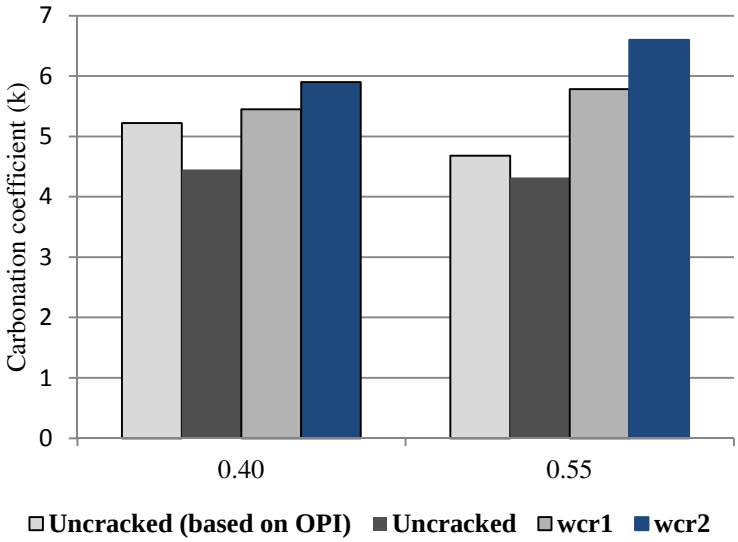

Figure 4.6 Carbonation coefficient for uncracked (OPI) and cracked PC concrete

In Figure 4.6 the actual carbonation coefficients that were obtained for the 0.40 PC specimens ranged from 4.45 for the uncracked specimen to 5.90 for the w_{cr2} specimen. The carbonation coefficients for the 0.40-w_{cr1} and 0.40-w_{cr2} concrete specimens were 22.% and 33% times respectively greater than the corresponding uncracked carbonation coefficients. Furthermore, the uncracked OPI carbonation coefficient for the 0.40 PC speciemen was 17% greater than the actual 0.40 PC uncracked carbonation coefficient.

Similarly with the 0.55 PC concrete the actual carbonation coefficients ranged from 4.32 for the uncracked specimen to 6.60 for the w_{cr2} specimen. This equated to 34% and 53% times greater carbonation coefficient for the 0.55- w_{cr1} and 0.55- w_{cr2} concrete as compared to the uncracked. In addition, the uncracked OPI carbonation coefficient for the 0.55 PC speciemen was 8% greater than the actual 0.55 PC uncracked carbonation coefficient.

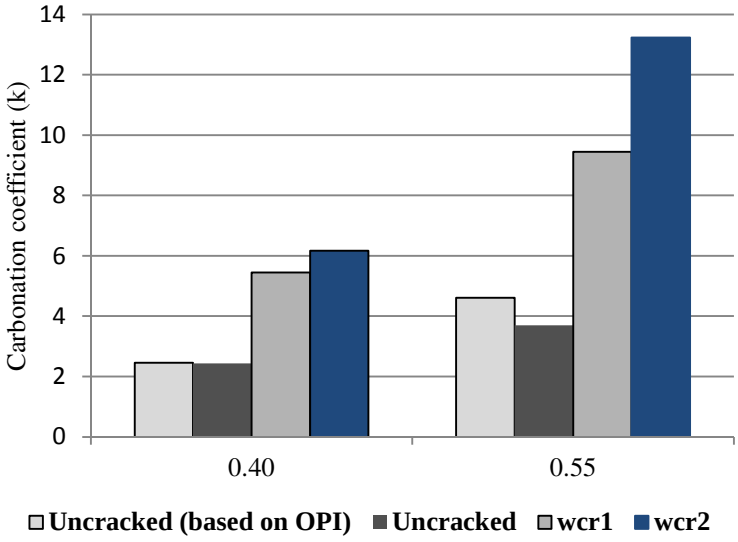

Figure 4.7 Carbonation coefficient for uncracked (OPI) and cracked PC/FA concrete

In Figure 4.7 the effects of cracking on carbon dioxide penetration was found to have the most marked influence in the PC/FA concrete. In the case of the 0.40 PC/FA concrete, the actual uncracked specimens displayed a carbonation coefficient values of 2.43. The w_{cr1} and w_{cr2} specimens produced carbonation coefficients of 5.45 and 6.17. This indicated a 124.0% and 154.0% greater effect of carbon dioxide diffusivity into the concrete as a result of the presence of cracks It can be seen that the uncracked OPI carbonation coefficient for the 0.40 PC/FA speciemen was fairly similar to the actual 0.40 PC uncracked carbonation coefficient, with a 1% greater difference.

In comparison to the 0.55 PC/FA concrete, an actual uncracked carbonation coefficient of 3.69 was obtained. The w_{cr1} and w_{cr2} samples produced carbonation coefficients of 9.44 and 13.23. This presented a 156.0% and 258.0% greater rate of carbon dioxide diffusivity into the cracked concrete than the uncracked concrete samples tested using the OPI durability approach, which is a considerable influence. The uncracked OPI carbonation coefficient for the 0.55 PC/FA speciemen was 25% greater than the actual 0.55 PC uncracked carbonation coefficient.

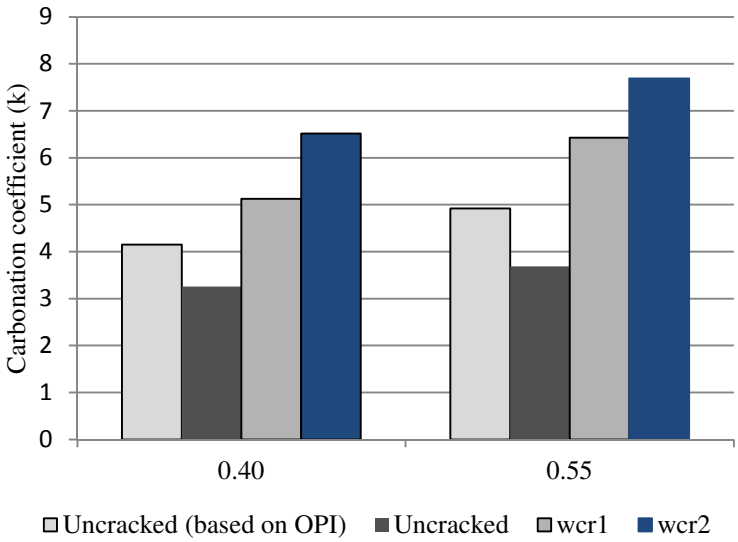

Figure 4.8 Carbonation coefficient for uncracked (OPI) and cracked PC/GGBS concrete

From Figure 4.8 the effect of cracks was found to have a significant influence on carbon dioxide penetration in PC/GGBS concrete. In the case of the 0.40 PC/GGBS concrete, the actual uncracked specimen displayed carbonation coefficient values of 3.26. The w_{cr1} and w_{cr2} specimens produced carbonation coefficients of 5.12 and 6.52; this implied a 57% and 100% greater effect of carbon dioxide diffusivity in to the cracked concrete. The uncracked OPI carbonation coefficient for the 0.40 PC/GGBS speciemen was 27% greater than the actual 0.40 PC/GGBS uncracked carbonation coefficient.

In contrast to the 0.55 PC/GGBS concrete where the carbonation coefficient for the actual uncracked reading was 3.69. The w_{cr1} and w_{cr2} specimens produced carbonation coefficients of 6.43 and 7.69, indicative of a 74% and 109% greater effect of carbon dioxide diffusivity into the cracked concrete. The uncracked OPI carbonation coefficient for the 0.55 PC/GGBS speciemen was 33% greater than the actual 0.55 PC/GGBS uncracked carbonation coefficient.

Hence it can be seen that the transport properties of PC/FA concrete were most affected as a result of the presence of cracks compared to the PC and PC/GGBS concretes based on the actual carbonation ceofficients obtained. Furthermore, the general trend exhibited for the carbonation coefficient obtained for a given binder increased in the following order: actual uncracked < OPI < w_{cr1} < w_{cr2}

4.4.3 Service life analysis of cracked and uncracked concrete based on carbonation resistance

In order to understand the implications of modified transport properties with respect to carbon dioxide ingress due to the presence of cracks in concrete, a service life prediction analysis was carried out. An analysis was carried out using the carbonation measurements that were obtained and considering a service life prediction of carbonation in 16 years. This age was selected as this was the natural time period that corresponded to the accelerated carbonation exposure period of 16 weeks, under an increased CO_2 concentration of 2%.

In the case of the uncracked concrete, Equation 2.17 (below) was used to predict the carbonation depth at 16 years (t), based on the carbonation coefficients (A) and power (n) that were obtained from the carbonation prediction model using the OPI results (Section 4.4).

$$\boldsymbol{D = At^n}$$

Table 4.5 illustrates the inputs used to obtain the carbonation depths from the OPI values when conducting the 16 year carbonation prediction analysis.

Table 4.5 Predicted carbonation depths in16 years based on the outputs of DI carbonation prediction model

	CARBONATION COEFFICIENT	n	PREDICTED CARBONATION DEPTH AFTER 16 YEARS (mm)
PC-0.40	5.22	0.33	13.03
PC/FA-0.40	2.46	0.40	7.46
PC/GGBS-0.40	4.15	0.33	10.36
PC-0.55	5.45	0.33	13.61
PC/FA-0.55	4.61	0.40	13.97
PC/GGBS-0.55	4.92	0.33	12.28

Table 4.6 illustrates the carbonation depths obtained from the OPI and cracked specimens when conducting the 16 year carbonation prediction.

	0.40			
	OPI	**Uncracked**	w_{cr1}	w_{cr2}
PC	13.03	11.11	13.03	14.40
PC/FA	7.46	7.77	16.53	18.71
PC/GGBS	10.36	9.13	12.79	16.27
	0.55			
	OPI	**Uncracked**	w_{cr1}	w_{cr2}
PC	13.61	10.78	12.69	16.48
PC/FA	13.97	11.20	28.62	40.12
PC/GGBS	12.28	9.81	16.05	19.20

Table 4.6 Estimated carbonation depths (mm) in 16 years based on carbonation coefficients obtained using OPI and cracked specimens

From Table 4.6 a general trend can be seen for all six concrete mixes, the actual uncracked carbonation followed by the OPI results produced the lowest carbonation depths results based on a 16 year prediction when compared with the carbonation depths obtained from the cracked concrete specimens. This could be attributed to the conservative nature of the transport properties in the uncracked concrete and in the OPI concrete.

In contrast the cracked carbonation coefficient that was used in the service life prediction analysis was indicative of the modified transport properties (increased concrete penetrability) as a result of the presence of cracks. This in turn resulted in the higher levels of carbon dioxide diffusing into the concrete matrix to facilitate carbonation, thereby promoting the onset of corrosion. Subsequently, the results of the 16 year prediction indicated the capacity of the carbonation coefficient when accounting for the modified transport concrete properties when considering the service life prediction of concrete prone to carbonation.

It can be noted that for a given binder type and w/b ratio, the predicted carbonation depth increased as the crack width increased. The influence of cracks on modifying the concrete properties due to carbon dioxide ingress was not as prominent in the 0.40 w/b ratio mixes as compared to the 0.55 w/b ratio mixes as seen from the predicted carbonation depths obtained for 16 year period. This highlighted the significance of concrete quality against carbonation resistance in cracked concrete.

In the case of 0.40 PC mixes, the difference between the actual predicted uncracked carbonation depths and w_{cr1} and w_{cr2} predicted carbonation depths were 1.92 mm (14.7 % greater) and 3.29 mm (29.6% greater) respectively. There was no significant difference (less than 10% difference) in the predicted carbonation depth for OPI specimens in comparison to the two crack width ranges (w_{cr1} and w_{cr2}) readings obtained.

In the case of 0.55 PC mixes, the difference between the actual predicted uncracked carbonation depths and w_{cr1} and w_{cr2} predicted carbonation depths were 1.91 mm (15.1 % greater) and 5.7 mm (52.8% greater) respectively. Considering the difference between the

uncracked (OPI) and w_{cr1} and w_{cr2} predicted carbonation depths were 0.92 mm (6 % lower) and 2.87 mm (21.1% greater) respectively for the 0.55 PC concrete.

For the 0.40 PC/FA mix, the difference between the actual uncracked and w_{cr1} and w_{cr2} predicted carbonation depths were 8.67 mm (52.9% greater) and 10.9 mm (140.8% greater) respectively. The difference between the uncracked (OPI) and w_{cr1} and w_{cr2} predicted carbonation depths were 9.07 mm (21.5% greater) and 11.25 mm (50.8% greater) respectively for the 0.40 PC/FA mix.

The 0.55 PC/FA mix was most permeable to the ingress of carbon dioxide through the presence of cracks. Hence this concrete produced the greatest carbonation depths for both crack width ranges (w_{cr1} and w_{cr2}) of 60.8% and 258.2% greater when compared to the actual uncracked carbonation depth. This concrete produced carbonation depths for both crack width ranges (w_{cr1} and w_{cr2}) of 104.8% and 187.1% greater when compared to the uncracked (OPI) carbonation depth.

The predicted carbonation depth for the 0.40 PC/GGBS mix was less significant when compared to the 0.40 PC/FA mix however greater than that of the 0.40 PC mix. The difference between the actual uncracked and w_{cr1} and w_{cr2} predicted carbonation depths were 3.66 mm (28.6% greater) and 7.14 mm (78.2% greater) respectively. The difference between the uncracked (OPI) and w_{cr1} and w_{cr2} predicted carbonation depths were 2.4 mm (23.4% greater) and 5.9 mm (57.5% greater) respectively.

Lastly, for the 0.55 PC/GGBS the difference between the actual uncracked and w_{cr1} and w_{cr2} predicted carbonation depths were 6.24 mm (38.8% greater) and 9.39 mm (95.7% greater) respectively. Considering the uncracked (OPI) and w_{cr1} and w_{cr2} was 3.77 mm (30.7% greater) and 6.92 mm (56.4% greater) respectively.

Firstly it can be concluded that cracks have a significant influence in modifying the transport properties (with respect to the carbonation coefficient) in concrete for a given concrete (w/b ratio and binder type). This difference was particularly prominent in the concrete mixes that contained supplementary binders (FA and GGBS).

Secondly, it can be concluded that the transport properties (in terms of carbonation coefficients) extracted from the OPI values (uncracked concrete) seem to be fairly conservative when compared to the cracked concrete transport properties (carbonation coefficients) for a given concrete (w/b ratio and binder type). The carbonation coefficients obtained from the OPIs were significantly lower (up to 57.1%) when compared to those obtained from the cracked concrete specimens.

The use of conservative outputs from the OPI model can have severe implication when assessing structures for carbonation, as illustrated in the 16 year carbonation service life prediction analysis. The use of concrete durability outputs in the carbonation service life prediction model, simulated a concrete that is less prone to carbonation-corrosion in the long-term. It can be seen that when using the DI approach for carbonation in both the material

testing and service life prediction, there are no accommodations made for the presence and influence of cracks on durability. Due to the significant influence that cracks have on the modifying the material properties of concrete, the results have shown that some reduction factors needed to be applied to the outputs from the DI approach to provide a more realistic characterization of the concrete and hence a realistic service life prediction.

4.5 Bulk Diffusion Test Results

Chloride transport in concrete can occur through a number of mechanisms such as diffusion, absorption, migration, convection and absorption. However in the case of bulk diffusion test, diffusion is the primary transport mechanism of chlorides (Song *et al.,* 2008).

4.5.1 General observations

Figure 4.9 shows a summary of the total chloride content profiles that were obtained from the uncracked concrete region of the uncracked concrete specimens, after being submerged in chloride solution for 16 weeks. The graph highlights the total chloride profiles obtained for all three binders tested (PC, PC/FA & PC/GGBS) and both w/b ratios (0.40 & 0.55).

Each data point plotted in the chloride profiles shown below, represents the average value taken from three concrete specimens, for a given w/b ratio and binder type. For each chloride profile plotted, six data points were extracted from the concrete specimens; one data point measurement was obtained at every 10 mm depth interval from the surface of the concrete up to a 60 mm depth.

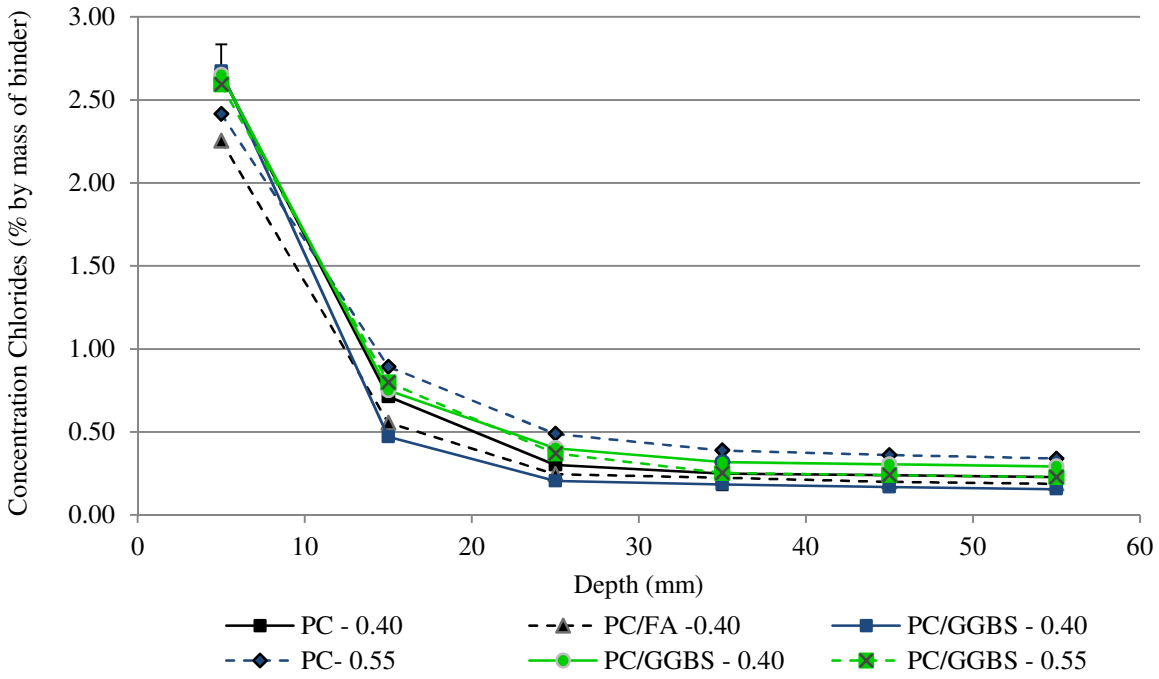

Figure 4.9 Total chloride content profiles obtained for all three concrete binders (PC, PC/FA & PC/GGBS) and both w/b ratios (0.40 & 0.55)

Based on the above figure (4.9) is can be seen that the uncracked concrete specimens exhibited an exponential decreasing trend with respect to the presence of chlorides through the depth of the concrete specimens (as was expected from literature (Luping *et al*., 2012)). When evaluating the influence of binder type on chloride ingress it can be seen in general that the PC/GGBS mixes displayed the lowest concentration of total chlorides in comparison to the chloride concentration obtained in the PC and PC/FA chloride profiles (Ayra *et al.,* 1995).

4.5.2 Effect of cracking on chloride diffusion

Due to the scatter of data that was obtained in the test results, a single chloride profile was used to represent the average chloride penetration in three specimens of cracked concrete. The errors bars for each data point plotted indicate the 95 % standard deviation for each set of bulk diffusion result obtained in the case of the uncracked, w_{cr1} (0.1 - 0.4 mm small crack range) and $w_{cr\,2}$ (0.5 - 0.8 mm big crack range) chloride profiles.

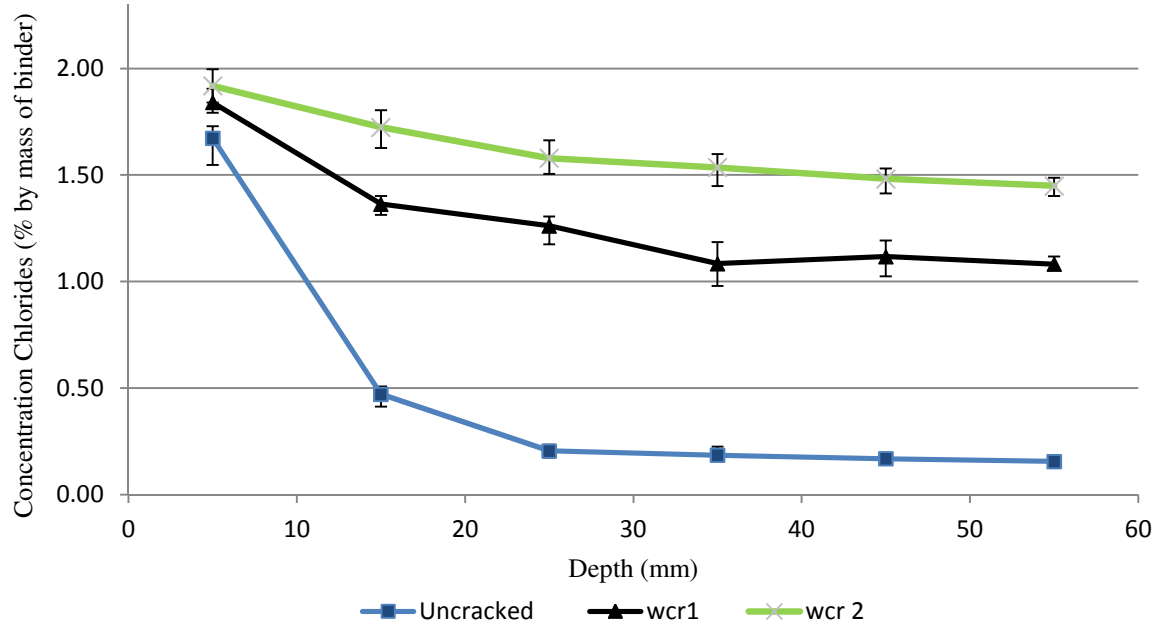

Figure 4.10 Chloride profiles obtained from the bulk diffusion results for 0.40 PC concrete

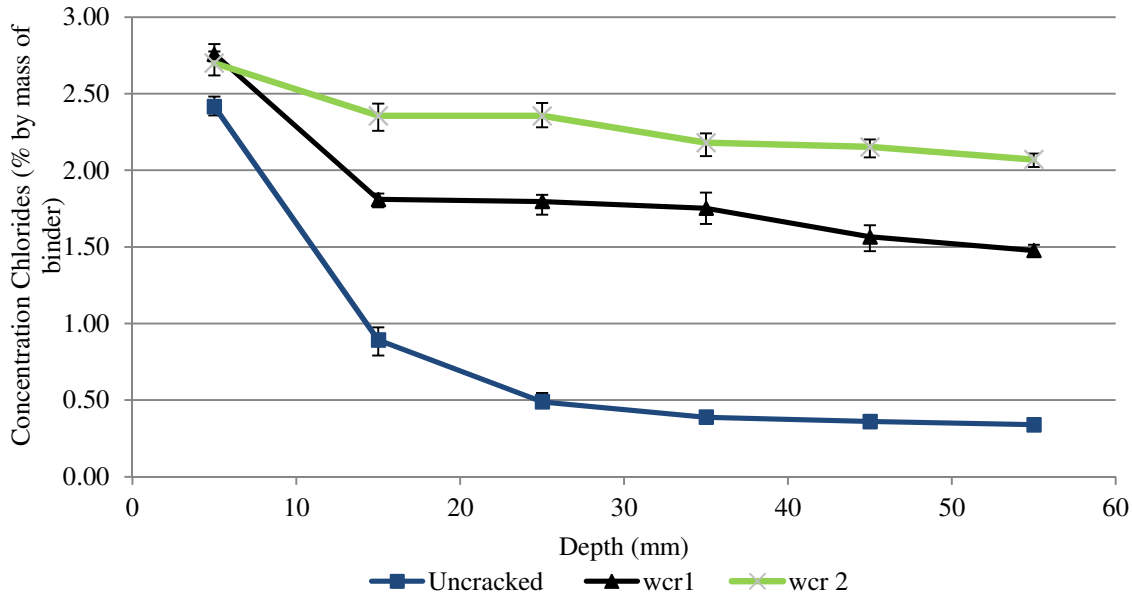

Figure 4.11 Chloride profiles obtained from the bulk diffusion results for 0.55 PC concrete

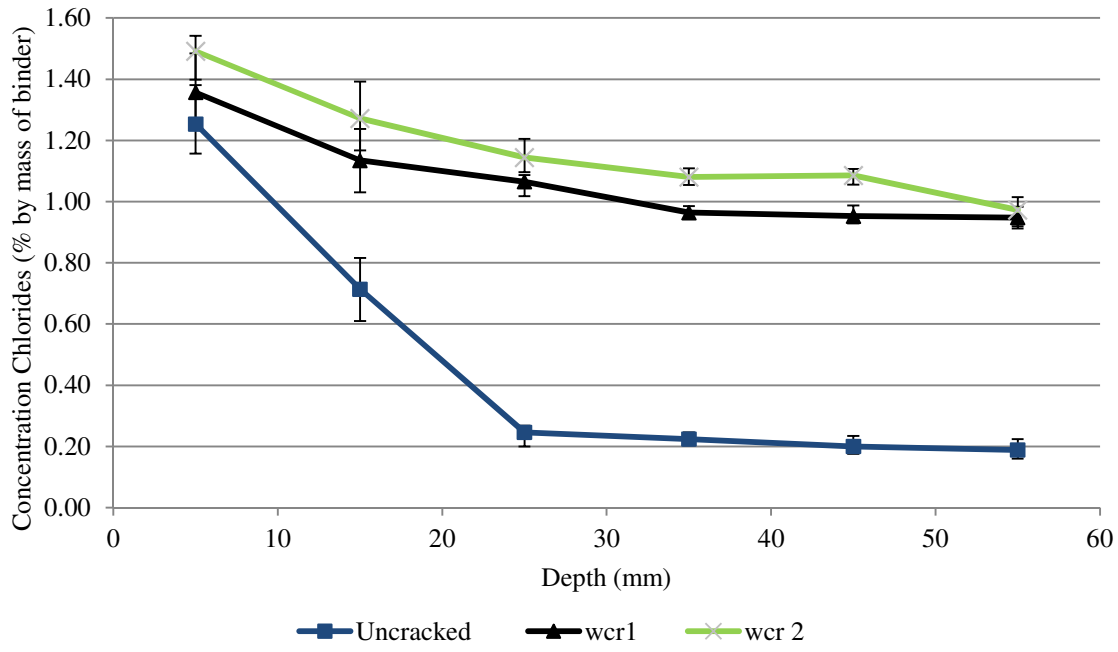

Figure 4.12 Chloride profiles obtained from the bulk diffusion results for 0.40 PC/FA concrete

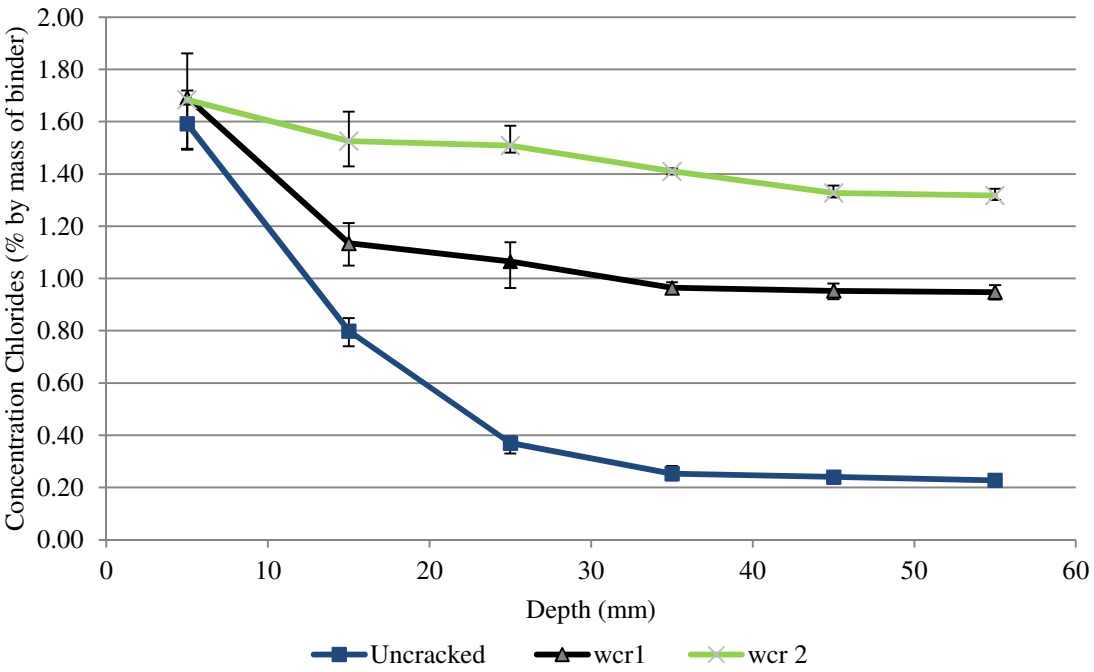

Figure 4.13 Chloride profiles obtained from the bulk diffusion results for 0.55 PC/FA concrete

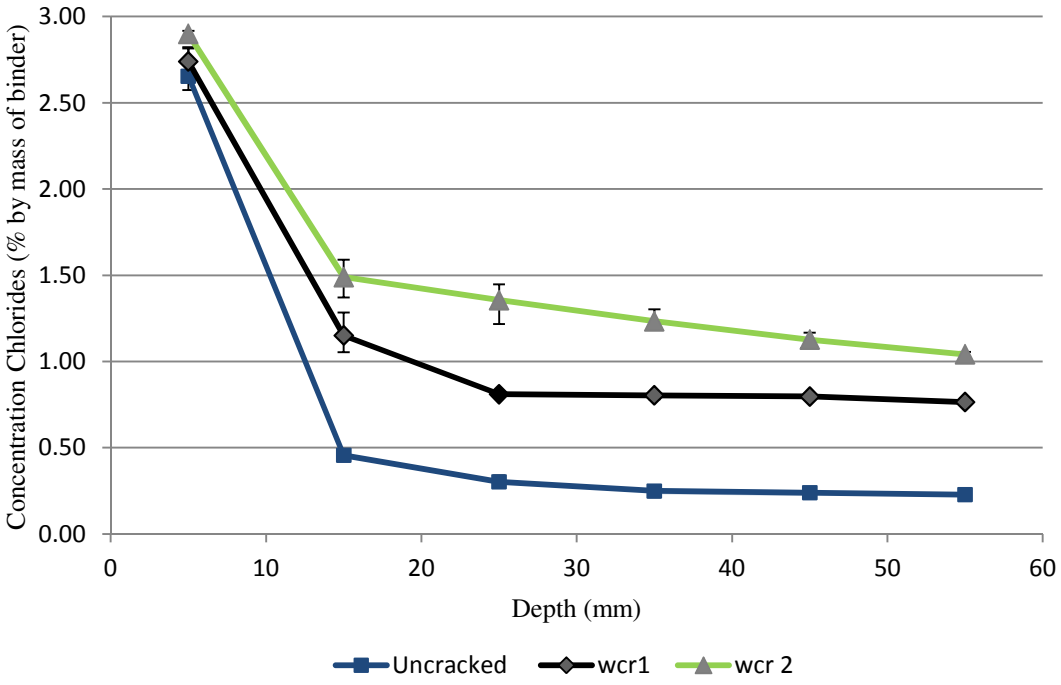

Figure 4.14 Chloride profiles obtained from the bulk diffusion results for 0.40 PC/GGBS concrete

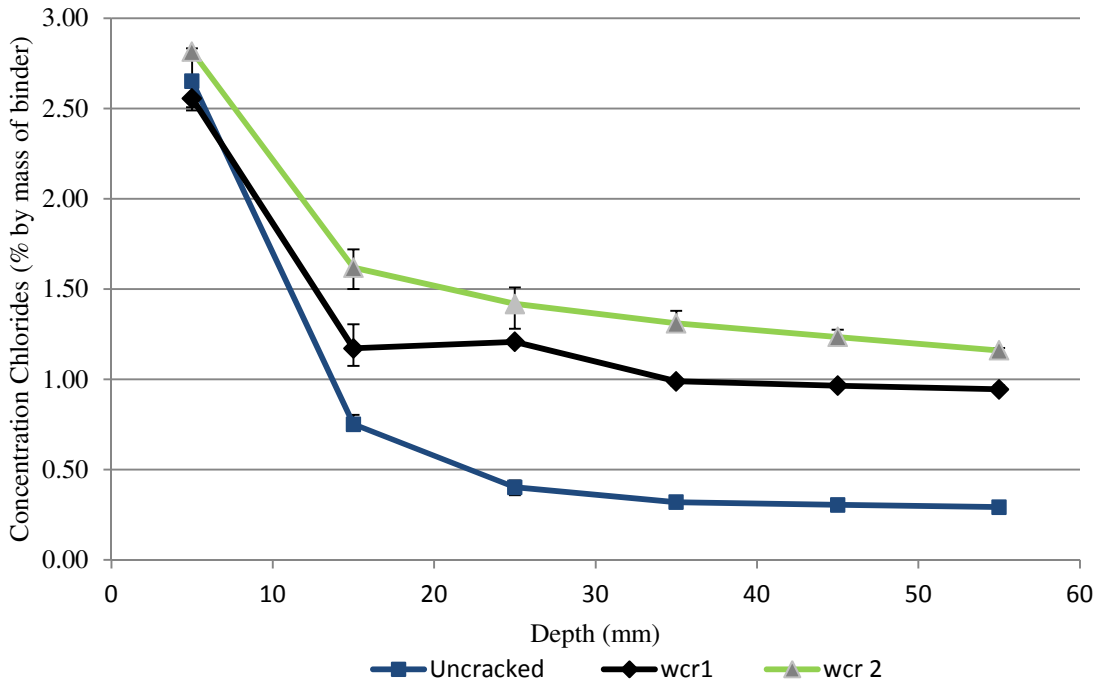

Figure 4.15 Chloride profiles obtained from the bulk diffusion results for 0.55 PC/GGBS concrete

The following general qualitative observations can be noted from Figure 4.10 to Figure 4.15:

The uncracked chloride profile (blue line) of a given mix displayed a typical exponential decrease in the presence of total chlorides at the surface of the concrete in relation to concentration of chlorides at an approximate depth of 60mm into the concrete specimen for a given binder type and w/b ratio. Furthermore it was noted that the uncracked chloride profiles displayed the lowest presence of chlorides in the concrete specimens throughout the depth of the concrete specimen in comparison to the concrete specimens that had the induced crack width w_{cr1} and w_{cr2} (for a given w/b ratio and binder type).

The two cracked concrete chloride profiles w_{cr1} (black line) and w_{cr2} (green line) also displayed a decrease in the presence of total chlorides at the surface in relation to the presence of total chloride at 60 mm depth in the specimens. However the decrease in chloride concentration did not fit a particular type of trend (i.e. exponential, linear, logarithmic). The presence of cracks substantially increased the ingress of chlorides into the concrete. In most instances, in the first 30 mm (from the surface) of the cracked chloride profiles (w_{cr1} and w_{cr2}) there was a variable scatter in the amount of chlorides present after which the profile tended to stabilise (to a given value) in the latter 30 mm depth of the specimen. Moreover, the w_{cr2} chloride profiles displayed the greatest variability in the amount of chlorides presence (as seen in the larger distance of the error bar from the mean value plotted) when compared to the w_{cr1} and uncracked chloride profiles for a given binder type and w/b ratio.

Firstly, the increase in chlorides can be attributed to the increased surface area created on the concrete specimen which then extended into the depth of the specimen as a result of the crack. The relationship between crack width range and depth to which the crack extended in the concrete did not form part of the scope of this study. The increased surface area on the concrete specimen exposed to sodium chloride solution facilitated increasing amounts of chlorides to diffuse into the concrete matrix. This led to deeper chloride ingress into the concrete specimen thus higher chloride concentrations exhibited through the depth of the concrete specimens, evident in the cracked chloride profiles (w_{cr1} and w_{cr2}).

Secondly, the large variation in the amount of chloride presence can be possibly attributed to the increased crack pathways created in the concrete matrix, as a result of the induced crack width in the concrete, and internal microcracking. When the tension load applied to the concrete specimen induced the required crack width, it forced a crack to propagate but it also promoted further micro cracking around the induced crack region. The degree of microcracking in the crack concrete specimen (which was outside the scope of this study) could have had a significant influence on the transport properties of the concrete. The microcracking would have allowed additional diffusion of chlorides into the concrete matrix, thus in turn increasing the presence of chlorides at a given depth, further studies are required to verify this.

It must be noted that based on the chloride profiles shown (Figure 4.10 to Figure 4.15), it is important to observe the percentage of chloride concentration by mass of binder that are present at the 55 mm depth for the each of the chloride profiles. This position is of interest as

this would, in some cases be the depth of reinforcement in concrete based on the Eurocode (CEN, 2007), to provide sufficient cover for concrete in a marine environment prone to chloride-induced corrosion. The reinforcement is only subject to chloride-induced corrosion once the percentage of chlorides percent exceeds the chloride threshold. This criteria was used as quantitative means to analysis the chloride profiles that were obtained for both the uncracked and cracked specimens.

At the onset an apparent trend exhibited was the chloride concentration at the 55 mm depth which exceeded the conservative chloride threshold value of 0.4% for both the crack widths ranges (w_{cr1} and w_{cr2}) for a given concrete mix. This was found to be the case for all binders (PC, PC/FA & PC/GGBS) and for both w/b ratios that were investigated. This highlighted the influence of cracks on modifying the transport properties in concrete with respect to chloride ingress. Furthermore, it is clear that the blended concretes were less prone to chloride ingress when compared to the PC concrete due to the beneficial effects of a denser microstructure and chloride binding as a result of using supplementary cementitious materials in the concrete. This trend is in agreement with results found in literature (Ayra & Xu, 1995)

It can be seen through the comparison of the uncracked 0.40 chloride profiles (PC, PC/FA & PC/GGBS) the PC mix provided the greatest resistance to the ingress of chlorides with 0.228 chloride concentration (% by mass of binder) whereas the PC/FA and PC/GGBS presented 20% and 46% more chlorides at 55 mm depth respectively. In the instance of the 0.40- w_{cr1}, it can be seen that the PC/GGBS mix presented the lowest percentage of chlorides with 0.765% chloride concentration (by mass of binder) at 55 mm depth in contrast to the PC/FA and PC mix which presented 21% and 46% more chlorides respectively. Lastly, in the case of the 0.40-w_{cr2}, the PC/FA exhibited the lowest percentage of chlorides 0.972% chloride concentration (by mass of binder), with the PC/GGBS and PC concretes exhibiting 7% and 49% more chlorides at the given depth respectively.

Similarly, when comparing the 0.55 chloride profiles (PC, PC/FA & PC/GGBS) the PC/FA mix provided the greatest chloride resistance of 0.227 chloride concentration (% by mass of binder) when compared to PC/GGBS and PC mix which presented 28% and 48% more chlorides (by % mass of binder) at the depth of 55 mm from the surface. In the instance of the 0.55- w_{cr1}, it can be seen that the PC/GGBS mix presented the lowest percentage of chlorides 0.945 chloride concentration (% by mass of binder) at 55mm depth in contrast to the PC/FA and PC mix which presented 1% and 56% more chlorides respectively. Furthermore the 0.55-w_{cr2} the PC/GGBS exhibited the lowest percentage of chlorides 1.160 chloride concentration (% by mass of binder), while the PC/FA and PC mix exhibiting 13% and 78% more chlorides at the given depth respectively.

Firstly, in the case of the PC/FA mixes, the results can be attributed to the fly ash reacting with calcium hydroxide leading to a lower degree of alkalinity of the pore solution and in turn a creates a higher capacity to bind chloride ions (Newman & Choo, 2003). Fly ash contains oxides of alumina that aid with the chloride binding process. The pozzolanic reaction

products further refine the concrete microstructure leading to a lower permeability concrete, which impede penetration by chlorides (Baert et al., 2008).

Due to the difficulty of quantitatively characterising the influence of cracks on transport properties particularly chloride ingress based on the chloride profiles. In the proceeding section, a description will be provided as to how the various chloride profiles were utilised to obtained diffusion coefficients. In doing so, a more quantitative analysis can be carried out to provide further information on the influence of cracks on chloride ingress.

4.6 Analysis of the chloride diffusion coefficients obtained from uncracked and cracked specimens through bulk diffusion

The CCI results that were obtained in Section 4.1 characterised the concrete's resistance to chloride ions. However, in order to compare the uncracked CCI result with the cracked bulk diffusion results, Equation 2.18 had to be applied. Recalling Equation 2.18 below:

$$C_{x,t} = C_s\left[1 - erf\left(\frac{x}{2\sqrt{D_a t}}\right)\right]$$

CCI – Diffusion coefficient

Firstly, the CCI values were used along with DI prediction model (Refer to Section 2.14.2 for further details) to determine the corresponding bulk diffusion values for the uncracked specimens. The chloride prediction in the DI spread sheet used the correlation that has been established between the CCI values and measured chloride ingress in concrete. The model also accounts for various environmental influences, the binder type and the age of the predicted chloride profile when predicting the chloride ingress.

One consideration that was made when using the DI prediction model, was the "age" of the CCI value used had to be same "age" of the bulk diffusion test specimens. The chloride conductivity tests were conducted after 16 weeks, corresponding to 112 days. Hence the value of 0.3068 years was used in the model. Table 4.7 shows the input parameters used in the DI Prediction Model and corresponding outputs that were determined particularly the diffusion coefficients of the uncracked (CCI) concrete specimens.

Table 4.7 Input and output parameters obtained using CCI values and DI prediction model

	Input			Output	
Mix	**CCI**	**Binder**	**Exposure**	**Dc (2 years) cm^2/s**	**Dc (age) cm^2/s**
0.40 - 100 PC	0.92	1	10	1.22E-08	2.10E-08
0.40 - 70/30 PC/FA	0.72	3	10	1.53E-08	2.10E-08
0.40 - 50/50 PC/GGBS	0.23	4	10	6.85E-09	2.45E-08
0.55 - 100 PC	1.29	1	10	2.21E-08	3.80E-08
0.55 - 70/30 PC/FA	1.25	3	10	3.05E-08	1.09E-07
0.55 - 50/50 PC/GGBS	0.48	4	10	9.25E-09	3.31E-08

*** Note the following notation was used as per the prediction model to represent the type of binder and environment used:**
Binder: 1 – 100% PC, 2 - 10% SF, 3 - 30% FA, 4 - 50% GGBS, 5 - 50% CS
Environment: 10 – Extreme, 20 – Very Severe, 30 – Severe

From Table 4.7 it can be seen that two diffusion coefficients were obtained using the six CCI results in conjunction with binder type and environmental exposure. It can be seen that the model determines the diffusion coefficient after 2 years (based on the established 2 year correlation that has been established from previous research) and then extrapolates the value to determine the diffusion coefficient at the age of interest (in this instance 0.3068 years). Hence there are two diffusion coefficients that were determined for a given mix type. It must be noted by the reader the difference in magnitude between the diffusion coefficients obtained at the younger (0.3068 years) and older age (2 years), a greater diffusion coefficient is obtained at the younger age compared to the older age for all concrete mixes tested. This result was expected as the concrete matures over time additional hydration occurs which serves to reduce the diffusion coefficient (Stanish & Thomas, 2003).

Obtaining diffusion coefficients from chloride profiles

The raw data obtained from the bulk diffusion tests that was used to plot the chloride profiles (Figure 4.15 - 4.20) were then used to determine the corresponding chloride diffusion coefficients. A MS Excel-based chloride-ingress modelling programme called CurveFit2003 developed by Tang C, was used for curve-fitting the chloride profiles to the error function solution of Fick's 2nd law to obtaining the apparent surface chloride concentration (C_s) and diffusion coefficient (D_a).

Five input parameters had to be defined prior to determining the various diffusion coefficients. The exposure period referred to the duration which the specimens was exposed to a chloride environment. The curve fitting parameter's refers to the various chlorides concentrations which correspond to a various depth in the concrete specimen for each chloride profile. In this instance "Depth 1", refers to the chloride concentration at the depth closest to the surface of the concrete specimen which is at approximately 5 mm. 10 mm intervals were used for each chloride profile, therefore "Depth 5" corresponded to a chloride concentration at a depth of approximately 55 mm from the surface of the concrete. The boundary condition defined how many surfaces of the concrete specimen were exposed to chlorides from an external environment. Table 4.8 below shows the input parameters that were used to obtain the relevant diffusion coefficients irrespective of the w/b ratio, binder type, crack width and chloride concentration of a concrete mix.

Table 4.8 Input parameters used in CurveFit2003 Model to obtained diffusion coefficient for a given w/b ratio, binder type, crack width and chloride concentration

Exposure data

Exposure time t, days:	112

Curve-fitting conditions

Curve-fitting start from the depth No.:	1
Curve-fitting end at the depth No.:	5
Exposure boundary:	One-sided
Thickness of specimen, mm:	100

Table 4.9 below shows the outputs in the form of diffusion coefficients that were obtained using the CurveFit2003 programme and the various chloride concentrations shown in Figure 4.10 to Figure 4.15. The surface chloride concentration and R^2 values corresponding to each diffusion coefficient can be found in Appendix H.

Table 4.9 Diffusion coefficients obtained from the various chloride profiles using CurveFit2003

		Diffusion Coefficient (Da) (x 10^{-12} m^2/s)		
		Uncracked(Bulk diffusion)	$_{wcr}1$	$_{wcr}2$
PC	0.40	1.70	512	1630
	0.55	2.78	675	1930
PC/FA	0.40	3.98	191	865
	0.55	6.96	512	1830
PC/GGBS	0.40	1.71	141	183
	0.55	2.72	470	618

From Table 4.9, it can clearly been seen that the diffusion coefficient significantly increases in magnitude in the following order: Uncracked < w_{cr1} < w_{cr2} for a given concrete type. This trend was displayed for all six concrete mixes that were tested.

Firstly, note the magnitude of the diffusion coefficients obtained with respect to the uncracked and cracked concrete (w_{cr1} and w_{cr2}) mixes. When comparing the uncracked diffusion coefficient to the w_{cr1} diffusion coefficient, the increase in diffusion typically ranged from 131 to 172 times more. Furthermore, the influence of the larger crack width on diffusion coefficient was more pronounced when compared to the uncracked concrete diffusion coefficient. The increase in diffusion ranged from 227 to 958 times greater when comparing the uncracked and w_{cr2} diffusion coefficient. These noteworthy increases in the diffusion coefficients can have a marked influence on the rate of ingress of aggressive species into concrete, which in turn de-passivates the reinforcement and resulting in the onset of chloride-induced corrosion.

4.6.1 Verification of chloride diffusion coefficient from CCI and Uncracked chloride profile

Similarly as was done with the carbonation coefficients, in order to compare the outputs from the DI models which the measured chloride profile results, the validity of the DI testing approach needed to be checked, with respect to the DI's ability to accurately predict chloride ingress behaviour in concrete. Consequently Figure 4.16 illustrates the chloride diffusion coefficients that were obtained from the CCI values (Model) and the uncracked chloride profile measurements (Actual). It must be noted that the diffusion coefficients that were obtained in the DI model were stated as cm^2/s whereas there diffusion coefficients that were obtained from the CurveFit 2003 were stated as m^2/s. In the figure below all diffusion coefficients are expressed as m^2/s.

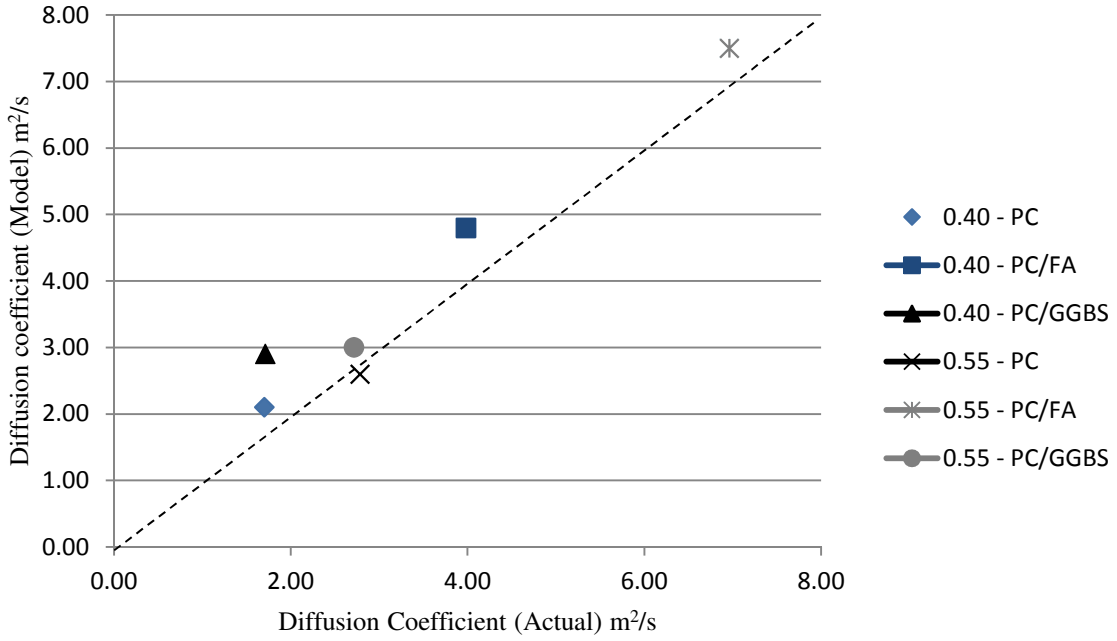

Figure 4.16 Actual diffusion coefficient Vs model diffusion coefficient

Similarly as with the carbonation coefficient, Figure 4.16 above serves to verify the ability of the CCI model to predict the chloride ingress in uncracked concrete, based on the diffusion coefficients that were obtained. Data points that fell on the forty five degree line illustrated that the predicted chloride diffusion coefficient from the DI model was the same as the diffusion coefficient obtained from the measured bulk diffusion results.

A 0.97 product moment correlation coefficient was obtained for the data points (for both w/b ratios (0.40 & 0.55) and the three binders used (PC, FA & GGBS)). It can be seen that all the data points do not lie on the 45 degree line, there was 0.03 variability present in the results that were obtained. It can also be noted that the diffusion coefficients obtained from the DI prediction model were relatively higher than the measured diffusion coefficient (except for the 0.40 PC/FA mix).

Similarly as discussed with the carbonation coefficient, the premise that the aim of the study was to not correct or modify the accuracy of the DI prediction model but to note the difference between the predicted model and measured values. Furthermore it ensured that there was not a substantial difference between the two variables as this would not provide an appropriate context to compare results and draw any conclusion.

4.6.2 Comparison of the diffusion coefficients obtained from the CCI and Bulk Diffusion Cracked concretes

The diffusion coefficient was used to assess the diffusivity of chlorides into uncracked and cracked concrete. Figure 4.17 to Figure 4.19 illustrates the diffusion coefficients that were obtained from the CCI tests simulating uncracked concrete, and the diffusion coefficient from the bulk diffusion tests for the uncracked concrete and the two crack width ranges w_{cr1} (0.1-0.4 mm crack width) and w_{cr2} (0.5-0.8 mm crack width) for a given binder type for both w/b ratios (0.40 & 0.55).

Generally, it can be observed from Figure 4.17 to Figure 4.19 that the diffusion coefficient obtained from the CCI values are substantially lower than those for the cracked specimens (w_{cr1} and w_{cr2}) from the cracked specimens. This was true for all three binders (PC, PC/FA & PC/GGBS) tested and w/b ratios (0.40 & 0.55) investigated.

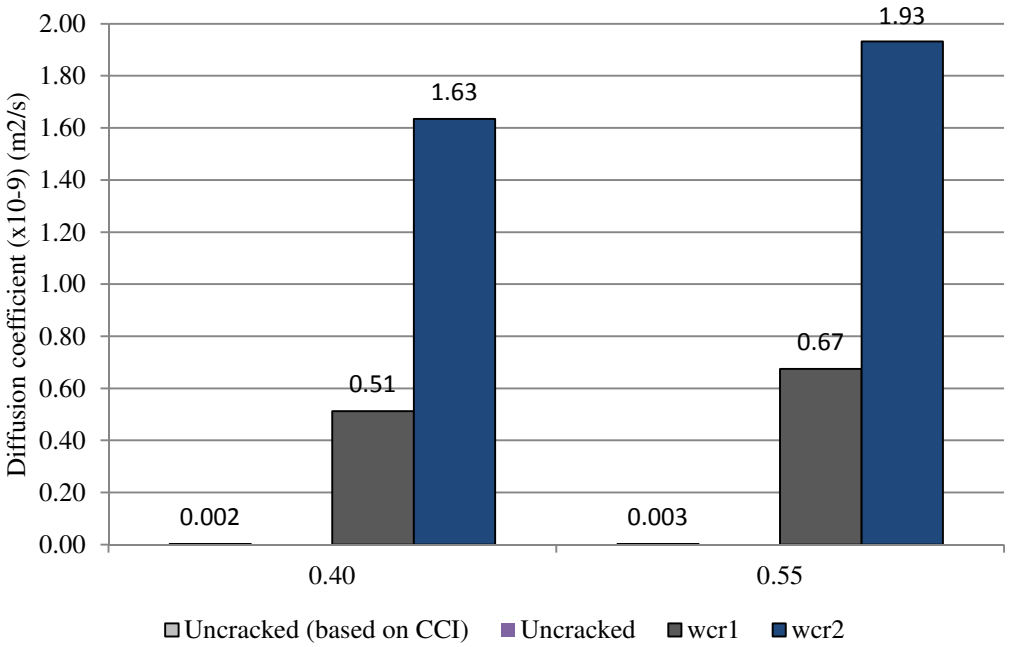

Figure 4.17 A comparison of the diffusion coefficients obtained from the uncracked CCI specimens with the diffusion coefficients from the bulk diffusion PC specimens (uncracked and cracked).

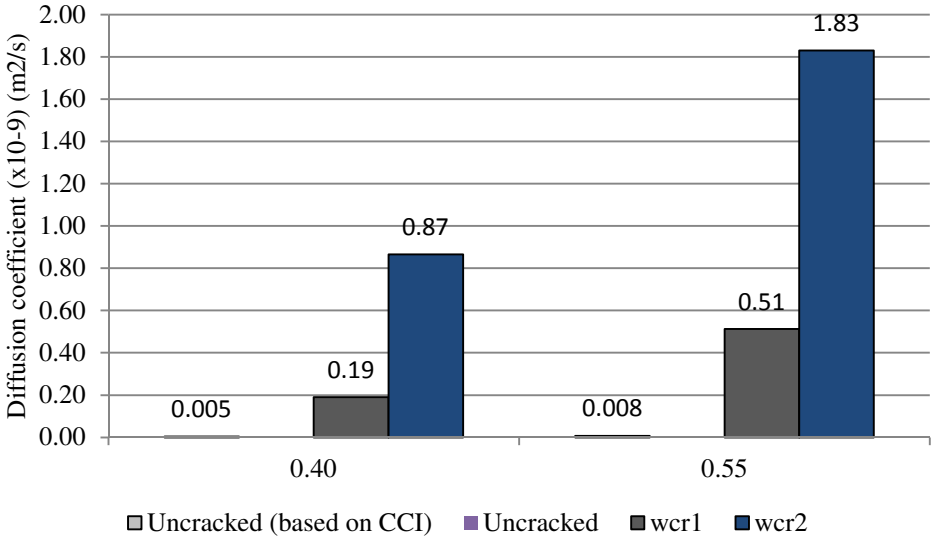

Figure 4.18 A comparison of the diffusion coefficients obtained from the uncracked CCI specimens with the diffusion coefficients from the bulk diffusion PC/FA specimens (uncracked and cracked).

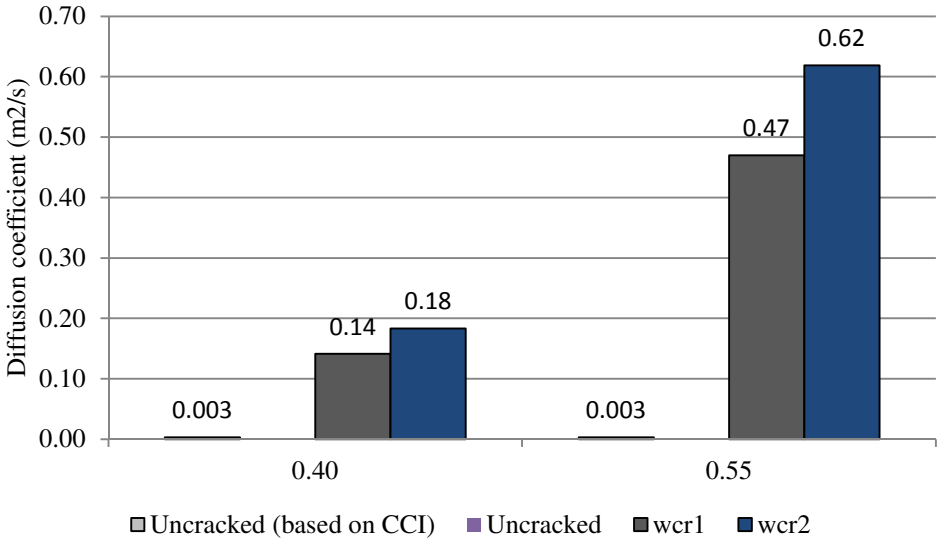

Figure 4.19 A comparison of the diffusion coefficients obtained from the uncracked CCI specimens with the diffusion coefficients from the bulk diffusion PC/GGBS specimens (uncracked and cracked).

A general trend can be observed from Figure 4.17 and Figure 4.19 the diffusion coefficients increased in the following order: Actual uncracked < CCI < w_{cr1} < w_{cr2}. It can be seen that in the presence of cracks (w_{cr1} and w_{cr2}) have a marked influence on the diffusion coefficients in comparison to the uncracked concrete diffusion coefficient (which due to their magnitude hardly appear on Figure 4.17-Figure 4.19). Furthermore, the PC cracked specimens exhibited the greatest diffusion of chloride based on the diffusion coefficient in relation to the PC/FA and PC/GGBS specimens. This result can be attributed to the binding of chlorides in concrete that contain supplementary binders in the concrete mixes.

It has been shown through numerous studies, that the chloride diffusion coefficients decreases with time (hence the diffusion coefficients obtained in the bulk diffusion tests are time dependent). Possible explanations for this is that the continuous hydration and binder reaction that densify the concrete over time (Luping *et al.,* 2012). This must be noted and taken into consideration when making service life predictions using time-dependent diffusion coefficients.

Furthermore, the significantly high (chloride) diffusion coefficients obtained for the cracked concretes also show that diffusion may not be the dominant transport mechanism as is assumed in the models. Further work should be done to establish other possible transport mechanisms that could contribute the increased diffusion coefficient in the cracked concretes.

When considering the effects of cracks, it can be noted that for a given binder type and w/b ratio, the diffusion coefficient increased as the crack width increased. The most prominent influence of cracks resulted in the increased rate of chloride ingress and subsequently increased diffusion coefficient was evident in the PC-055 mix. For example, the PC-055 w_{cr1} diffusion coefficient obtained was 335 times greater (from 0.002 to 0.67 $x10^{-9}$ m/s ^{2}) in relation to the PC-0.55 uncracked diffusion coefficient. Additionally, the PC-055 w_{cr2} diffusion coefficient obtained was 965 times greater (from 0.002 to 1.93 $x10^{-9}$ m/s ^{2}) in relation to the PC-0.55 uncracked diffusion coefficient.

It is clear from the result in Figure 4.17-4.19 that the used of the uncracked diffusion parameters (bulk diffusion and CCI) in service life modelling provides fairly conservative chloride penetration results when compared to the results from the uncracked diffusion parameters. This outcome can have severe implications when assessing the service life of a given structure with regards to the degree of damage in the form of corrosion. The use of a conservative service life output will provide an unrealistic assessment of the structure, if there are cracks present on the structure. This could possibly led to pre-mature failure of the structure due to the lack of maintenance and repair conducted because no accommodation was made for the influence of cracks in the assessment of concrete's durability .

5 CONCLUSION

The main objective of this study was to investigate the of flexural crack width on transport property of concrete, and their effect on the DI testing approach.

Firstly, the results indicate that the presence of surface cracks modifies the transport properties in the concrete, by promoting a rapid increase of ingress of aggressive species into the concrete matrix. This can be attributed to the increase surface area created by the presence of the crack in the concrete specimen, which allows more species to penetrate the concrete. Furthermore, the presence of the crack in the concrete also created a local region of microcracks in the vicinity of the main crack, which promoted the ingress of species into the concrete matrix. Other factors being constant, an increase in surface crack width lead to increased rates of ingress of carbon dioxide into the concrete, although to a greater extent in the blended cements specimens. However, in the case of diffusion of chlorides into concrete, an increase in surface crack width lead to greater chloride diffusion and to a lesser extent in the blended cements specimens

Secondly, the results demonstrated that the durability indices extrapolated from the DI testing approach using sound concrete specimens produced unconservative durability parameters for the tested concrete specimens in contrast to the durability parameters obtained from the cracked concrete specimens that were tested.

Subsequently, when the sound (DI) and cracked durability parameters where used in carbonation and chloride ingress service predictions, it was found that the DI service life predictions outputs were significantly unconservative in relation to service life outputs from the durability parameters obtained from cracked concrete specimens. These results highlighted the degree of influence which the presence of cracks can have on modifying transport properties in concrete. Furthermore, it also highlights the impact that the presence of cracks can have on the service life of RC structures and the prediction of long-term carbonation- and chloride- induced corrosion.

Lastly, the research conducted showed that some modification needs to be made when using the DI approach to assess the durability of structures, particularly if cracks are present on the structure, as is always the case. Failure to make such provisions in the analysis, would result in over-estimation of service-life. This could led to pre-mature failure of the structure.

These factors will be critically evaluated in this chapter in a more general sense based on the results and discussion presented in Chapter 4.

5.1 The influence of cover cracking and binder type on the ingress of carbon dioxide in concrete

The results showed that the rate of ingress of carbon dioxide (measured from the carbonation depth) increases with increasing crack width but is sensitive to concrete quality. For a given binder type and w/b ratio, the carbonation depth increased with increasing crack width. These observations can be summarised as two distinct scenarios as follows:

(i) For a given crack width, carbonation rate is sensitive to binder type.

(ii) For a given binder type and w/b ratio, carbonation rate is sensitive to crack width.

A comparison of the carbonation depth of all the specimens indicate that an increase in carbonation rates with increasing crack width was most significant in the fly ash and ground blastfurnace slag specimens (PC/FA-0.40, PC/FA-0.55, PC/GGBS-0.40 & PC/GGBS-0.55).

In general the results agreed with the trends that were found in literature for the uncracked concrete mixes, this was explained by the increased amount of $Ca(OH)_2$ that are available for carbonation in plain Portland cement. Furthermore, similar trends were also displayed in the cracked specimens.

For example, at the end of the 16^{th} week, a crack width range of 0.1 mm to 0.4 mm (w_{cr1}) in an PC/FA-0.40 specimen resulted in 4 times greater (from 16.53 mm to 4.07 mm) carbonation depth when compared to PC-0.40 specimens of the same crack width. While for the same crack width range (w_{cr1}) a PC/GGBS-0.40 resulted in 2.05 times greater carbonation depth reading when compared to PC-0.40 specimen of the same crack width.

5.2 The influence of the (uncracked) OPI carbonation coefficient and cracked carbonation coefficient parameters on service life predictions

Based on the carbonation depth results that were obtained, the carbonation coefficients were obtained (from both the OPI and cracked concrete specimens) and used as inputs in carbonation service life prediction model to assess the degree which cracks modified the transport properties in the concrete and the implication on service life of RC structures.

It can be concluded that the transport properties (carbonation coefficients) extracted from the OPI values (uncracked concrete) seem to be fairly conservative when compared to the cracked concrete transport properties (carbonation coefficients) for a given concrete (w/b ratio and binder type). The carbonation coefficients obtained from the OPIs were significantly lower (up to 57.1% lower) when compared to the carbonation coefficients obtained from the cracked concrete specimens. This substantial difference was particularly prominent in the concrete mixes that contained supplementary binders (FA and GGBS) which exhibited a denser microstructure (Kawamura & Torii, 1989).

5.3 The influence of cover cracking and binder type on chloride ingress

The results showed that the rate of chloride-ingress (measured from the chloride profiles) increases with increasing crack width but is sensitive to concrete quality. For a given binder type and w/b ratio, the chloride ingress (measured by the centration of chlorides by mass of binder) increased with increasing crack width. These observations can be summarised as two distinct scenarios as follows:

(i) For a given crack width, chloride ingress is sensitive to binder type.

(ii) For a given binder type and w/b ratio, chloride ingress is sensitive to crack width.

The uncracked chloride profiles displayed the lowest presence of chlorides in the concrete specimens over the overall depth of the concrete specimen in comparison to the cracked concrete specimens (for a given w/b ratio and binder type). A comparison of the chloride profiles of all the specimens indicated, an increase in chloride diffusion with increasing crack

width was most significant in the PC specimens (PC-0.40, PC-0.55). This trend was consistent with the results found in literature with regards to chloride profiles in uncracked concrete specimens.

It can be concluded that the transport properties (diffusion coefficients) obtained from the CCI values (uncracked concrete) seem to be fairly unconservative when compared to the cracked concrete transport properties (diffusion coefficients) for a given concrete (w/b ratio and binder type).

The results showed that the durability parameters on the CCI results, produced the diffusion coefficient for a given binder type and w/b ratio when compared to the corresponding cracked width ranges $w_{cr1} < w_{cr2}$. This trend was exhibited for all three binder types (PC, PC/FA & PC/GGBS) investigated.

The most prominent influence of cracks resulted in the increased rate of chloride ingress and subsequently increased diffusion coefficient was evident in the PC-055 mix. For example, the PC-055 w_{cr1} diffusion coefficient obtained was 335 times greater (from 0.002 to 0.67 $x10^{-9}$ m/s ^{2}) in relation to the PC-0.55 uncracked diffusion coefficient. Additionally, the PC-055 w_{cr2} diffusion coefficient obtained was 965 times greater (from 0.002 to 1.93 $x10^{-9}$ m/s ^{2}) in relation to the PC-0.55 uncracked diffusion coefficient.

5.4 Influence of cracking on the Durability Index (DI) testing Approach

It is clear from the results that the used of the Durability Index testing approach (particularly with respect to the OPI and CCI) produces fairly conservative durability parameters in comparison to durability parameters obtained from bulk diffusion and accelerated carbonation tests that account for the presence of cracks.

The use of these conservative outputs from the DI model can have severe implication when assessing the in-situ durability of a given structure. For a given structure the use of the DI provided fairly conservative outputs (Figure 4.11 - 4.12 and Figure 4.22 - 4.24) which are not realistic reflection of the durability potential of the concrete. The use of the outputs in the carbonation or chloride ingress service life prediction model simulates a material behaviour less prone to carbonation- or chloride- induced corrosion in the long-term. It can be seen that when using the DI approach for both material testing and service life prediction, there are no allowances made for the presence and influence of cracks on durability. This could possibly led to pre-mature failure of the structure due to the lack of maintenance and repair conducted because no allowance was made for the influence of cracks in the assessment of concrete's durability.

Due to the significant influence that cracks have on the modifying the material properties of concrete, the results have shown that some reduction factors needed to be applied to the outputs from the DI approach to provide a more realistic material and service life prediction of a RC structure. Further research into understanding how other crack parameters (e.g. crack depth, frequency, etc.) modify transport properties in concrete will led to a better insight into dealing with and accounting for the presence of cracks in RC structures.

6 RECOMMENDATIONS

The following recommendations for further work are put forward based on this study:

I. Quantification of microcracks in a localized region in the vicinity of an induced crack

In this study, the scope of investigation was limited to influence of macrocracks ranging from 0.1 mm to 0.8 mm. on modifying transport mechanism in concrete. Further work should be carried out to establish what extent microcracks that develop in the localized region of an induced crack have on modifying transport properties in concrete. Additionally how do you characterize and account for the presence of the microcracks in concrete and subsequently in service life predictions.

II. Quantification of crack width vs. cover depth

The limitation of the surface crack width for RC durability purposes should be related to the cover depth. Further work should be done to establish the relationship between the ingress of aggressive species and different surface crack widths and concrete covers for various binder types.

III. ***Correlation with on-site corrosion rate measurements***

The carbonation and chloride ingress rates obtained in the laboratory especially for the cracked concrete should be correlated with on-site measurements. In this study, the influence of cracks on chloride and carbon dioxide was carried out in controlled environments. This study can be further extended by carrying out the same experiments using on-site RC structures that exhibit cracks. This will provide as more complex output on the influence of cracks on the penetration of aggressive species as numerous variables that are constantly changing (temperature, humidity & concentration of aggressive species).If necessary, correction factors may be applied in order to reliably predict corrosion rates.

IV. Further laboratory experiments- Quantification of various crack parameters

This study can be extended by carrying out long term laboratory experiments, introducing more variables (smaller crack widths ranges, w/b ratios, crack types). Additional crack parameters such as crack length and density should be studied with regards to their influence on chloride and carbon dioxide ingress. Due to the variability of a given crack, there are a number of parameters that can be considered in trying to model the crack. Hence more data that is available for a given crack characteristic, a more realistic perspective can be obtained by combining the effects of the different characteristic. The ultimate focus should be to develop a correlation between these various factors and their influence on the ingress of species in cracked concrete. Also to investigate the influence of these factors with respect to modifying transport mechanism in concrete when they act in con-junction with other factors and

not in isolation (which is often the case in on-site). This will lead to a more realistic approach to understanding and predicting the behaviour of cracks in RC structures. Subsequently this will provide a platform for incorporating the influence of cracks in service life prediction

V. Durability index testing approach and service life predictions

It can be seen that based on the concrete specimens tested from RC structures that contains cracks, the DI parameters obtained provides a more conservative assessment of the concrete durability as compared to the assessment of the cracked concrete specimens for the same concrete. The DI service life prediction model can be modified to account for the presence of cracks on RC structures; however it requires substantial information (which is still lacking) on the ingress of aggressive species through cracks. Once there is a general consensus on the influence of cracks, a modification factor can be established for the chloride or carbonation service life predictions. This will allow for more realistic service life prediction behaviour of RC structure that have cracks presence.

~~V.~~VI. Determing crack width as function of compressive strength and bending capacity

Due to the conservative nature of structural codes, with respect to the increase in load and resultant crack width. A possible area of investigation would be to assess the influence of loading as a percentage of compressive strength or bending capacity on crack width and resultant ingress of aggressive species. This would allow for a practical input from engineers and application in the industry.

7 REFERENCES

ACI Commitee, 2001. *224R-01-Control of cracks in concrete structures,* s.l.: ACI Committee 224.

ACI, 1995. (ACI318-95). In: *Building Code Requirements for Structural Concrete and Commentary.* MI: American Concrete Institue, Farmington Hills.

ACI, 1996. Corrosion of Metals in Concrete. In: *(ACI 222r-96).* Commitee 222, Detriot(MI): s.n.

ACI, 2002. Building Code Requirements for Structural Concrete and Commentary. In: *(ACI 318-02).* MI: American Concrete Institue, Farmington Hills.

Alexander, M. G., 1993. Two experimental techniques for studying the effects of the interfacial zone between cement paste and rock. *Cement and Concrete Research,* pp. 567-575.

Alexander, M. G., Ballim, Y. & Mackecknie, J., 2008. A framework for uses of durability indexes in performance-based design and specifications fro reinforced concrete structures. *Materials and Structures,* pp. 921-936.

Alexander, M. G., Beushausen, H. & Otieno, M. B., 2012. *Corrosion of steel in reinforced concrete: Infleunce of binder type, water/binder ratio, cover and cracking.* Cape Town: University of Cape Town, Concrete Materials and Structural Integrity Research Unit, MSc Thesis.

Alexander, M. G., Mackechnie, J. R. & Ballim, Y., 1999. Guide to the use of durability indexes for achieving durability in concrete structures. *Research Monology, No.2.*

Alonso, C., Andrade, C., Castellote, C. & Castro, P., 2000. Chloride threshold values to depassivate reinforcing bars embedded in a standardized OPC mortar. *Cement and Concrete Research,* pp. 1047-1055.

Alonso, C., Castellote, M. & Andrade, C., 2002. Chloride Threshold Dependence of Pitting. *Electrochim Acta,* pp. 469-3481.

Ammouche, Riss, J., Breysse, D. & Marchand, J., 2001. Image anaylsis for the automated study of microcracks in concrete. *Cement and Concrete composite,* pp. 267-278.

Ampadu, K. O., Torii, K. & Kawamura, M., 1999. Beneficial effect of fly ash on chloirde diffusivity of hardened cement paste. *Cemenat and concrete Research,* pp. 585-590.

Andrade, C., Sanjuan, M. A. & Alonso, M. C., 1993. *Measurement of chloride diffusion coefficient from migration tests.* s.l., s.n., pp. 289-98.

Angst, U. & Vennesland, O., 2009. *Critical chloride content in reinforced concrete – State of the art.* London, Taylor & Francis Group.

Anik, D. et al., 1997. Chloride binding capacity of carious hydrated cement systems. *Advance Cement-Based Materials,* pp. 28-35.

Arya, C. & Newman, J. B., 1990. *Problem of predicting risk of corrosion of steel in chloride contaminated concrete.* s.l., Proceedings of the institution of Civil Engineers (London). Part 1- Design and Construction, pp. 875-888.

Ayra, C., Buenfeld, N. R. & Newman, J. B., 1990. Factors influencing chloride-binding in concrete. *Cement and Concrete Research,* pp. 291-300.

Ayra, C. & Ofori-darka, F. K., 1996. Infleunce of crack frequency on reinforcement corrosion in concrete. *Cement and Concrete Research,* pp. 345-353.

Ayra, C. & Xu, Y., 1995. Effect of cement type on chloirde binding and corrosion of steel in concrete. *Cement and Concrete Research,* pp. 893-902.

Baert, G., Gruyaert, E., Audenaert, K. & De Belie, N., 2008. *Chloride ingress in high-volume fly ash concrete.* s.l., RILEM Publications, pp. 473-482.

Ballim, Y., Alexander, M. G. & Beushausen, H. D., 2009. Durability of concrete. In: *Fulton's Technology.* s.l.:s.n., pp. 164-171.

Ballim, Y., Grieve, G. R. & Alexander, M. G., 2004. *Reinforced concrete duarbility of concrete durability design status and prospect in South Africa.* Midrand, s.n.

Barnett, V., Lewis, T. & Rothamsted, V., 1994. Outliers in Statistical Data. In: *Wiley Series in Probability and mathematics statistics, appplied probability and statistics.* s.l.:John Wiley & Sons.

Basheer, L., Kropp, J. & Cleland, D. J., 2001. Assessment of the durability of concrete from its permeation properties: A review. *Construction and Buidling Materials,* pp. 93-103.

Baweja, D., Roper, H. & Sirvivatnanon, V., 1998. Chloirde-induced steel corrosion in concrete:Part 1 corrosion rates, corrosion activity, and attack areas. *ACI Materials Journal,* pp. 207-217.

Bazant, Z. P., 1979. Physical model for steel corrosion in concrete sea structures-theory. *ASCE Journal of the structural division,* pp. 1137-1153.

Beushausen, H. & Alexander, M., 2008. The South African durability index tests in an international comparision. *Journal of the South African Institute of Civil Engineers,* pp. 25-31.

Bisschop, J. & Van Mier, J., 1999. Quantification of shrinkage microcracking in young mortar with fluorescence light microscopy. *Delft Univesity of Technology.*

Brooks, J., 2003. Elasticity, shrinkage, creep, and thermal movements. In: *Advance Concrete Technology Set.* Leeds, UK: Butterwoth Heinemann, pp. 1-18.

Broomfield, J. P., 1994. Assessing corrosion damage on reinforced concrete structures. In: *Corrosion and corrosion protection of steel in concrete.* s.l.:Sheffield Academic Press.

Broomfield, J. P., 2007. *Corrosion of steel in concrete.* Abington, Oxon: Talyor & Francis Group.

Browne, R. D., 1980. *Mechanims of corrosion of steel in concrete in relation to design, inspection, and repair of offshore and coastal structures.* s.l., s.n., pp. 169-203.

Bruwhiler, E. & Whittmann, F. H., 1990. The wedge splitting test, a new method of performing stable frature meachincs tests. *Enigineering fracture mechanics,* pp. 117-125.

C1202, A., 2010. *Stanadard Test Method For Electrical Indication of Concrete's Ability to Resist Chloride Ion Penetration ,* West Conshohocken, PA: ASTM International .

C-496, A., n.d. *Standard test Method for Splitting Tensile Strength of Cylindrical Concrete Specimens,* s.l.: American Society for Testing and Materials.

Castellote, M., Fernandez, L., Andrade, C. & Alonso, C., 2009. Chemical chamge and paste analysis of OPC pastes carbonated at different carbon dioxide concentratrions. *Materials and structures,* pp. 515-525.

Castellote, M., Marcialis, A. & Turriziani, R., 1970. The kinetics of penetration of chloride ions into concrete. *Cemnto II,* pp. 157-164.

CEB, 1992. Durable concrete structures. In: UK: Thomas Telford.

CEB, 1992. *Durable Concrete Structures.* s.l.:s.n.

CEN, 2007. *EN 1992-1 Design of concrete structures - Part 1-1: General rules and rules for buildings,* Italy: Luxembourg:Publications office of the European Union.

Choinska, M., Khelidji, A., Chatzigeorgiou, G. & Pijaudier-Cabot, G., 2007. Effect and interaction of temperature and stress level realeted damage on permeability of concrete. *Cement and Concrete Research,* pp. 79-88.

Choi, Y. S., Kim, J. G. & Lee, K. M., 2006. Corrosion Behavior of Steel Bar Embedded in fly ash concrete. *Corrosion Science,* pp. 1733-1745.

Collepordi, M., Marcialis, A. & Tuniziani, R., 1972. Penetration of chloride ions into cement pastes and concretes. *Journal of Ceramic Society,* pp. 534-535.

Cui, H. et al., 2015. Experimental study on effects of CO2 concentrations on concrete. *Construction and Building Materials,* pp. 522-527.

Day, R. & Clarke, J., 2003. Plastic and Thermal Cracking. In: *Advance Concrete Technology Set.* Berkshire, UK: The Concrete Society, Century House, Telford Avenue, pp. 3-17.

Dhir, R. K., McCarthy, M. J. & Zhou, S., 2004. *Role of cement content in specifications for concrete.* s.l., s.n., pp. 113-127.

Edvardsen, C., 1999. Water permeambility and autogenous healing of crack in concrete. *ACI Materials Journal,* pp. 448-454.

Elahi, A., Basheer, P. A., Nanukuttan, S. V. & Khan, Q. U., 2010. Mechanical and duarbility properties of high performance concretes containing supplementary cementitious materials. *Construction and Building Materials,* pp. 292-299.

El-Reedy, M. A., 2008. *Steel reinforced concrete structures: Assessment and repair of corrosion.* s.l.:Taylor & Francis Group .

Elsener, B. et al., 2003. Half-cell potential measurements -potential mapping on reinforced concrete structures. *Materials Structures Journal,* pp. 461-471.

EN1990, 2002. *Eurocode - Basis of structural design,* Brussels: CEN.

EN1992, 2004. *Design of concrete structures,* Brussels: EUROCODE 2.

Feldman, R. F., Chan, G. W., Brousseau, R. J. & Tumidajski, P. J., 1994. Investigation of the Rapid Chloride Permeability Test. *ACI Materials Journal,* pp. 246-255.

Feldman, R., Prudencio, L. R. & Chan, G., 1999. Rapid chloirde permeability test on blended cement and other concretes:correlation between charge, initial current and conductivity. *Construction and Building Materals,* pp. 149-154.

Folic, R., 2009. Durability design of concrete strcutures- Part 1 Analysis fundamentals. *Architecture and Civil Engineering,* pp. 1-18.

Folic, R., 2009. Durability design of concrete structures-Part 1:Analysis fundamentals. *Architecture and Civil Engineering,* pp. 1-18.

Gerard, B. & Marchand, J., 1999. Influence of cracking on the diffusion properties of cement-based materials. Part-1: Influence of continuous cracks on the steady-state regime. *Cement and concrete Research,* pp. 37-43.

Glasser, F. P., Marchand, J. & Samson, E., 2008. Durability of concrete- Degredation phenomena involving detrimental chemical reactions. *Cement and Concrete Research,* pp. 226-246.

Gopalan, M. K., 1996. Sorptivity of fly ash concrete. *Cement and Concrete Research,* pp. 1189-1197.

Gowriplanan, N., Sirivivatnanon, V. & Lim, C. C., 2000. Chloride Diffusivity of concrete cracked in flexure. *Cement and Concrete Research,* pp. 725-730.

Grantham, M., 2003. Diagnosis, inspection, testing and repair of reinforcement concrete structures. In: *Advance Concrete technology Set.* Middlesex, UK: Butterworth Heinemann, pp. 1-54.

Grieve, G., 2009. Cementitious Materials. In: *Fulton's Concrete Technology.* s.l.:Cement & Concrete Institute.

Gruyaert, E., Heede, P. V. d. & Belie, N. D., 2013. Carbonation of slag concrete:Effect of the cement replacement level and curing on the carbonation coefficient-Effect of carbonation on the pore structure. *Cement and Concrete Composites,* pp. 39-48.

Gulikers, J., 2005. Theroretical consideration on the supposed linear relationship between concrete resistivity and corrosion rate of steel reinforcement. *Materials Corrosion,* pp. 393-403.

Guneyisi, E. & Gesoglu, M., 2008. A study on durability properties of high performance concretes incorperating high volumes of slag. *Materials and Structures,* pp. 479-493.

Hadjsadok, A. et al., 2012. Durability of mortars and concretes containing slag with loe hydraulic activity. *Cement and Concrete composites,* pp. 671-677.

Hansson, C. M., Poursaee, A. & Laurent, A., 2006. Macrocell and microcell corrosion of steel in ordinary Portland cement and high performance concretes. *Cement and Concrete Research,* pp. 2098-2102.

Haque, M. N. & Kayyali, O. A., 1995. Free and water soluble chloirde in concrete. *Cement and Concrete Research,* pp. 531-542.

Hassan, K. E., Cabrera, J. G. & Maliehe, R. S., 2000. The efffect of mineral admixtures on the properties of high-performance concrete. *Cemenat and Concrete Composites,* pp. 267-271.

Hearn, N., 1991. Effect of skrinkage and load-induced cracking on water permeability of concrete. *ACI Materials Journal,* pp. 234-240.

Heckroodt, R. O., 2002. *Guide to deterioration and failure of building materials.* Heron Quay, London E14 4JD: Thomas Telford Ltd.

Heiyantuduwa, R. & Alexander, M. G., 2009. Studies on prediction models for concrete durability. In: London: Taylor & Francis Group, pp. 303-309.

Hetek, 1996. *Chloride penetration into concrete, State of the Art Report,* Denmark: Road Directorate.

Hilsdorf, H., 1995. Concrete conpresive strength, transport characteristics and durability. In: *Performanc criteria for concrete durability.* London: E & FN Spon, pp. 108-125.

Hobbs, D. W., 1996. *Chloride ingress and chloride-induced corrosion in reinforcement concrete member.* Cambridge, Society of Chemical Industry, pp. 124-135.

Ho, D. S. & Lewis, R. K., 1987. Carbonation of concrete and its prediction. *Cement and concrete Research,* pp. 489-504.

Hong, C. Z. & Parrott, L. J., 1989. Air permeability of cover concrete and the effects of curing. In: s.l.:British Cement Association Report, pp. 24-25.

Hoseini, M., Bindiganavile, V. & Banthia, N., 2009. The effect of mechanical stress on permeability of concrete:A review. *Cement and Concrete Research,* pp. 213-220.

Houston, A. & Ferguson, P. M., 1972. *Corrosion of reinforcing steel embedded in structural concrete,* University of Texas at Austin: Center for Highway Research.

Houst, Y. F. & Wittmann, F. H., 2002. Depth profiles of carbonates formed during natural carbonation. *Cement and Concrete Research,* pp. 1923-1930.

Huang, R. & Yang, C. C., 1997. Conditions assessment of reinforced concrete beams relative to reinforcement corrosion. *Cement and Concrete,* pp. 131-137.

International, A., 2000. Corrosion:Understanding the basics. In: *Corrosion.* Ohio: ASM International.

Isaia, G. C., Gastadini, A. L. & Moraes, R., 2003. Physical and pozzolanic action of mineral additions on the mechanical strength of high-performance concretes. *Cement and concrete composites ,* pp. 69-76.

Ismail, M., Toumi, A., Francois, R. & Gagne, R., 2004. Effect of crack opening in the local diffusion of chlorides in inert materials. *Cement and Concrete Research,* pp. 711-716.

Jaggi, S., Bohni, H. & Elsener, B., 2007. Macrocell corrosion of steel in concrete-experiments and numerical modelling. In: *Corrosion of reinforcement in concrete-mechanisms, monitoring, inhibitors and rehabilitation techniques in concrete.* s.l.:Woodhead Publishing Limited, CRC Press, pp. 75-88.

Jang, S. Y., Kim, B. S. & Oh, B. H., 2011. Effect of crack width on chloride diffusion coefficient of concrete by steady-state migration tests. *Cement and concrete,* pp. 9-19.

Joseph, H. & Ramamurthy, K., 2009. Influence of fly ash on strength and sorption characteristics of cold-bonded fly ash aggregate concrete. *Construction Building and Materials,* pp. 747-760.

Kawamura, M. & Torii, K., 1989. *Chloride permebility of concrete containing fly ash and blast furnace slag.* s.l., s.n., pp. 411-416.

Khatri, R. & Sirvivantnanon, V., 1997. Methods for the Determination of Water Permeability of Concrete. *ACI Materials Journal,* pp. 167-172.

Koch, G. H. et al., 1999. *Corrosion costs and preventive strategies in the United States,* s.l.: FJWA-RD-01-156.

Kolias, S. & Gerorgiou, C., 2005. The effect of paste volume and of water content on the strength and. *Cement and Concrete Composites,* pp. 211-216.

Kropp, J., 1995. Relation between transport characteristics and durability.. In: *Performance criteria for concrete durability (Rilem report 12).* London: E & FN Spon: s.n., pp. 97-137.

Kumar, A. & Roy, D. M., 1986. The effect of desiccation on the porosity and pore structure of freeze dried hardened portland cement and slag-blended pastes. *Cement and Concrete Research,* pp. 74-78.

LethaboCompliance, 2013. *Chemical anaylsis of fly ash.* s.l.:s.n.

Li, L. & Sagues, A. A., 2001. Chloride Corrosion Threshold of Reinforcing Steel in Alkaline. *Corros,* pp. 19-28.

Lindvall, A., 2007. Chloirde ingress data from field and laboratory exposure-Influence of salinity and temperature. *Cement and Concrete Composities,* pp. 88-93.

Luping, T., Nilsson, L. & Basheer, P. M., 2012. *Resistance of concrete to chloride ingress:Testing and modelling.* New York: Spon Press.

Lu, X., Li, C. & Zhang, H., 2002. Relationship between the Free and Total Chloride. *Cement and Concrete Research,* pp. 323-326.

Maage, M. et al., 1996. Service life predictions of exisiting structures exposed to marine environments. *ACI Materials Journal,* Vol. 93(No.6), pp. 1-8.

MacDonald, D. D., El-Tantawy, Y. A., Rocha-Filho, R. C. & Urquidi-MacDonald, M., 1991. *Evaulation of electrochemical Impedance Techniques for detecting Corrosion on Rebar in Reinforced Concrete.* s.l.:s.n.

Mackechnie, J., 2001. *Predictions of reinforced concrete durability in the marine environment.* s.l.:University of Cape Town.

Mackechnie, J. R., 1996. *Predictions of Reinforeced Concrete Durability in the Marine Environment.* s.l.:University of Cape Town.

Mackechnie, J. R. & Alexander, M. G., 2001a. *Durability predictions using early-aged Durability Index Testing: Achieving quality in concrete construction:Workshop 1- Specifiying reinforced concrete for the year 2001,* s.l.: Concrete Society of South Africa.

Mackechnie, J. R. & Alexander, M. G., 2002. *Durability predictions using early age durability index testing.* Brisbane, Australia, CSIRO.

Mackechnie, J. R. & Alexander, M. G., 2002. *Durability predictions using early-aged durability index testing.* Brisbane, Australian Corrosion Association, p. 11.

Malhotra, V. M., 1987. *Properties of fresh and hardened concrete incorporating ground granulated blastfurnace slag.* Ottawa, Canda: Canadian Government Publishing Centre.

Marsavina, L. et al., 2009. Experimental and numerical determination of the chloride penetration in cracked concrete. *Construction and Building Materials,* pp. 264-274.

Metha , P. K., 2006. *Durability of concrete- A zigzag course of progress.* Montreal, Canada, American Concrete Institute, pp. 1-16.

Metha, P. K. & Burrows, R. W., 2001. Building durable structures in the 21st Century. *The Indian Concrete Journal,* pp. 437-443.

Metha, P. & Monterio, P. J., 2006. *Concrete: Microstructure, Properties and Materials.* United States of America: McGraw-Hill Companies.

Miller, J. H., 2006. *Protecting potential landmarks through demolition review,* Washington, D.C: National Trust for Historic Preservation.

Mohammed, B., Sakai, K., Banthai, N. & Yoshida, H., 2003. Predictions of chloirde ions ingress in uncracked and cracked concrete. *ACI Materials Journal,* pp. 38-48.

Mohammed, T. U. & Hamada, H., 2003. Relationship between free chloirde and total chloride content in concrete. *Cement and Concrete Research,* pp. 1487-1490.

Mohammed, T. U., Otsuki, N., Hisada, M. & Shibata, T., 2001. Effect of crack width and bar type on corrosion. *Journal of Materials in Civil Engineering,* pp. 194-201.

Monfore, G. E. & Verbeck , G. J., 1960. Corrosion of Prestressed Wire in Concrete. *ACI Materials Journal,* pp. 491-497.

Motohashi, K. & Masuda, Y., 2005. *Comparision of neutralization depth determined by thermal gravimetric anaylsis of CaCO3 and a phenophthalein method in an accelarated carbonation test.* France, s.n.

Mu, S., De Schutter, G. & Ma, B.-g., 2013. Non-steady state chloride diffusion in concrete with different crack density. *Materials and Structures,* pp. 123-133.

Nedhi, M., Shahria Alam, M. & Youssef, M. A., 2010. Development of corrosion-free concrete beams-column joint with adequate seismic energy dissipation. *Engineering Structure,* pp. 2518-2528.

Neville, A., 1981. *Properties of concrete (3rd Edition).* Great Britain: The Pitmann Press.

Neville, A., 2003. Can we determine the age of cconcrete by measuring carbonation? Part 1. *Concrete International.*

Newman, J. & Choo, B. S., 2003. *Advanced Concrete Technology 1: Constituent Materials.* Oxford: Butterworth-Heinemann.

Nikam, V. S. & Tambvekar, V. Y., 2003. *Effect of Different Supplementary Cementious Materials on the Microstructure and its Resistance Against Chloride Penetration.* s.l., s.n., pp. 1-10.

Nolan, E., Basheer, P. A. & Long, A. E., 1995. The effect of durability enhancing products on the physical properites of near surface concrete. *Construction and Building Materials,* pp. 267-272.

Nordtest method, N. B. 4., 1995. *Concrete, Hardened: Accelarated Chloride Penetration,* s.l.: Nordtest.

Nordtest, 1997. *Concrete, Mortar and Cement Based Repair Materials: Chloride Diffusion Coefficient from Migration Cell Experiments.* 2nd ed. Finland: Espoo.

Oh, B. H. & Jang, S. Y., 2007. Effects of material and environmental parameters on chloirde penetration profiles in concrete structures. *Cement and Concrete Research,* pp. 47-53.

Okada, K. & Miyagawa, T., 1980. *Chloride corrosion of reinforcing steel in cracked concrete.* s.l., s.n., pp. 237-254.

Otieno, M., Alexander, M. & Beushansen, H., 2010. Corrosion in cracked and uncracked concrete-influence of crack width, concrete quality and crack re-opening. *Magazine of Concrete Research,* pp. 393-404.

Pa Pa, W., Watanabe, M. & Machiba, A., 2004. Penetration profile of chloride ion in cracked reinforced concrete. *Cement and Concrete,* pp. 1073-1079.

Page, C. L. & Vennesland, O., 1983. Pore solution composition and chloride binding capacity of silica fue cement paste. *Materials and Structures,* Volume 1, pp. 19-25.

Papadakis, V. G., 2000. Effect of supplementary cementing materials on concrete resistance against carbonation and chloride ingress. *Cement and Concrete Research,* pp. 291-299.

Papadakis, V. G., Fardis, M. N. & Vayenas, C. G., 1992. Hydration and carbonation of pozzolanic cements. *ACI Materials Journal,* pp. 119-130.

Papadakis, V. G., Vayaenis, C. & Faradis, M. N., 1989. Fundamental modeling and experimental investigation of concrete carbonation. *American Institute of Civil Engineers,* pp. 1639-1650.

Papdakis, V. G., Vayenis, C. G. & Faradis, M. N., 1991. Fundamental modelling and experimental investigation of concrete carbonation. *ACI Materials Journal,* pp. 363-373.

Park, S.-S., Kwon, S.-J., Hwa, S. & Lee, S.-W., 2012. Modeling of water permeability in early aged concrete with cracks based on mocro pore structure. *Construction and Buidling Materials,* pp. 597-604.

Parrot, L. J., 1987. *A review of carbonation in reinforced concrete.,* UK: Cement and Concrete Association under a BRE contract.

Parrot, L. J., 1992. Variations of water absorption rate and porosity with depth from an exposed concrete. *Cement and Concrete Research,* pp. 1077-1088.

Parrott, L. & Hong, C. Z., 1991. Some factors influencing air permeation measurements in cover concrete. *Materials and structures,* pp. 403-408.

Parrott, L. J., 1987. *A review of Carbonation in Reinforced Concrete.* United Kingdom: British Cement Association.

Pfeifer, D., McDonald, D. & Krauss, P., 1994. The Rapid Chloirde Permeability Test and its correlation to the 90-Day Chloirde Ponding Test. *PCI Journal,* pp. 38-47.

Polder, R. B., 1997. *Chloride diffusion and resistivity testing of five concrete mixes for marine environment.* St-Remy-les-Chevreuses, RILEM.

Poulsen, E., 1990. *The chloride diffusion characteristics of concrete:appriximate determination by linear regression analysis, Nordic Concrete Research No.1 ,* s.l.: Nordic Concrete Federation.

Poulsen, E. & Mejlbro, L., 2006. *Diffusion of chlorides in concrete, Theroy and Application.* s.l.:Editors Taylor & Francis.

Ramezanianpour, A. A. & Malhotra, V. M., 1995. Effect of curing on the compressive strength, resistance to Chloride-Ion Penetration and porosity of concrete incorporating slag, fly ash or silica fume. *Cement and Concrete Composites,* pp. 125-133.

Raupach, M., 1996. Chloride-induced macrocell corrosion of steel. *Construction and buidling Material,* pp. 329-338.

Regourd, M., 1980. *Microanalytical studies(X-Ray Photo Electron Spectrometry) of surface hydration reactions of cement compounds.* London: Series A.

Reinhardt, H., 2007. *Fluid transport in wedge-split cracked concrete.* Belgium, s.n.

Richardson, M. G., 2002. *Fundermentals of durable concrete:Modern concrete technology.* London: Spoon Press.

Roy, D. M. & Idorn, G. M., 1993. *Concrete Microstructure,* Washington, DC: Strategic Highway Research Program.

Samacha, H. R. & Hover, K. C., 1992. Influence of microcracking on the mass transport properties of concrete. *Materials Journal,* pp. 416-424.

SANS10100-2, 1994. South African National Standards, Materials and execution of work. In: *The structural use of concrete.* s.l.:s.n.

SANS3001-PR5, 2011. *South African National Standards -Civil enginering test methods, Part 5: Computation of soil-mortarpercentages, course sand ratio, grading modulus and fineness modulus,* s.l.: s.n.

SANS5861-2, 1994. *South African National Standards, Concrete tests - Sampling of freshly mixed concrete. First revision,* s.l.: s.n.

SANS5861-3, 1994. *South African National Standards, Concrete tests - Making and curing of test specimens. First edition,* s.l.: s.n.

Sasatani, T., Torll, K. & Kawamura, M., 1995. *Five-year exposure test on long-term properties of concretes containing fly ash, blast-furnace slag and silica fume.* Milwaukee, ACI, pp. 283-296.

Schangen, E., Yoon, I.-S. & De Rooij, M. R., 2007. *Measurement of chloride ingress in cracked concrete.* Ghent, Belgium, Uitgeverij Acco, pp. 19-25.

Schiebl, P. & Raupach, M., 1997. Labouratory studies and calculations on the influence of crack width on chloride induced corrosion of steel in concrete. *ACI Materials Journal,* pp. 56-62.

Schiessl, P., 1988. *Corrosion of Steel in Concrete.* New York: Chapman & Hall.

Shah, S. P. & Slate, F. O., 1965. *Internal Microcracking, Mortar-aggregate bond and stress-strain curve of concrete.* London, A.E Brooks & K Newman, pp. 82-91.

Shalon, R. & Raphael, M., 1964. *Corrosion of reinforcing steel in hot countries.* Paris, s.n.

Sherman, M. R., McDonald, D. B. & Pfeifer, D. W., 1996. Durability aspects of precast prestressed concrete. Part 2:Chloirde permeability study. *PCI Journal,* pp. 76-95.

Shi, H.-S., Xu, B.-W. & Zhou, X.-c., 2009. Influence of mineral admixtures on compressive strength, gas permeability and carbonation of high performance concrete. *Construction and Building Materials,* pp. 1980-1985.

Simon , P., 2004. Improved current distribution due to a unique anode mesh placement in a steel reinforcement concrete parking garage slab CP system. *NACE Corrosion,* Issue No. 04345.

Song, H.-W. & Kwon, S.-J., 2007. Permeability characteristics of carbonated concrete considering capillary pore structure. *Cement and Concrete Research,* pp. 909-915.

Song, H.-W. & Kwon, S.-J., 2007. Permeability characteristics of carbonated concrete considering capillary pore structure. *Cement and Concrete Research,* pp. 909-915.

Song, H.-W., Kwon, S.-J., Byun, K.-J. & Park, C.-K., 2006. Predicting carbonation in early-aged cracked concrete. *Cementa dn Concrete Research,* pp. 979-989.

Song, H. W., Lee, C.-H. & Ann, K. Y., 2008. Factors influencing chloride transport in concrete structures exposed to marine environments. *Cement and Concrete Composites,* pp. 113-121.

St. John, D. A., Poole, A. & Sims, I., 1998. *Concrete Petrography:A handbook of Investigative techniques.* New York, NY: John Wiley & Sons Inc.

Stanish, K. & Thomas, M., 2003. The use of bulk diffusion tests to establish time-dependent concrete chloride diffusion coefficient. *Cement and Concrete,* pp. 55-62.

Streicher, P. E., 1997. *The development of a Rapid Chloride Test for concrete and its use in engineering practice.* s.l.:University of Cape Town.

Sugiyama, T., Bremner, T. & Holm, T., 1996. Effect of stress on gas permeability in concrete. *Materials Journal,* pp. 443-450.

Suryavanshi, A. K., Scantleburg, J. D. & Lyon, S. B., 1998. Corrosion of reinforcement steel embedded in high water-cement ratio concrete contaminated with chloirde. *Cement and Concrete Research,* pp. 263-381.

Sutter, L. et al., 2008. *The Deleterious Chemical Effects of Concentrated Deicing Solutions,* Pierre: South Dakota Department of Transportation.

Swamy, R. N., 1997. *Design for durability and strength through the use of fly ash and slag in concrete.* New Zealand, ACI, pp. 1-72.

T277, A., n.d. *Standard Method of Test for Rapid Determination of the Chloride Permeability of Concrete,* s.l.: s.n.

Takewaka, K. & Mastumoto, S., 1988. Quality and cover thickness of concrete based on the esitmation of chloirde penetration in marine environment. *ACI SP,* pp. pg 381-400.

Tang, L., 1967. *Chloride transport in Concrete-Measurement and prediction; Publication P-96:6,* Goteberg: Chalmers University of Technology.

Temper, B., 1947. *The corrosion of reinforcing steel in cracked concrete.* s.l., s.n., pp. 1137-1144.

Thangavel, K. & Rengaswamy, N. S., 1998. Relationship between chloride/hydroxide ratio and corrosion rate of steel in concrete. *Cement and concrete composites,* pp. 283-292.

Thomas, M. D. & Bamforth, P. E., 1999. Modelling Chloride Diffusion in Concrete: Effect. *Cement and Concrete Research,* pp. 487-495.

Thomas, M. D. & Matthews, J. D., 1992. The permeability of fly ash concrete. *Materials and Structures,* pp. 388-396.

Torrent, R., Basheer, M. & Goncalves, A. F., 2007. *Chapter3. Non-destructive methods to measure gas permeability,* s.l.: RILEM TC 189-NEC:State-of-the-art Report.

Torrent, R. J., 1992. A two-chamber vacuum cell for measuring the coefficient of permeability to air of the concrete cover on site. *RILEM Materials and Structures,* pp. 358-365.

Turner, L., 1937. The autogenous healing of cement and concrete: its relation to vibrated concrete and cracked concrete. *Internation Association of Testing Materials.*

Tuuti, K., 1982. Corrosion of steel in Concrete. *CBI forskning research, Swedish Cement and Concrete Research Institute, Institute of Technology, Stockholm.*

Underhill, L. & Bradfield, D., 2007. *Introstat.* Cape Town: Department of Statistical Science.

Uysal, M. & Akyuncu, V., 2012. Durability performance of concrete incoperating Class F and Class C fly ash. *Construction and Building materials,* pp. 170-178.

Van Delinder, L. S., 1984. *Corrosion - A Natural but Controllable Process.* Houston TX: NACE International Corrosion Society.

Victor, C. L. & Yang, E.-H., 2008. Self healing in concrete Materials. In: *Springer Series in Materials Science.* s.l.:Springer, pp. 161-193.

Vida, T., Castel, A. & Francois, R., 2004. Analyzing crack wodth to predict corrosion inreinforced concrete. *Cement and Concrete Research,* pp. 165-174.

Walter, R., Ostergaard, L., Olesen, J. F. & Stang, H., 2005. Wedge splitting test for a steel–concrete interface. *Engineering Fracture Mechanics,* pp. 2565-2583.

Wang , K., Jansen, D., Karr, A. & Shah, S. P., 1997. Permeability study of cracked concrete. *Cement and concrete research,* 27(3), pp. 381-393.

Wang, K., Jansen, D. C. & Shah, S. P., 1997. Permeability study of cracked concrete. *Cement and Concrete Research,* pp. 381-398.

Whiting, D., 1981. *Rapid Measurement of the Chloride Permeability of Concrete,* Washington: FHWA/RD-81/11, Federal Highway Admistration.

Wilkins, N. M. & Lawrence, P. F., 1983. *Corrosion of reinforcement in concrete construction,* s.l.: A.P Crane.

Win, P., Watanabe, M. & Machida, A., 2004. Penetration profile of chloride ion in cracked reinforced concrete. *Cement and Concrete Research,* pp. 1073-1079.

Wittmann, F. H., Zhang, P. & Zhao, T. J., 2011. *Application of Neutron Radiography to study mositure movement in cracked and cracked concrete.* s.l., RILEM Publications SARL, pp. 515-522.

Woodson, R. D., 2009. Causes of distress and deterioration of concrete. In: *Concrete Structures: Protection, repair and rehabilitation.* s.l.:Butterworth Heinemann, pp. 19-29.

Yahia, A., Tanimura, M. & Shimoyama, Y., 2005. Rheological properties of highly/flowable mortar containing limestone filler-effect of powder content and W/C ratio. *Cement and Concrete Research,* pp. 532-539.

Yang, C. S. H. R., 2002. The relationship netween charge passed and the chloride-ion concentration in concrete using steady state chloride migration test. *Cement and Concrete Researcg,* pp. 217-222.

Yang, E., Yang, Y. & Li, V., 2007. Use of high volumes of fly ash to improve ECC mechanical properties and material greenness. *ACI Materials Journal,* pp. 1809-1813.

Yeau, K. Y. & Kim, E. K., 2005. An experimental study on corrosion resistance of concrete with ground granulate blast-furnace slag. *Cement and Concrete Research,* pp. 1391-1399.

Yi, S.-T., Hyun, T.-Y. & Kim, J.-K., 2011. The effects of hydraulic pressure and crack width on water permeability of penetration crack-induced concrete. *Construction and Building Materials,* pp. 2576-2583.

Yoon, I., Schlagen, E., De Roji, M. & Van Breugel, K., 2007. The effects of cracks on chloride penetration into concrete. *Key Engineering Materials,* pp. 769-772.

Young , F. J., 1988. Review of the Pore Structure of Cement Paste and Concrete and its Influence on Permeability. *ACI SP-108,* pp. 1-18.

Yuan, Q. et al., 2009. Chloride binding of cement-based materials subjected to external chloride environment-A review. *Construction Buidling Materials,* pp. 1-13.

Zhang, S.-f., Lu, C.-h. & Liu, R.-g., 2011. *Experimental determination of chloride penetration in cracked concrete beams.* s.l., s.n., pp. 380-384.

8 APPENDIX A: DURABILITY INDEX TESTS

Durability of concrete may be defined as its ability to remain serviceable in a given exposure environment over its expected design life, without significant deterioration. Deterioration is often associated with ingress of aggressive agents in a liquid, vapour, gas or ionic form, which can penetrate the concrete from the exterior. Hence the near-surface concrete quality largely controls durability.

In recent years, the durability performance of concrete has increasingly become a point of concern since it is primarily this aspect that has been responsible for the failure of concrete structures. Most National codes and specifications set limits on the water/binder ratio's, cements, cover, etc., but without adequately addressing the issue of achieving adequate quality of the concrete cover.

Three durability test have been developed to characterize concrete according to the transport mechanisms; oxygen permeability for permeation, water sorptivity for absorption and chloride conductivity for diffusion (Alexander ***et al.,*** 1999).

8.1 Oxygen permeability test

Permeability involves the process of movement of fluids through the pore structure under externally applied pressure whilst the pores are saturated with the particular fluid. The permeability test involves forcing a gas through the specimen and thus is dependent on the path for the flow of gas through the specimen. These paths provided by pores extending through the length of the specimen, and are referred to as continues pores. The permeability of concrete is dependent on the concrete microstructure, the moisture condition of the material and the characteristics of the permeability fluid.

Test Apparatus

The oxygen permeability tests that were conducted used a falling head permeameter that was developed by Ballim at the University of the Witwatersrand. The test is based on deriving the Darcy coefficient of permeability by measuring the pressure gradient through concrete under a sustained pressure head. Figure 6.2 shows a schematic arrangement of the oxygen permeability apparatus.

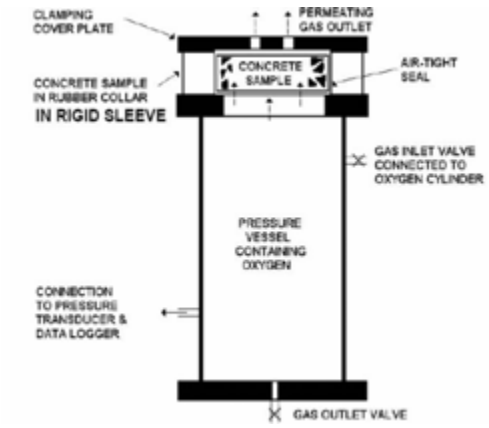

Figure 8.1 Schematic diagram of oxygen permeability apparatus

A compressible rubber collar as shown in Figure 7.2 is needed for each cell. The collar allows for a tight fit around the specimen which eliminates any leakage of oxygen, except through the pores of the specimen.

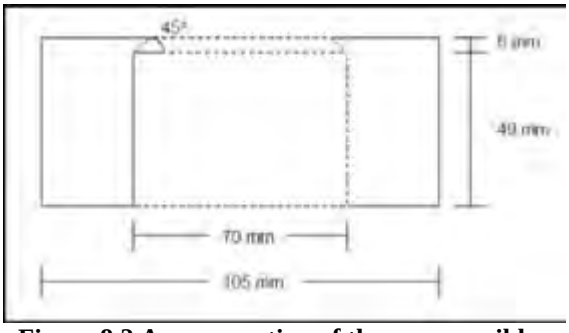

Figure 8.2 A cross-section of the compressible collar

Test method

Upon removal from the oven, the specimens weighted on a measuring scale, they were then placed in a desiccator and allowed to cool. The specimens were allowed to cool down for a period of two hours, after which they were removed and weighed. The specimens were then placed in the compressible collar with the near-surface face at the bottom. The collar and rigid sleeve were then placed on the top of the chamber, so that it covers the hole. The screws on the cover plate were then tightened, till it was adequately sealed.

Both the inlet and outlet values were opened, and oxygen was allowed to travel through the permeameter for 5 seconds. This allowed the chambers to be purged of gases other than oxygen. The outlet value was closed and the pressure was allowed to build up to 100±5 kPa. Thereafter the gas inlet valve was closed and the time and pressure was recorded. The decrease in pressure with time was recorded electronically on a computer. The test was terminated when the pressure had dropped to 50kPa or after 6 hours, which ever occurred first. The gas release valve was then opened and the specimen removed.

Calculation of Permeability

The equation governing the falling head permeameter is shown in Equation 1 below:

$$\boldsymbol{k = \frac{\omega V g d}{R A \sigma t}\, ln \frac{P_0}{P}} \qquad \textbf{Equation 7.1}$$

where: K = coefficient of permeability (m/s)

ω = molecular mass of permeating air (kg/mol)

V= volume of the pressure cylinder (m^3)

g = acceleration due to gravity (m/s^2)

d = specimen thickness (m)

R = universal gas constant (Nm/Kmol)

A = cross-sectional area of specimen (m^2)

σ = absolute temperature (K)

t = time (s)

P_o = pressure at the start of test (kPa)

P = pressure at time t

The coefficient of permeability was simplified by defining the permeability index (OPI) as the negative logarithm of the coefficient of permeability as shown in Equation 5:

$$\boldsymbol{OPI = -log_{10} k} \qquad \textbf{Equation 8.2}$$

8.2 Sorptivity test

Absorption involves the process whereby fluid is drawn into a porous, unsaturated material under the action of capillary forces. The capillary suction is dependent on the pore geometry and the saturation level of concrete. The rate of movement of a wetting front through a porous material under the action of capillary forces is defined as sorptivity.

Specimen preparation and test method

Upon the completion of the permeability test, the vertical curved sides of the specimens were sealed using packaging tape, to ensure uni-directional absorption. The specimens were weighed as well as the diameter and thicknesses were measured. A prepared solution of sodium hydroxide was poured into a tray that contained ten layers of paper towel. The paper towel was saturated and the water was visible on the top surface.

The specimens were placed with the near-surface side on the wet paper towel and began timing the start of the test using a stopwatch, as illustrated in Figure 7.3. The mass of the specimens were recorded at 3, 5, 7, 9, 12, 16, 20 and 25 minutes. Prior to the specimen being

weighed the excess solution was removed by patting the specimen on a damp piece of absorbent paper.

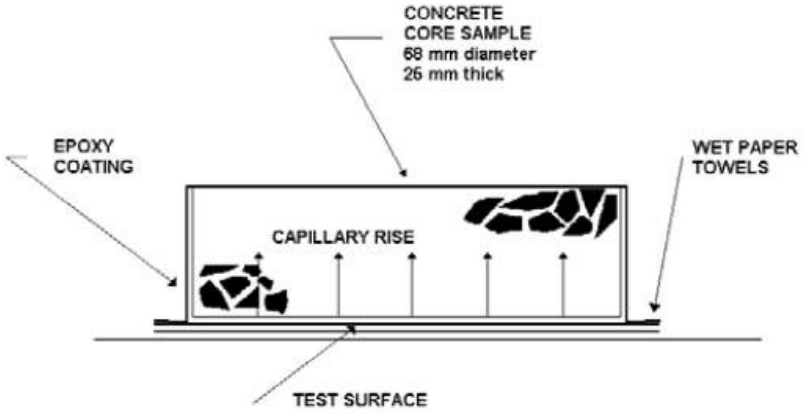

Figure 8.3 Schematic diagram of water sorptivity test

The specimens were then placed in a vacuum saturation tank, as illustrated in Figure 6.5, in such a way as to maximise the exposed surface area.

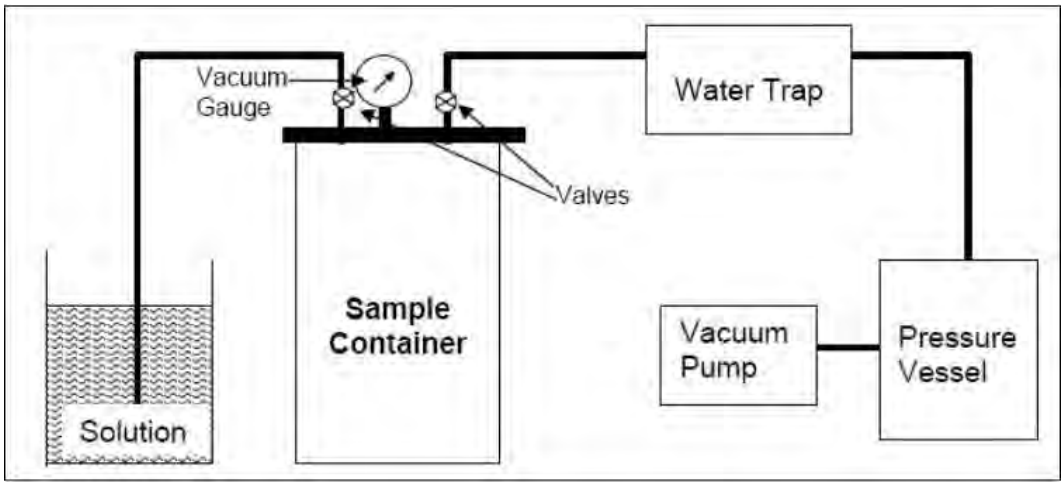

Figure 8.4 Schematic of vacuum saturation tank use to pre-saturate specimens

The vacuum tank was sealed using petroleum jelly after which a vacuum pressure of 75kPa was applied to the chamber. This was maintained for three hours after which calcium hydroxide solution was allowed to flow into the chamber. The pressure was re-established to 75kPa and this was maintained for a period of an hour. Thereafter the vacuum was released and air was allowed to flow into the chamber. The specimens were allowed to soak for a period of 18 hours, after which they were removed from the chamber and weighed to determine the vacuum saturate mass of the specimen.

8.3 Chloride conductivity test

Diffusion involves the process by which liquid, gas or ions move through a porous material under the action of a concentration gradient. The chloride conductivity test, involves measuring diffusion, which is an internal transport mechanism for concrete structure exposed to salts.

These methods have an important role to play in the development of durability indexes since all aggressive agents do not enter concrete via a single mechanism.

Specimen preparation and test method

Once the specimens were removed from the oven, their thickness and diameter were measured using a vernier calliper. The dry mass of the specimen was also recorded. The specimens were then placed in a vacuum saturation tank, as illustrated in Figure 7.4, in such a way as to maximise the exposed surface area.

The vacuum tank was sealed using petroleum jelly, and the specimens were maintained under a vacuum pressure of between -75 and -80kPa for three hours. After three hours, 5.0M sodium chloride solution was allowed to enter the vacuum tank and cover the specimens to an approximate depth of 40mm. The vacuum pressure was re-established to between -75 and -80kPa. After a period of one hour, the vacuum pressure was released and air was allowed to enter the chamber. After 18 hours of soaking the specimens were removed and weighed immediately. The specimens were now ready to be tested.

The specimens were placed within the flexible collar of the rigid central ring as shown in Figure 7.Both the anode and cathode parts of the cells were filled with 5.0M sodium chloride solution. The central portion of the cell was screwed into the cathode section of the cell the combined section was then screwed into the anode part of the cell. The ammeter and voltmeter was then connected. The power supply was then switched on and the DC power supply was adjusted till the voltage applied across the specimen is approximately ten volts. The current and voltage readings were recorded simultaneously.

Calculation of chloride conductivity

The chloride conductivity of the specimen can be calculated using Equation 8.3:

$$\sigma = \frac{it}{VA} \qquad \textbf{Equation 8.3}$$

Where: σ = conductivity of the specimen, (mS/cm)

i = electric current, (mA)

V = voltage, (V)

t = specimen thickness, (cm)

A = cross-sectional area, (cm^2)

References

Alexander. M.G, 2001. Durability index tests- Further notes on aspects related to testing and variability

9 APPENDIX B – TESTING AND VARIABILITY

The test result that was calculated for each of the tests conducted was based on the mean of three or four test determinations on the same material. In order to assess the test results variability, an established statistical procedure for determining 'outliers' was applied based on mathematical statistics. An outlier is defined as an observation or data point which does not appear to fall within the expected distribution for a particular data set (Barnett *et al.,* 1994). They can seriously affect the results of analyses.

The confidence interval for the sample was calculated using the t-distribution. The t-distribution was developed by W.S Gosset in 1908 in a need to do statistical tests using small samples (Underhill. L & Bradfield. D, 2007). The decision to use a 95% confidence interval was made. The equation for obtaining the confidence interval is highlighted below.

$$\left(\bar{X} - t^{*}_{n-1}\frac{s}{\sqrt{n}}, \bar{X} + t^{*}_{n-1}\frac{s}{\sqrt{n}}\right) \qquad \textbf{Equation 9.1}$$

Where: n= Size of random sample

$\bar{X}$= Sample mean

s=Sample standard deviation

t = T value obtained from the t-distribution tables, for a 95% confidence interval the corresponding t value was 4.303.

The sample deviation for the sample is calculated using the equation below.

$$s = \left(\frac{n\sum x_i^2 - (\sum x_i)^2}{n(n-1)}\right)^{\frac{1}{2}} \qquad \textbf{Equation 9.2}$$

where: n= Size of random sample

x_i= Individual test results

Using the equation above it was possible to determine a range which consisted of a low side and high side value for a 95% confidence interval. The confidence interval, allowed for data that fell out of the 95% confidence range to be identified as outliers. The outliers were then rejected and not included in the sample population.

References

Underhill. L (Underhill & Bradfield, 2007)and Bradfield. D, 2007. Introstat. Department of statistical Science, University of Cape Town, January 2007

10 APPENDIX C - COMPRESSIVE STRENGTH RESULTS

Table 10.1 28 Day Compressive Strength Results

0.40			0.55		
PC		**Average**	**PC**		**Average**
	Strength (MPa)	60.0		Strength (MPa)	45.7
	Mass (g)	2376		Mass (g)	2391
	Std. Dev.	0.6		Std. Dev.	2.0
	Range (95%)	58.6		Range (95%)	40.9
		61.3			50.6
PC/FA		**Average**	**PC/FA**		**Average**
	Strength (MPa))	57.9		Strength (MPa)	35.6
	Mass (g)	2402		Mass (g)	2386
	Std. Dev.	1.7		Std. Dev.	0.5
	Range (95%)	53.7		Range (95%)	34.5
		62.0			36.8
PC/GGBS		**Average**	**PC/GGBS**		**Average**
	Strength (MPa))	56.2		Strength (MPa))	39.5
	Mass (g)	2438		Mass (g)	2386
	Std. Dev.	2.5		Std. Dev.	1.8
	Range (95%)	49.9		Range (95%)	35.2
		62.5			43.9

*Note - The results presented in Table 9.1 are an average of three specimens tested.

11 APPENDIX D – DURABILITY INDEX TESTS RESULTS

Table 11.1 OPI results for 0.40 concrete mixes after 16 weeks

0.40			Mean	Coefficient of permeability (k)	Standard deviation	Variance	n	SE	t (n-1)	95% Cl (Max)	95% Cl (Min)	SE value
PC	#1	9.87	*9.82*	15.20	0.07	0.0045	4	0.03	2.35	9.90	9.74	0.08
	#2	9.83										
	#3	9.72										
	#4	9.85										
PC/FA	#1	10.22	10.18	6.68	0.10	0.0103	4	0.05	2.35	10.30	10.06	0.12
	#2	10.29										
	#3	10.05										
	#4	10.16										
PC/GGBS	#1	9.84	9.96	11.00	0.09	0.0072	4	0.04	2.35	10.06	9.85	0.10
	#2	9.95										
	#3	10.04										
	#4	9.99										

*Notes:

n – Number of specimens tested
SE – Standard Error
t - T value obtained from the t-distribution tables, for a 95% confidence

Table 11.2 OPI results for 0.55 concrete mixes after 16 weeks

0.55			Mean	Coefficient of permeability (k)	Standard deviation	Variance	n	SE	t (n-1)	95% CI (Max)	95% CI (Min)	SE value
PC	#1	9.90	9.79	16.32	0.10	0.0107	4	0.05	2.35	9.91	9.66	0.12
	#2	9.75										
	#3	9.66										
	#4	9.83										
PC/FA	#1	10.05	9.90	12.53	0.16	0.0254	4	0.08	2.35	10.09	9.71	0.19
	#2	9.99										
	#3	9.86										
	#4	9.69										
PC/GGBS	#1	9.82	9.84	14.30	0.10	0.0101	4	0.05	2.35	9.96	9.72	0.12
	#2	9.95										
	#3	9.87										
	#4	9.71										

*Notes:

n – Number of specimens tested
SE – Standard Error
t - T value obtained from the t-distribution tables, for a 95% confidence

Table 11.3 CCI values for 0.40 concrete mixes after 16 weeks

0.4			Mean	Standard deviation	n	SE	t (n-1)	95% CI (Max)	95% CI (Min)	SE value
PC	#1	0.98	0.92	0.11	4	0.06	2.353	1.05	0.78	0.13
	#2	0.90								
	#3	0.76								
	#4	1.02								
PC/FA	#1	0.78	0.72	0.09	4	0.04	2.353	0.82	0.61	0.10
	#2	0.68								
	#3	0.61								
	#4	0.80								
PC/GGBS	#1	0.22	0.24	0.04	4	0.02	2.353	0.28	0.19	0.04
	#2	0.19								
	#3	0.26								
	#4	0.27								

*Notes:

n – Number of specimens tested
SE – Standard Error
t - T value obtained from the t-distribution tables, for a 95% confidence

Table 11.4 CCI values for 0.55 concrete mixes after 16 weeks

0.55			Mean	Standard deviation	n	SE	t (n-1)	95% Cl (Max)	95% Cl (Min)	SE value
PC	#1	1.35	1.29	0.15	4	0.07	2.353	1.46	1.12	0.17
	#2	1.09								
	#3	1.28								
	#4	1.44								
PC/FA	#1	0.55	0.48	0.21	4	0.11	2.353	0.72	0.23	0.25
	#2	0.74								
	#3	0.33								
	#4	0.28								
PC/GGBS	#1	0.49	0.51	0.09	4	0.05	2.353	0.61	0.40	0.11
	#2	0.62								
	#3	0.51								
	#4	0.40								

Table 11.5 WSI results for 0.40 concrete mixes after 16 weeks

0.4			Mean	Standard deviation	n	SE	t (n-1)	95% CI (Max)	95% CI (Min)	SE value
PC	#1	9.95	9.90	0.17	4	0.09	2.353	10.10	9.70	0.20
	#2	9.65								
	#3	9.96								
	#4	10.04								
PC/FA	#1	9.08	9.20	0.20	4	0.10	2.353	9.43	8.97	0.23
	#2	9.28								
	#3	9.00								
	#4	9.44								
PC/GGBS	#1	8.84	8.50	0.27	4	0.14	2.353	8.82	8.18	0.32
	#2	8.58								
	#3	8.35								
	#4	8.22								

Table 11.6 WSI results for 0.55 concrete mixes after 16 weeks

0.55			Mean	Standard deviation	n	SE	t (n-1)	95% CI (Max)	95% CI (Min)	SE value
PC	#1	11.38	11.35	0.29	4	0.15	2.353	11.69	11.00	0.34
	#2	11.09								
	#3	11.17								
	#4	11.74								
PC/FA	#1	9.81	9.75	0.15	4	0.07	2.353	9.93	9.58	0.18
	#2	9.93								
	#3	9.68								
	#4	9.59								
PC/GGBB	#1	10.94	10.90	0.17	4	0.08	2.353	11.10	10.70	0.20
	#2	10.83								
	#3	11.11								
	#4	10.72								

12 APPENDIX E – CARBONATION DEPTH RESULTS

Table 12.1Carbonation depths (mm) for the 0.40 uncracked, w_{cr1} & w_{cr2} mixes after 16 weeks

	Uncracked							
	Mix	**#1**	**#2**	**#3**	**Average**	**Stdev**	**Max**	**Min**
	PC	3.58	3.49	3.81	3.63	0.03	3.67	3.58
	PC/GGBS	8.49	9.15	9.76	9.13	0.40	9.81	8.45
	PC/FA	7.40	6.84	7.87	7.37	0.26	7.81	6.92
	w_{cr1}							
	Mix	**#1**	**#2**	**#3**	**Average**	**Stdev**	**Max**	**Min**
0.40	**PC**	3.94	4.05	4.23	4.07	0.02	4.11	4.04
	PC/GGBS	12.66	13.13	12.59	12.79	0.09	12.94	12.64
	PC/FA	15.57	17.97	16.04	16.53	1.62	19.25	13.80
	w_{cr2}							
	Mix	**#1**	**#2**	**#3**	**Average**	**Stdev**	**Max**	**Min**
	PC	5.19	4.28	4.74	4.74	0.21	5.09	4.39
	PC/GGBS	15.98	16.10	16.75	16.27	0.17	16.56	15.99
	PC/FA	17.19	19.97	18.98	18.71	1.99	22.06	15.36

*Notes:

- All carbonation readings in Table 12.1 are recorded in millimetres.
- Stdev - Standard deviation

Table 12.2 Carbonation depths (mm) for the 0.55 uncracked, w_{cr1} & w_{cr2} mixes after 16 weeks

	Uncracked							
	Mix	**#1**	**#2**	**#3**	**Average**	**Stdev**	**Max**	**Min**
	PC	10.33	11.88	11.23	10.78	0.81	12.14	9.42
	PC/GGBS	8.57	9.23	9.83	9.21	0.40	9.88	8.54
	PC/FA	12.26	10.59	10.76	11.20	0.84	12.62	9.78
	w_{cr1}							
	Mix	**#1**	**#2**	**#3**	**Average**	**Stdev**	**Max**	**Min**
0.55	**PC**	12.14	13.24	12.86	12.69	0.32	13.22	12.16
	PC/GGBS	16.87	16.15	15.14	16.05	0.76	17.33	14.77
	PC/FA	29.81	27.12	28.94	28.62	1.88	31.78	25.46
	w_{cr2}							
	Mix	**#1**	**#2**	**#3**	**Average**	**Stdev**	**Max**	**Min**
	PC	15.60	16.78	17.06	16.48	0.60	17.49	15.47
	PC/GGBS	18.01	19.59	20.01	19.20	1.12	21.09	17.32
	PC/FA	38.34	41.05	40.97	40.12	2.37	44.11	36.12

*Notes:

- All carbonation readings in Table 12.1 are recorded in millimetres.
- Stdev - Standard deviation

13 APPENDIX F – CARBONATION COEFFICIENTS OBTAINED FROM CARBONATION DEPTH RESULT

Table 13.1 Carbonation coefficients obtained from carbonation depth reading

Uncracked		Carbonation depth (mm)	time (t)	exponent (n)	Coefficient (A)
0.40	OPC	3.63	16	0.33	1.45
	OPC/FA	7.37	16	0.40	2.43
	OPC/GGBS	9.13	16	0.33	3.66
0.55	OPC	10.78	16	0.33	4.32
	OPC/FA	11.20	16	0.40	3.69
	OPC/GGBS	9.21	16	0.33	3.69

w_{cr1}		Carbonation depth (mm)	time (t)	exponent (n)	Coefficient (A)
0.40	OPC	4.07	16	0.33	1.63
	OPC/FA	16.53	16	0.40	5.45
	OPC/GGBS	12.79	16	0.33	5.12
0.55	OPC	12.69	16	0.33	5.78
	OPC/FA	28.62	16	0.40	9.44
	OPC/GGBS	16.05	16	0.33	6.43

w_{cr2}		Carbonation depth (mm)	time (t)	exponent (n)	Coefficient (A)
0.40	OPC	4.74	16	0.33	1.90
	OPC/FA	18.71	16	0.40	6.17
	OPC/GGBS	16.27	16	0.33	6.52
0.55	OPC	16.48	16	0.33	6.60
	OPC/FA	40.12	16	0.40	13.23
	OPC/GGBS	19.20	16	0.33	7.69

14 APPENDIX G – BULK DIFFUSION RESULTS

Table 14.1 Chloride concentration (% by mass of binder) for the 0.40-PC uncracked, w_{cr1} & w_{cr2} mixes after 16 weeks

Uncracked	*Specimen*	*1*	*2*	*3*	*1*	*2*	*3*	*Average*
	Depth (mm)	**[Cl] Concrete**	**[Cl] Concrete**	**[Cl] Concrete**	**[Cl] Binder**	**[Cl] Binder**	**[Cl] Binder**	**[Cl] Binder**
	5	0.355	0.330	0.360	1.706	1.584	1.728	1.673
	15	0.103	0.086	0.106	0.494	0.412	0.507	0.471
	25	0.036	0.043	0.049	0.174	0.207	0.233	0.205
	35	0.035	0.033	0.047	0.169	0.159	0.226	0.184
	45	0.032	0.032	0.041	0.155	0.154	0.197	0.168
	55	0.029	0.030	0.038	0.139	0.144	0.182	0.155
w_{cr1}	*Specimen*	*1*	*2*	*3*	*1*	*2*	*3*	*Average*
	Depth (mm)	**[Cl] Concrete**	**[Cl] Concrete**	**[Cl] Concrete**	**[Cl] Binder**	**[Cl] Binder**	**[Cl] Binder**	**[Cl] Binder**
	5	0.397	0.380	0.373	1.905	1.824	1.792	1.840
	15	0.292	0.273	0.287	1.402	1.312	1.377	1.364
	25	0.272	0.272	0.245	1.305	1.304	1.174	1.261
	35	0.226	0.204	0.247	1.087	0.980	1.185	1.084
	45	0.214	0.249	0.236	1.025	1.193	1.134	1.117
	55	0.233	0.219	0.224	1.117	1.053	1.076	1.082
w_{cr2}	*Specimen*	*1*	*2*	*3*	*1*	*2*	*3*	*Average*
	Depth (mm)	**[Cl] Concrete**	**[Cl] Concrete**	**[Cl] Concrete**	**[Cl] Binder**	**[Cl] Binder**	**[Cl] Binder**	**[Cl] Binder**
	5	0.383	0.400	0.416	1.840	1.920	1.996	1.919
	15	0.363	0.339	0.376	1.740	1.627	1.805	1.724
	25	0.346	0.327	0.314	1.663	1.569	1.505	1.579
	35	0.333	0.325	0.302	1.598	1.561	1.449	1.536
	45	0.319	0.313	0.295	1.530	1.502	1.414	1.482
	55	0.310	0.304	0.292	1.488	1.459	1.402	1.449

Table 14.2 Chloride concentration (% by mass of binder) for the 0.55-PC uncracked, w_{cr1} & w_{cr2} mixes after 16 weeks

Uncracked	*Specimen*	*1*	*2*	*3*	*1*	*2*	*3*	*Average*
	Depth (mm)	**[Cl] Concrete**	**[Cl] Concrete**	**[Cl] Concrete**	**[Cl] Binder**	**[Cl] Binder**	**[Cl] Binder**	**[Cl] Binder**
	5	0.376	0.365	0.358	2.482	2.408	2.358	2.416
	15	0.148	0.120	0.138	0.976	0.791	0.911	0.893
	25	0.083	0.070	0.069	0.547	0.461	0.458	0.489
	35	0.062	0.059	0.055	0.412	0.389	0.365	0.389
	45	0.058	0.055	0.051	0.382	0.363	0.336	0.360
	55	0.054	0.052	0.049	0.356	0.341	0.323	0.340
w_{cr1}	*Specimen*	*1*	*2*	*3*	*1*	*2*	*3*	*Average*
	Depth (mm)	**[Cl] Concrete**	**[Cl] Concrete**	**[Cl] Concrete**	**[Cl] Binder**	**[Cl] Binder**	**[Cl] Binder**	**[Cl] Binder**
	5	0.428	0.418	0.409	2.819	2.759	2.699	2.759
	15	0.274	0.277	0.273	1.809	1.824	1.799	1.811
	25	0.272	0.275	0.271	1.792	1.813	1.786	1.797
	35	0.255	0.274	0.269	1.682	1.807	1.771	1.753
	45	0.240	0.241	0.232	1.580	1.590	1.527	1.566
	55	0.233	0.226	0.213	1.537	1.490	1.406	1.478
w_{cr2}	*Specimen*	*1*	*2*	*3*	*1*	*2*	*3*	*Average*
	Depth (mm)	**[Cl] Concrete**	**[Cl] Concrete**	**[Cl] Concrete**	**[Cl] Binder**	**[Cl] Binder**	**[Cl] Binder**	**[Cl] Binder**
	5	0.425	0.408	0.395	2.804	2.691	2.602	2.699
	15	0.379	0.342	0.350	2.499	2.258	2.309	2.355
	25	0.358	0.379	0.335	2.361	2.499	2.207	2.356
	35	0.338	0.348	0.306	2.229	2.293	2.017	2.180
	45	0.336	0.341	0.303	2.216	2.247	1.997	2.153
	55	0.333	0.321	0.289	2.193	2.115	1.904	2.071

Table 14.3Chloride concentration (% by mass of binder) for the 0.40-PC/FA uncracked, w_{cr1} & w_{cr2} mixes after 16 weeks

Uncracked	*Specimen*	*1*	*2*	*3*	*1*	*2*	*3*	*Average*
	Depth (mm)	**[Cl] Concrete**	**[Cl] Concrete**	**[Cl] Concrete**	**[Cl] Binder**	**[Cl] Binder**	**[Cl] Binder**	**[Cl] Binder**
	5	0.251	0.210	0.222	1.380	1.157	1.224	1.254
	15	0.111	0.145	0.148	0.610	0.798	0.816	0.714
	25	0.036	0.048	0.049	0.199	0.264	0.268	0.246
	35	0.037	0.041	0.045	0.204	0.223	0.246	0.224
	45	0.032	0.035	0.043	0.176	0.190	0.234	0.200
	55	0.029	0.033	0.041	0.160	0.182	0.223	0.188
w_{cr1}	*Specimen*	*1*	*2*	*3*	*1*	*2*	*3*	*Average*
	Depth (mm)	**[Cl] Concrete**	**[Cl] Concrete**	**[Cl] Concrete**	**[Cl] Binder**	**[Cl] Binder**	**[Cl] Binder**	**[Cl] Binder**
	5	0.260	0.238	0.241	1.433	1.311	1.328	1.357
	15	0.210	0.207	0.202	1.157	1.137	1.110	1.135
	25	0.190	0.198	0.192	1.048	1.090	1.057	1.065
	35	0.172	0.181	0.173	0.947	0.994	0.951	0.964
	45	0.171	0.172	0.177	0.940	0.945	0.973	0.953
	55	0.161	0.178	0.177	0.886	0.981	0.976	0.948
w_{cr2}	*Specimen*	*1*	*2*	*3*	*1*	*2*	*3*	*Average*
	Depth (mm)	**[Cl] Concrete**	**[Cl] Concrete**	**[Cl] Concrete**	**[Cl] Binder**	**[Cl] Binder**	**[Cl] Binder**	**[Cl] Binder**
	5	0.279	0.280	0.254	1.534	1.542	1.399	1.492
	15	0.212	0.253	0.228	1.168	1.393	1.256	1.272
	25	0.219	0.206	0.199	1.205	1.132	1.096	1.144
	35	0.192	0.201	0.196	1.054	1.109	1.079	1.081
	45	0.192	0.201	0.199	1.056	1.107	1.094	1.086
	55	0.166	0.180	0.184	0.912	0.990	1.015	0.972

Table 14.4Chloride concentration (% by mass of binder) for the 0.55-PC/FA uncracked, w_{cr1} & w_{cr2} mixes after 16 weeks

Uncracked	*Specimen*	*1*	*2*	*3*	*1*	*2*	*3*	*Average*
	Depth (mm)	**[Cl] Concrete**	**[Cl] Concrete**	**[Cl] Concrete**	**[Cl] Binder**	**[Cl] Binder**	**[Cl] Binder**	**[Cl] Binder**
	5	0.235	0.210	0.226	1.671	1.493	1.613	1.592
	15	0.104	0.119	0.114	0.741	0.848	0.809	0.799
	25	0.054	0.055	0.046	0.387	0.395	0.330	0.371
	35	0.032	0.035	0.040	0.227	0.250	0.282	0.253
	45	0.030	0.034	0.037	0.215	0.245	0.261	0.240
	55	0.030	0.031	0.034	0.214	0.223	0.244	0.227
w_{cr1}	*Specimen*	*1*	*2*	*3*	*1*	*2*	*3*	*Average*
	Depth (mm)	**[Cl] Concrete**	**[Cl] Concrete**	**[Cl] Concrete**	**[Cl] Binder**	**[Cl] Binder**	**[Cl] Binder**	**[Cl] Binder**
	5	0.241	0.237	0.235	1.719	1.685	1.672	1.692
	15	0.170	0.161	0.147	1.212	1.144	1.049	1.135
	25	0.160	0.153	0.135	1.139	1.092	0.963	1.065
	35	0.138	0.135	0.132	0.985	0.964	0.943	0.964
	45	0.138	0.135	0.129	0.980	0.959	0.921	0.953
	55	0.137	0.133	0.129	0.974	0.950	0.919	0.948
w_{cr2}	*Specimen*	*1*	*2*	*3*	*1*	*2*	*3*	*Average*
	Depth (mm)	**[Cl] Concrete**	**[Cl] Concrete**	**[Cl] Concrete**	**[Cl] Binder**	**[Cl] Binder**	**[Cl] Binder**	**[Cl] Binder**
	5	0.261	0.238	0.210	1.861	1.694	1.497	1.684
	15	0.230	0.212	0.201	1.639	1.509	1.429	1.526
	25	0.223	0.208	0.210	1.585	1.482	1.496	1.509
	35	0.196	0.200	0.198	1.398	1.421	1.411	1.410
	45	0.190	0.185	0.184	1.355	1.315	1.310	1.327
	55	0.189	0.184	0.183	1.343	1.311	1.300	1.318

Table 14.5Chloride concentration (% by mass of binder) for the 0.40-PC/GGBS uncracked, w_{cr1} & w_{cr2} mixes after 16 weeks

Uncracked	*Specimen*	*1*	*2*	*3*	*1*	*2*	*3*	*Average*
	Depth (mm)	**[Cl] Concrete**	**[Cl] Concrete**	**[Cl] Concrete**	**[Cl] Binder**	**[Cl] Binder**	**[Cl] Binder**	**[Cl] Binder**
	5	0.500	0.457	0.457	2.815	2.575	2.573	2.654
	15	0.078	0.086	0.079	0.440	0.485	0.444	0.456
	25	0.050	0.060	0.051	0.279	0.339	0.290	0.303
	35	0.047	0.048	0.038	0.264	0.272	0.214	0.250
	45	0.044	0.046	0.037	0.247	0.261	0.210	0.239
	55	0.040	0.044	0.037	0.228	0.250	0.207	0.228
w_{cr1}	*Specimen*	*1*	*2*	*3*	*1*	*2*	*3*	*Average*
	Depth (mm)	**[Cl] Concrete**	**[Cl] Concrete**	**[Cl] Concrete**	**[Cl] Binder**	**[Cl] Binder**	**[Cl] Binder**	**[Cl] Binder**
	5	0.501	0.480	0.478	2.823	2.704	2.691	2.739
	15	0.228	0.198	0.187	1.284	1.115	1.054	1.151
	25	0.146	0.141	0.144	0.823	0.793	0.814	0.810
	35	0.145	0.139	0.144	0.817	0.781	0.812	0.803
	45	0.145	0.138	0.142	0.815	0.778	0.799	0.797
	55	0.133	0.135	0.140	0.747	0.760	0.787	0.765
w_{cr2}	*Specimen*	*1*	*2*	*3*	*1*	*2*	*3*	*Average*
	Depth (mm)	**[Cl] Concrete**	**[Cl] Concrete**	**[Cl] Concrete**	**[Cl] Binder**	**[Cl] Binder**	**[Cl] Binder**	**[Cl] Binder**
	5	0.518	0.510	0.516	2.917	2.873	2.906	2.899
	15	0.282	0.267	0.244	1.591	1.506	1.372	1.490
	25	0.257	0.249	0.216	1.447	1.403	1.218	1.356
	35	0.214	0.231	0.211	1.208	1.302	1.189	1.233
	45	0.207	0.200	0.193	1.167	1.127	1.087	1.127
	55	0.182	0.185	0.187	1.026	1.043	1.055	1.041

Table 14.6Chloride concentration (% by mass of binder) for the 0.55-PC/GGBS uncracked, w_{cr1} & w_{cr2} mixes after 16 weeks

Uncracked	*Specimen*	*1*	*2*	*3*	*1*	*2*	*3*	*Average*
	Depth (mm)	**[Cl] Concrete**	**[Cl] Concrete**	**[Cl] Concrete**	**[Cl] Binder**	**[Cl] Binder**	**[Cl] Binder**	**[Cl] Binder**
	5	0.388	0.348	0.377	2.771	2.489	2.692	2.651
	15	0.113	0.102	0.101	0.804	0.731	0.720	0.752
	25	0.050	0.062	0.057	0.359	0.440	0.409	0.403
	35	0.049	0.042	0.043	0.349	0.301	0.310	0.320
	45	0.046	0.042	0.040	0.329	0.297	0.289	0.305
	55	0.042	0.042	0.039	0.302	0.298	0.277	0.292
w_{cr1}	*Specimen*	*1*	*2*	*3*	*1*	*2*	*3*	*Average*
	Depth (mm)	**[Cl] Concrete**	**[Cl] Concrete**	**[Cl] Concrete**	**[Cl] Binder**	**[Cl] Binder**	**[Cl] Binder**	**[Cl] Binder**
	5	0.370	0.352	0.351	2.644	2.516	2.507	2.556
	15	0.168	0.165	0.158	1.203	1.182	1.130	1.172
	25	0.166	0.189	0.152	1.186	1.351	1.087	1.208
	35	0.144	0.136	0.136	1.029	0.970	0.968	0.989
	45	0.140	0.130	0.135	1.001	0.931	0.964	0.965
	55	0.137	0.129	0.131	0.976	0.921	0.937	0.945
w_{cr2}	*Specimen*	*1*	*2*	*3*	*1*	*2*	*3*	*Average*
	Depth (mm)	**[Cl] Concrete**	**[Cl] Concrete**	**[Cl] Concrete**	**[Cl] Binder**	**[Cl] Binder**	**[Cl] Binder**	**[Cl] Binder**
	5	0.398	0.393	0.391	2.844	2.806	2.793	2.814
	15	0.230	0.225	0.225	1.641	1.606	1.608	1.618
	25	0.199	0.200	0.196	1.422	1.429	1.401	1.417
	35	0.186	0.182	0.182	1.329	1.303	1.298	1.310
	45	0.180	0.177	0.161	1.287	1.267	1.149	1.234
	55	0.162	0.167	0.158	1.155	1.196	1.129	1.160

15 APPENDIX H - CURVEFIT2003 MODEL RESULTS

Table 15.1Diffusion coefficient results obtained using the CurveFit2003 Model for 0.40 concrete mixes

		Uncracked	w_{cr1}	w_{cr2}
0.40-PC	Surface Cl content Cs, mass%:	2.394	1.586	1.881
	Diffusion Coefficient (D_a)	7.87E-12	5.12E-10	1.63E-09
	R^2	0.981	0.879	0.871
0.40-PC/FA	Surface Cl content Cs, mass%:	2.031	1.527	1.308
	Diffusion Coefficient (D_a)	1.38E-11	1.91E-10	8.65E-10
	R^2	0.954	0.732	0.828
0.40-PC/GGBS	Surface Cl content Cs, mass%:	3.741	2.218	2.517
	Diffusion Coefficient (D_a)	8.59E-12	1.41E-10	1.83E-10
	R^2	0.975	0.629	0.709

Table 15.2 Diffusion coefficient results obtained using the CurveFit2003 Model for 0.55 concrete mixes

		Uncracked	w_{cr1}	w_{cr2}
0.55-PC	Surface Cl content Cs, mass%:	2.518	1.428	2.611
	Diffusion Coefficient (D_a)	3.78E-10	6.75E-10	1.93E-09
	R^2	0.725	0.901	0.858
0.55-PC/FA	Surface Cl content Cs, mass%:	1.716	1.586	1.677
	Diffusion Coefficient (D_a)	1.96E-11	5.12E-10	1.83E-09
	R^2	0.947	0.879	0.922
0.55-PC/GGBS	Surface Cl content Cs, mass%:	3.000	1.692	1.882
	Diffusion Coefficient (D_a)	1.51E-11	4.70E-10	6.18E-10
	R^2	0.934	0.717	0.783